RUPRECHT-KARLS-UNIVERSITÄT HEIDELBERG

DOCTORAL THESIS

Stellar Tidal Streams as Cosmological Diagnostics: Comparing data and simulations at low galactic scales

---

Author:
Gustavo MORALES

Referees:
Prof. Dr. Eva K. GREBEL
Prof. Dr. Volker SPRINGEL

Astronomisches Rechen-Institut
Heidelberg Graduate School of Fundamental Physics
Department of Physics and Astronomy

14th May, 2018

DISSERTATION
submitted to the
Combined Faculties of the Natural Sciences and Mathematics
of the Ruperto-Carola-University of Heidelberg, Germany
for the degree of
DOCTOR OF NATURAL SCIENCES

Put forward by
GUSTAVO MORALES
born in Copiapo
ORAL EXAMINATION ON JULY 26, 2018

Stellar Tidal Streams as Cosmological Diagnostics:
Comparing data and simulations at low galactic scales

Referees:
Prof. Dr. Eva K. GREBEL
Prof. Dr. Volker SPRINGEL

NOTE: Some parts of the written contents of this thesis have been adapted from a paper submitted as a co-authored scientific publication to the Astronomy & Astrophysics Journal: Morales *et al.* (2018).

NOTE: Some parts of this thesis have been adapted from a paper accepted for publication in the Astronomy & Astrophysics Journal: Morales, G. *et al.* (2018). "Systematic search for tidal features around nearby galaxies: I. Enhanced SDSS imaging of the Local Volume". arXiv:1804.03330. DOI: 10.1051/0004-6361/201732271

Abstract

In hierarchical models of galaxy formation, stellar tidal streams are expected around most galaxies. Although these features may provide useful diagnostics of the ΛCDM model, their observational properties remain poorly constrained. Statistical analysis of the counts and properties of such features is of interest for a direct comparison against results from numerical simulations. In this work, we aim to study systematically the frequency of occurrence and other observational properties of tidal features around nearby galaxies. The approach featured here is based on a visual classification of diffuse features around a sample of nearby galaxies, using a post-processing of optical survey imaging optimized for the detection of low-surface-brightness stellar structure. At the limiting surface brightness of this sample, $14-17\%$ of the galaxies exhibit evidence of diffuse features likely to have arisen from minor merging events. For simulated images, the frequency is $16-19\%$. Our technique recovers all previously known streams in the selected sample and yields a number of new candidates. We conclude that this methodology provides a reliable foundation for the statistical analysis of diffuse circumgalactic features in wide-area imaging surveys, and for the identification of targets for follow-up studies.

Zusammenfassung

In hierarchischen Modellen der Galaxienentstehung wird erwartet, dass die meisten Galaxien von Gezeitenströmen umgeben sind. Obwohl diese Strukturen möglicherweise hilfreiche Aufschlüsse über das ΛCDM Modell liefern könnten, sind ihre beobachtbaren Eigenschaften nach wie vor unzulänglich bekannt. Eine statistische Analyse der Anzahl und Eigenschaften dieser Strukturen ist von Interesse für den direkten Vergleich mit Ergebnissen aus numerischen Simulationen. Meine Arbeit hatte zum Ziel systematisch die Häufigkeit des Auftretens und andere beobachtbare Eigenschaften von Gezeitenströmen um nahegelegene Galaxien zu untersuchen. Die hier dargelegte Vorgehensweise basiert auf einer visuellen Klassifizierung von diffusen Strukturen um eine Stichprobe von nahen Galaxien, wofür eine auf die Detektion von stellaren Strukturen mit niedriger Flächenhelligkeit optimierte Nachbearbeitung von optischen Durchmusterungen eingesetzt wurde. Bei der limitierenden Flächenhelligkeit dieser Stichprobe zeigen $14-17\%$ der Galaxien Hinweise auf diffuse Strukturen, die wahrscheinlich von kleineren Verschmelzungsereignissen herrühren. Für simulierte Bilder liegt die Häufigkeit bei $16-19\%$. Mein Verfahren zeigt alle bisher bekannten Ströme in der ausgewählten Stichprobe und liefert einige neue Kandidaten. Ich gefolgere, dass diese Methodik eine verlässliche Grundlage für die statistische Analyse von diffusen galaxienumgebenden Strukturen in großflächigen bildgebenden Durchmusterungen und für die Identifikation von Zielen für Nachfolgeuntersuchungen liefert.

Acknowledgements

I would like to thank my whole Ph.D. committee and examinators, in particular to Eva K. Grebel, David Martínez-Delgado, and Volker Springel. Without their guidance, support and nearly infinite patience, I never would have been able to finish this humble but enriching, rewarding project.

To my colleagues Andrew Cooper, Carlos Frenk, Roberto DePropris, Thomas Puzia, Rolando Dünner, Behnam Javanmardi, Carolin Wittmann, and so many others, for their insightful comments and professionalism; and to the whole administrative staff of the ARI, from whom I always received help and support.

Special mention to my good, fresh, strong, always dear friends, whom made me company and trusted in me during this quest. Mauricio Carrasco, Fabián Olivares, Eduardo Bañados, Lucy Maxton, Agnese Miral, Santiago Casas, Christine Lansche, Felipe Montellano, Priyata Kalra, Gabriel Torrealba, Néstor Espinoza, Cristóbal Sifón, Miguel Campos, Nicolás González, Marcelo Tala, Melissa Navarro, Oscar García: you will never be forgotten.

Last but not least, to my dear family. My dad, mom, and my brothers, for whom I live, work, and fight for. Thank you for tolerating this weird dream I had since I was twelve.

Contents

List of Figures

List of Tables

List of Abbreviations

ΛCDM	Λ-**C**old **D**ark **M**atter
COCO	**Co**pernicus **Co**mplexio
DM	**D**ark **M**atter
DECaLS	**D**ark **E**nergy **Ca**mera **L**egacy **S**urvey
GALEX	**Gal**axy **E**volution E**x**plorer
J&B	Bullock and Johnston (2005) and Johnston et al. (2008)
MW	**M**ilky **W**ay
MBD11	Miskolczi, Bomans, and Dettmar (2011)
NED	**N**ASA **E**xtragalactic **D**atabase
PM, **P^3M**	**P**article(-**P**article-**P**article) **M**esh
SDSS	**S**loan **D**igital **S**ky **S**urvey
SNR	**S**ignal-to-**N**oise-**R**atio
SPH	**S**moothed-**P**article **H**ydrodynamics
STSS	**S**tellar **T**idal **S**tream **S**urvey
UV	**U**ltra **V**iolet

A mi Papá y mi Mamá. Por siempre.

Chapter 1

Introduction

> In a nutshell, the universe is 4% visible, 23% undetectable and 73% unimaginable. Welcome to the cosmos, full of mass you can measure but not manhandle, driven by a force you can infer but not explain.
>
> Tim Radford

Astronomy tackles the problem of understanding the Universe by studying celestial objects and all kind of extraterrestrial phenomena, spanning a wide range of physical scales, objects and processes, and testing natural explanations for every set of measurements possible. A key element of astrophysics as a scientific discipline includes the study of the physical nature of galaxies, while applying the laws and theories of physics to the interpretation of astronomical observations related to them. In this context, the formation and evolution of galaxies in particular is the central node of this work.

1.1 Some historical context

In the late 1920s, the so-called island universes became of uttermost relevance in the discovery of the expansion of the Universe, thanks to redshift measurements (Hubble, 1929). Later, many more extra-galactic objects were classified as galaxies and sorted according to their morphology.

Later, in the decades of 1950s and 1960s, it was noted that many galaxies had distinct features. While the majority of bright galaxies could be classified as either elliptical, spiral or barred-spiral, it was clear that many peculiar morphologies would not fit into these three families. Numerous authors started to report the discovery of twisted shapes and faint extensions outside of the central region of these galaxies, subsequently gathered in atlases and catalogues: Zwicky et al. (1961), Zwicky, Herzog, and Wild (1963), Vorontsov-Vel'Yaminov and Arkhipova (1962), Vorontsov-Vel'Yaminov and Arkhipova (1964), and Arp (1966).

These peculiar galaxies were linked to interacting galaxies, with connecting or outgoing filaments being the dominant signature. These 'bridges' and 'tails' were noticeable different from spiral arms, sometimes showing signs of high star formation activity. As Duc and Renaud (2013) pointed out, being always challenging to observe, Arp

(1966) even suggested that pure gravitation should not be the only element influencing peculiar galaxies and their small scale structures.

As also noted by Duc and Renaud (2013), Toomre and Toomre (1972) provided huge insight into the debate after a series of numerical experiments. By simulating collisions of a satellite galaxies on eccentric orbits, and varying the degree of disk inclination with respect to the orbital plane, it was shown that galaxies in such strong tidal field would develop structures with the same shapes as the ones referenced in the catalogues. In this way, they noted that close encounters of these kind had the potential to change the orbits of the stars in the disk in a non random way, leading to the creation of coherent sub-galactic structures, within or around the host galaxies. By varying several the inclination of the disks or the eccentricity of the orbit, they showed that gravitation was enough to reproduce the structures observed in interacting systems. Duc and Renaud (2013) Also pointed how many other computational works followed, allowing to conclude on the tidal origin of several observed features (Danziger and Schuster, 1974; Stockton, 1974; Yabushita, 1977). Since then, gravitational tides have been considered as the major cause of the creation of filaments in interacting galaxies, either by systematically exploring a large volume of the parameter space, or by simulating specific, observed galaxies in order to bring new lights when interpreting the observations. This is why such features are often refered to as tidal structures.

Currently, the research on interacting galaxies, and more specifically, tides in colliding galaxies, is mainly focused on three aspects: (1) the cosmological approach, mainly based on the ΛCDM paradigm applied to galaxy formation through repeated accretion of satellites; (2) work based on the central region of mergers, where the formation of AGNs and its associated feedback is dicussed; and (3) the study of the stellar populations of the interacting galaxies and the properties of the star clusters and the dwarf galaxies they may contain. This thesis can be understood as an example of the first approach.

1.2 From cosmology to stellar halos

In the Λ Cold Dark Matter (ΛCDM) cosmology, structures grow hierarchically under the influence of gravity through numerous mergers of smaller structures consisting mainly of dark matter (DM) (e.g., Press and Schechter, 1974; White and Rees, 1978; Blumenthal et al., 1984; Davis et al., 1985; Lacey and Cole, 1993). Baryonic matter collects in the potential wells of DM halos, then (in sufficiently massive halos) cools and condenses, eventually leading to star formation. State-of-the-art cosmological simulations seek to model the assembly of dark and baryonic mass, star formation, stellar evolution, and so-called 'feedback' processes such as supernovae ab initio in order to demonstrate how complex interactions between these processes give rise to the observed diversity of the cosmic galaxy population (e.g., Kauffmann, White, and Guiderdoni, 1993; Cole et al., 2000; Croton et al., 2006; Vogelsberger et al., 2014; Schaye et al., 2015).

In such models, the stellar content of galaxies forms partly in situ through the condensation of gas in the galaxies themselves, and partly through the accretion of stars tidally stripped from other galaxies that they encounter over cosmic time, which may be partially disrupted or have merged completely by the present day (e.g., Searle and Zinn, 1978; Abadi, Navarro, and Steinmetz, 2006; Purcell, Bullock, and Zentner, 2007). The assembly histories of galaxies with a stellar mass comparable to the mass of the

Milky Way (MW) vary widely in these models (Guo and White, 2008). This is supported by observational results from the detailed study of nearby galaxies. Our Milky Way, for instance, appears to have experienced a relatively quiescent merger history (Hammer et al., 2007), while its neighbor M31 shows a much more extended stellar structure, including a variety of bright stellar streams with different morphologies (e.g., Zucker et al., 2004; McConnachie et al., 2009; Ibata et al., 2014; Thomas et al., 2017). Models also predict that merger rates were higher at higher redshifts (e.g. Maller et al., 2006), and that the merger history depends in characteristic ways on environment (e.g. Gottlöber, Klypin, and Kravtsov, 2001).

1.3 Stellar haloes and the formation of tidal streams

In principle, a galaxy contains dark matter, stars, gas and dust, and tends to keep all of its material bound because of gravitational forces. However, when it moves in an external potential, created for instance by neighbor galaxies, it can experience gravitational forces which vary across distance. This situation typically depicts a galaxy in a tidal field.

Mergers between interacting or colliding galaxies occurring in a tidal field can be classified due to the properties of the merging galaxies, such as their number (binary or multiple), their gas richness (wet, dry, damped and mixed mergers), and their comparative size (major or minor).

Minor mergers occur when one of the galaxies is significantly larger than the other(s)[1]. Tidal features of interest of this thesis are mainly a signature of these minor mergers, typically referred in the literature as tails, rings, ripples, shells, loops and warps. The process by which bound stars and gas can be (partially) re-arranged into tidal features is called tidal stripping, with the tidal radius being the distance at which a star within a satellite becomes unbound or stripped and becomes bound instead to the host galaxy about which the satellite orbits.

In this context, Read et al. (2005) improved the analytical derivation for the tidal radius of satellites in galaxies, and using N-body simulations, confirmed what others (Toomre and Toomre, 1972; Keenan and Innanen, 1975) established previously: (1) that the orbits of stars are critical in determining the tidal radius for the satellite in the process of stripping; and (2), that both radial and prograde orbits are more efficient in tidal stripping, when compared to retrograde orbits. Also noteworthy by Read et al. (2005) were the studies by Kazantzidis et al. (2004) and Kravtsov, Gnedin, and Klypin (2004), reporting that satellites showed tangential velocity anisotropy near the tidal radius, and that radially biased velocity distributions were more rapidly stripped. Comparable experiments made with groups of stars submerged in tidal fields, like globular clusters and star clusters, showed identical results (Takahashi, Lee, and Inagaki, 1997; Baumgardt and Makino, 2003).

Another relevant effect for the presence of tidal features is called ram pressure stripping. In galaxy clusters, groups of galaxies are permeated by hot, X-ray emitting gas known as the intra-cluster medium (e.g. Wężgowiec et al., 2012). As galaxies move in this field, said gas creates a ram pressure effect that, if strong enough to overcome the gravitational potential of the galaxy, ends up removing the gas content from the galaxy. Evidence for ram pressure stripping can be found in many galaxy clusters, of

[1] As opposed to a major merger, where the two bodies have similar size or masses.

which one of them can be expressed in terms of streamers of gas and dust trailing behind the motion of a given galaxy, effectively changing the colors of stars in different regions of it (Mayer et al., 2006).

1.4 Tidal streams as a motivation for this thesis

A well-established prediction is that most of the mass in stellar halos of present-day Milky Way-mass galaxies was contributed more than 9 Gyr ago by a few satellites in the mass range of 10^8 to 10^9 $M_\odot$ (e.g., Bullock and Johnston, 2005; De Lucia and Helmi, 2008; Cooper et al., 2010; Pillepich, Madau, and Mayer, 2015; Amorisco, 2017b). While stars that formed in situ are expected to dominate the stellar mass profiles of galaxies at small galactocentric radii, accreted stars have a much wider range of binding energies and can give rise to stellar halos extending as far as the virial radius of the host DM halo (e.g., Bullock et al., 2001; Font et al., 2006; Cooper et al., 2013; Rodriguez-Gomez et al., 2016). Long dynamical times in the outer regions of DM halos allow coherent structures formed by tidal stripping, such as streams and shells, to persist for many gigayears (Johnston, Sackett, and Bullock, 2001). Dynamical friction causes the few most massive satellites to deposit their stars at small galactocentric radii, while the outer regions of stellar halos are more likely to consist of material contributed by a number of less massive satellites (e.g., Bullock and Johnston, 2005; Amorisco, 2017a). Owing to their low stellar densities and intrinsically low luminosities, it is hard to determine both the full extent of stellar halos and their contributions to the innermost regions of galaxies. Together with other difficulties, this makes it challenging to constrain stellar fractions observationally ex situ (e.g., Cooper et al., 2013; D'Souza et al., 2014; Merritt et al., 2016; Harmsen et al., 2017).

It is more straightforward to detect recent and ongoing accretion events involving satellites that are sufficiently luminous to give rise to bright tidal streams in the outskirts of massive galaxies. A growing number of such features have been detected beyond the Local Group in recent years, and further extragalactic surveys reaching sufficiently low surface brightness have recently been completed or are currently ongoing (e.g., Schweizer and Seitzer, 1990; Martínez-Delgado et al., 2007; Martínez-Delgado et al., 2008a; Mouhcine and Ibata, 2009; Miskolczi, Bomans, and Dettmar, 2011; Ludwig et al., 2012; Duc et al., 2015; Okamoto et al., 2015; Merritt et al., 2016; Crnojević et al., 2016; Spavone et al., 2017; Harmsen et al., 2017).

Mergers between galaxies with very different stellar masses (typically mass ratios of around 1:10 or higher) are often called minor mergers. These generally involve long-period orbits, little orbital decay or angular momentum loss for the less massive galaxy (which we refer to hereafter as the 'satellite'), and little disturbance of the central structure of the more massive galaxy. Consequently, thin, coherent stellar tidal streams are a distinctive observable signature of such mergers, more so for less massive, more recently accreted, and kinematically 'colder' satellites (Johnston et al., 2008). Gaseous tidal streams are commonly observed around interacting galaxies and can be easily traced through 21 cm observations. They usually overlap with the stellar features unless, for instance, ram pressure separates them. Their observable properties can also be measured in optical data, for example, using their Hα emission, or looking for galactic dust. Pure gaseous streams (such as the trailing Magellanic Stream) are rare, whereas pure stellar streams are more common around massive galaxies following the dispersal of any previously associated gas, or when gas-deficient early-type

satellites are disrupted. For a review, see Duc and Renaud (2013). In the case of MW-like hosts, we expect minor merger events to be less frequent in the present-day Universe and the coherent structures they generate (such as tidal tails) to persist only for a few billion years before they become undetectable (Wang et al., 2017). Observationally, however, the frequency with which such streams occur around MW-like hosts and their distribution of morphologies are poorly constrained.

1.5 Data surveys and simulations used in this work

Over the past decade, the Stellar Tidal Stream Survey (STSS) has carried out an ultra-deep, wide-field imaging exploration of several nearby spiral galaxies, based on data taken with amateur robotic telescopes (Martínez-Delgado et al., 2007; Martínez-Delgado et al., 2010; Martínez-Delgado et al., 2015a). This survey has revealed striking stellar tidal streams of different morphologies with unprecedented depth and detail. Subsequently, Miskolczi, Bomans, and Dettmar (2011) (*MBD*11 from now on) developed a search strategy for low-surface brightness tidal structures around a sample of 474 galaxies in the Sloan Digital Sky Survey (SDSS) Data Release 7 archive (Abazajian et al., 2009). The authors calibrated images taken from the SDSS archive and processed them in an automated manner. Searching for possible tidal streams by visual inspection, they found that at least 6% of their sample showed distinct stream-like features (with a total of 19% presenting faint features of any kind). This study demonstrated that detecting a meaningful sample of tidal features close to the detection limit of the SDSS images is feasible.

Although considerable progress has been made by *MBD*11 and other works, studies of structure with low surface brightness in the outskirts of galaxies remain predominantly discovery-driven and qualitative. To enable a meaningful statistical comparison between data with low surface brightness and cosmological models of galaxy formation, two further advances are urgently required: samples with both a well-defined selection function and uniform imaging data, and the development of automated methods to detect and quantify features with low surface brightness.

The majority of existing deep-imaging studies have been targeted at galaxies that are either very nearby or have known features detected in shallower imaging. It is clearly impossible to draw any conclusions about how frequent such features are from these data alone. Furthermore, prior work has focused on structures associated with Milky Way-type galaxies. This definition is subjective; it typically includes galaxies that are sufficiently bright, morphologically regular, and have late Hubble type. Not only does a subjective selection make it harder to compare one observational sample to another, but it is almost impossible to apply a comparable qualitative selection to models. Although commendable efforts by, for example, Snyder et al. (2015), have made great progress, currently even the most sophisticated hydrodynamical simulations do not reliably reproduce the full range of morphological details that such judgments are based on. Moreover, selection of Milky Way analogues by qualitative criteria will almost certainly result in a wide sampling of the distribution of fundamental quantities such as stellar mass, and a highly incomplete sample at a given stellar mass. It is much more straightforward, and statistically sound, to carry out comparisons in terms of observable quantities that can be robustly constrained in models, stellar mass being the most obvious choice[2].

[2]In principle, constraining our sample only by stellar mass, without any consideration on morphology, would mean to also cover all galaxies from early to late types. This would include, for example,

Therefore, to make a meaningful comparison between data and models, deep imaging surveys with simple, quantitative selection functions based on fundamental quantities are necessary. Ideally, these would exploit the statistics of brighter circumgalactic features that can be detected in large samples drawn from shallow wide-area surveys, since the expense of targeted deep imaging is often hard to justify for surveys in which substantial numbers of (statistically important) non-detections are to be expected. Low surface brightness features are often said to be ubiquitous, but such statements must take into account the brightness of the features, the depth of the observations, and also, the environment on which the host galaxies are found. A known (and for a given sample, uniform) limit on depth is crucial to make meaningful statements about counts of structures. Finally, since the role of accretion in the galaxy formation process can be investigated through correlations between structure with low surface brightness and other galaxy properties, it would be very useful (and arguably necessary) to examine large numbers of host galaxies of similar mass without restriction to specific morphologies.

1.5.1 The Stellar Tidal Stream Survey

This thesis is heavily influenced by the work published by the STSS. Their current data has also been used as a way to confirm new detections. Its main objective is to impose observational constraints on the rate and consequences of minor mergers in spiral galaxies of the local volume, by targeting isolated spiral Milky Way analogues ($M_B < -20.5$) within the local volume (~ 10 Mpc), allowing a direct comparison with available ΛCDM models of stellar halos, in order to explore if the Milky Way and the Andromeda galaxy merging history is typical by comparing with other nearby galaxies. In this respect, the work featured in this thesis can be understood as a natural extension towards a more robust, reliable comparison.

The Pilot Survey was originally published in Martínez-Delgado et al. (2010). In an effort to study spatially extended stellar tidal features of low surface brightness, the authors carried out deep, wide field imaging of eight field spiral galaxies in the local volume, with data taken at small robotic telescopes, but with reported surface brightness sensitivity reaching $\mu_{\rm lim}(V) \approx 28.5$ mag arcsec^{-2}.

This initial observational effort led to the discovery of six previously unpublished extensive (to ~ 30 kpc) stellar structures in the halos surrounding these galaxies, which were interpreted to be likely debris from tidally disrupted satellites. The team also confirmed several enormous stellar overdensities previously reported in the literature, but never before interpreted as tidal streams. It also put into perspective the highly diverse morphological characteristics of these extended stellar features, as it can be seen in Figures 1.1 and 1.2: great circle-like features akin to the Sagittarius stream surrounding the Milky Way, disconnected ripples and shells and giant clouds of presumed tidal debris far beyond the main stellar body, as well as long and straight, coherent features emerging from galactic disks. Along with the remains of already disrupted counterparts, these observations also captured the remains of satellites caught in the middle of tidal disruption processes.

Throughout the papers published by the STSS team, qualitative comparisons with available simulations set in a ΛCDM cosmology (that model the stellar halo as the result of satellite disruption evolution) showed that the extraordinary variety of stellar

low-mass ellipticals or barred spirals, which are not Milky Way-type galaxies. Nevertheless, in practice, a more accessible way to learn more about Milky Way analogues is to select a larger sample that can be segmented afterwards according to a more appropriate criteria.

morphologies detected in the pilot survey matched that seen in those simulations. The common existence of these tidal features around disk galaxies and the morphological match to the simulations constituted new evidence that these theoretical models also apply to a large number of other Milky Way-mass disk galaxies in the local volume, and it was one of the main motivations when starting this project. Now it also provides ways of follow-up confirmation (see Section 4.1.1).

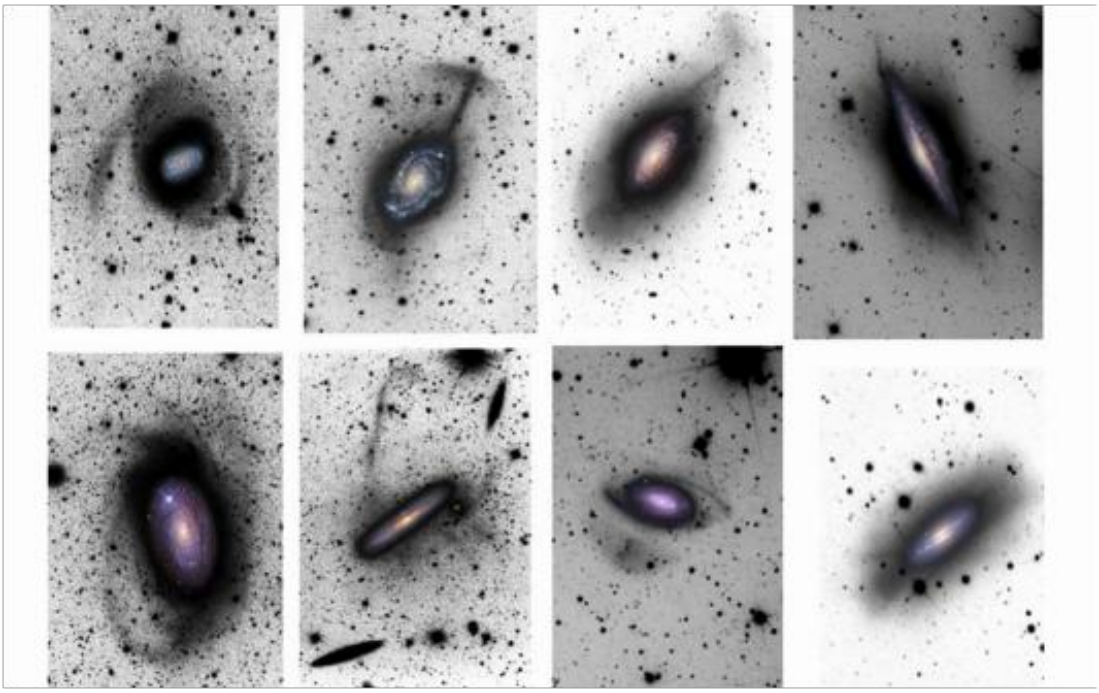

FIGURE 1.1: Super-stretched images with color insets taken from Martínez-Delgado et al. (2010), showing a wide diversity of tidal overdensities. From left to right (top row): huge plumes around NGC 1084; a tidal debris structure typically referred as "umbrellas" in NGC 4651; diffuse, more coherent mixed features around NGC 3521; an inner, spiked halo in NGC 1055. From left to right (bottom row): a gaseous stream resembling Sgr-stream in M63; satellites in the middle of disruption processes in NGC 4216; an giant, visually disconnected stellar cloud in NGC 7531; and a conspicuous spike and large wedge-shaped structure in NGC 5866.

The majority of the studies published by the STSS focused on surveying the Universe in particular case studies.

In Martínez-Delgado et al. (2008b), a large-scale halo structure of tidal origin was discovered in NGC 5907 (see Figure 1.3), clearly linked to low-mass satellite accretion. This structure confirmed that halos of spiral galaxies in the local universe may still contain a significant number of galactic fossils from their hierarchical formation. *N*-body simulations were used to show that these observed features could be explained in the context of external accretion, specifically by the tidal disruption of a dwarf galaxy-like system in a disk galaxy plus dark halo potential. This paper not only highlighted the relevance of stream progenitors when explaining galactic evolution of seemingly isolated galaxies (e.g. warped disks), but also pointed for the first time towards the need of obtaining a statistically significant census of tidal streams for the local Universe, to be compared with simulations later.

Then, Martínez-Delgado et al. (2009) reported the discovery of a giant, loop-like stellar structure around the edge-on spiral galaxy NGC 4013 (see Figure 1.3), confirmed

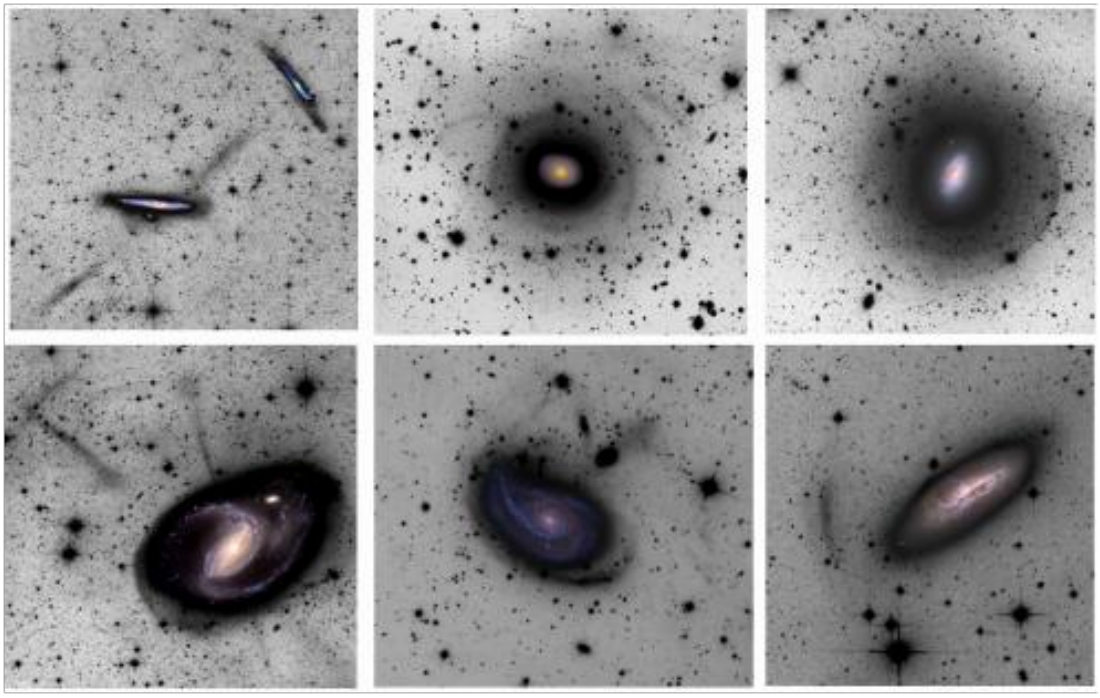

FIGURE 1.2: Super-stretched images with color insets taken from Martínez-Delgado et al. (2015a), showing a wide diversity of more complex tidal overdensities. From left to right (top row): a giant stellar tidal stream in the halo of NGC 4631; ripples and shells of debris in NGC 3682 and NGC 4414. From left to right (bottom row): an extended, multi-component stellar stream encircling NGC 1097; and two coherent, disconnected stellar features in NGC 5364 and NGC 4145.

with three different sets of data from three different telescopes. The authors used simulations to show that the sky-projected morphology of said structure was consistent with the theoretical predictions for an edge-on, projected view of a stellar tidal stream of a dwarf satellite moving in a low inclined, nearly circular orbit, with an estimated mass of 6×10^8 $M_\odot$. The estimated age of the surviving structure was consistent with a stream of ~ 2.8 Gyr old. Once again, these results showed that a seemingly isolated galaxy (with clear signs of disk warping in *HI* maps) could also be explained by recent minor merging events.

In another case study, Trujillo et al. (2009), the authors offered a panchromatic, deep multiwavelength analysis ($0.15 - 160$ μm) of the outer region of the nearby galaxy M94 (see Figure 1.3). Here the origin of M94's bright outer star-forming disk is discussed, arguing that although an external origin of the extended disk (e.g., due to the accretion of a satellite galaxy) cannot be ruled out with the data at hand, the gravitational distortion of the oval region (bar and disk) is favored, as it explains more naturally the existence of an inner ring, plus the enhanced star formation activity in the outer disk of M94.

Later, in Sollima et al. (2010), the authors offered a multi-wavelength analysis of M81's optical ring-like structure, also known as Arp's Loop (see Figure 1.3). Usually interpreted as the byproduct of a tidal interaction with M82, it is argued that the optical measurements of this structure includes scattered light from the same Galactic cirrus that is responsible for the bulk of the far-infrared emission, highlighting the relevance of Galactic contamination in low-surface-brightness structures.

Another important step leading towards the realization of this thesis was the work

done by Chonis et al. (2011), who presented deep surface photometry of a very faint, giant arc-loop feature in the halo of the nearby spiral galaxy NGC 5055 (see Figure 1.3), which proved to be consistent with tidal debris resulting from ongoing satellite accretion in the ΛCDM-based models of Bullock and Johnston (2005), Johnston et al. (2008), and Cooper et al. (2010).

In Martínez-Delgado et al. (2012), a diffuse stellar substructure apparently linked to the irregular galaxy NGC 4449 (see Figure 1.3) was mapped with a modest (0.5-m) telescope in combination with high-resolution wide-field images from the 8-m Subaru Telescope, which resolved the extended feature into a stream of red giant branch stars, confirming its physical association with NGC 4449. The properties of the stream implied a massive dwarf spheroidal progenitor, with a stellar mass ratio between the two galaxies of $\sim$ 1:50, while the indirectly measured dynamical mass ratio, when including dark matter, was estimated to be $\sim$ 1:10 $-$ 1:5. This system was then referred as a stealth merger, where an infalling satellite galaxy is nearly undetectable by conventional means, but still has a substantial dynamical influence on its host galaxy. This discovery also suggested that satellite accretion can play a significant role in building up the stellar halos of low-mass galaxies, and possibly in triggering their starbursts.

In Beaton et al. (2014), a low surface brightness stellar stream was identified in NGC 5387 using SDSS imaging, along with a blue progenitor using the Galaxy Evolution Explorer (GALEX) Deep Imaging Survey, and spectroscopy from the Large Binocular Telescope to estimate their redshifts. The favored interpretations were that the blue overdensity was a region of enhanced star formation in the outer disk of NGC 5387 (see Figure 1.3) induced by the minor accretion event, or the progenitor of the stellar stream experiencing enhanced star formation.

Foster et al. (2014) performed a complete analysis the dynamics of faint stellar substructures around NGC 4651 (see Figure 1.3), the Umbrella Galaxy, which hosts a complex system of streams and shells formed through the tidal disruption of a dwarf elliptical galaxy. Colours, luminosities and stellar masses were computed using multiband Subaru/Suprime-Cam images, while candidates for kinematic tracers (i.e. globular clusters, planetary nebulae, *HII* regions) were identified, later followed up with Keck/DEIMOS (DEep Imaging Multi-object Spectrograph) spectroscopy to obtain velocities, including the progenitor of the stream. Most importantly, this work confirmed that the kinematics of low surface brightness substructures can indeed be recovered and modelled using discrete tracers.

Also noteworthy were the efforts of Cooper et al. (2011), who presented new deep observations of "shell" structures in the halo of the nearby elliptical galaxy NGC 7600 (see Figure 1.3), together with an ab initio cosmological simulation showing how continuous accretion of clumps of dark matter and stars creates a broad region of diffuse circumgalactic structures strikingly similar to those of NGC 7600. As far as simulations of shell galaxies go, this work confirmed that tidal shells can be generated by the disruption of a satellite system in a radial orbit, but presented for the first time an episodic generation of shells, in contrast with earliest simulation attempts, which were characterized by a single instantaneous disruption event that liberates all the stars from the progenitor. Thus, the evolution of the orbit of the main shell progenitor was shown to be complex, where tidal structures are transient and interact with one another, and shell-like features are contributed by more than one progenitor.

FIGURE 1.3: Examples from the Stellar Tidal Stream Survey. From left to right: NGC 5907, NGC 4013, M94 (top row); M81, NGC 5055, NGC 4449 (middle row); NGC 5387, NGC 4651, NGC 7600 (bottom row).

1.5.2 The Dark Energy Camera Legacy Survey

This thesis also searched for images of galaxies with visible low-surface-brightness features in the optical images from the third data release (DR3) of the Dark Energy Camera Legacy Survey (DECaLS, Blum et al., 2016a), which is part of the NOAO Large Surveys programs. This survey uses the Dark Energy Camera (DECam), a wide-field CCD imager at the CTIO Blanco 4-m telescope, to obtain optical imaging covering 14000 deg^2 in three optical bands (g,r,z). Since the footprint is mostly in the equatorial and southern sky, and only a fraction of the DECaLS data have been publicly released, only a few targets have been imaged with sufficient quality and depth to aid in the interpretation of the processed SDSS images.

1.6 This Thesis: scope and outline

This work is about testing some very particular concepts of galaxy formation theory by contrasting available data and simulations systematically, specifically at low scales. The main objective is to assess the relevance and prominence of minor merging events in the local Universe via their frequency.

In particular, we take a step toward this more systematic approach by making a statistical assessment of the number of features detected in a survey of a volume-, magnitude-, and size-limited sample of nearby Milky Way-mass[3] (as opposed to Milky Way-type) host galaxies. To keep the study consistent, we select our sample on the basis of mass and recessional velocity. We apply a custom image reduction process uniformly to images of each galaxy in our sample from Data Release 10 of the SDSS (Ahn et al., 2014), and estimate the detection limit in surface brightness. We present both observational results and some advancements in the mock catalogue generation, in an effort to contribute to form the basis of further investigations into the structure and sub-structure of stellar halos and their comparisons with theoretical predictions from ΛCDM models.

There are at least three important notes to consider: first, stellar halos are believed to have formed through a series of accretion events occurring over the lifetime of their host galaxies. Debris associated with the most ancient mergers and those with intrinsically faint progenitors is likely to have extremely low surface brightness at the present day (below 30 mag arcsec^{-2}). The technique we describe here is therefore well suited to studying evidence for more recent ($t_{\rm lookback} \sim 4-5$ Gyr) interactions and mergers with more massive satellite galaxies, rather than ancient, well-mixed halo components or the contribution of fainter satellites.

Secondly, throughout the text, we use the term 'overdensity' to refer to any kind of diffuse feature in the processed image that is not obviously the outward continuation of the brighter isophotes of the host galaxy, without making claims regarding their origin or nature (including whether they are real stellar or gaseous features, or are physically associated with the host galaxy). Minor merger signatures, and more specifically, stellar tidal streams, are understood as a particular class of overdensities, arising from stars distributed around the orbit of a current or former satellite, or else a tidal distortion of the host galaxy. In cases where a host galaxy interacts with a companion of comparable mass (typically referred to as a major merger), both may be severely distorted. Our sample contains very few of these non-equilibrium systems, which we exclude from further consideration.

Finally, several previous surveys of tidal features have been published, albeit with some key differences in sample selection. Kaviraj (2010) focused on early-type galaxies (ETGs) and found that $\sim$ 18% of their sample exhibited signs of disturbed morphologies (e.g., shells). This sample was also based on SDSS multiband photometry, but combined with the significantly ($\sim$ 2 mag) deeper monochromatic images from the SDSS Stripe 82. Atkinson, Abraham, and Ferguson (2013) studied faint tidal features in galaxies with a wide range of morphologies using the wide-field component of the Canada–France–Hawaii Telescope Legacy Survey. Their sample consisted of 1781 luminous galaxies in the magnitude range $15.5 < r < 17.0$. A classification of tidal features according to their morphology (e.g., streams, shells, and tails) was performed, with no major interpretation in terms of their physical origin, especially when distinguishing between major and minor mergers. They found that about 12% of the galaxies in their sample showed clear tidal features at their highest confidence level. This fraction increased to about 18% when they included systems with weaker tidal features. The colors and stellar masses of central galaxies were found to influence these numbers significantly: linear features, shells, and fans were more likely in galaxies with stellar masses $> 10^{10.5}$ M$_\odot$, and red galaxies were found to be twice more likely to show tidal features than blue galaxies. Table 1 from Atkinson, Abraham,

[3] We will consider the mass of the Milky Way to be $\sim 10^{12}$ M$_\odot$, according to McMillan (2011) and McMillan (2017).

and Ferguson (2013) summarizes an overview of faint substructures studies from earlier work in the literature. We note that no publication attempted a less restricted but still controlled sample, especially focused on a future comparison with state-of-the-art simulations.

Chapter 2 characterizes the sample selection and image post-processing technique used. Chapter 3 presents the simulations and how they were processed. Chapter 4 describe and discuss the results of this project, including reports of the discovery of several new streams and a list of tidal feature candidates for follow-up observations, and the current role of the simulations in the general comparison to data. Chapter 5 summarizes these results while considering directions for future work. Auxiliary tables and complementary figures referenced throughout this thesis are presented in Appendices A and B.

Chapter 2

The Data

> Without data you are just another person with an opinion
>
> W. Edwards Deming

This thesis made use of the dataset publicly available from the Spitzer Survey of Stellar Structure in Galaxies (S4G, Sheth et al., 2010); and the imaging data from the Sloan Digital Sky Survey (SDSS, Gunn et al., 1998), Data Release 10 (DR10; Ahn et al., 2014). These data were processed based on the work done by Miskolczi, Bomans, and Dettmar (2011). Results described in Chapter 4 were also complemented by the last results from the Tidal Stream Survey (STSS, Martínez-Delgado et al., 2010), and by the optical images from the Dark Energy Camera Legacy Survey (DECaLS, Blum et al., 2016a). Complementary data have been extracted using the Nasa Extragalactic Database[1] (NED).

2.1 The Spitzer Survey of Stellar Structure in Galaxies

In galaxy formation theory, knowing the distribution of stellar material in a galaxy is extremely useful. Encoded within its structure is the fossil record of the assembly history and evolutionary processes through cosmic time. Thus, obtaining an statistically significant census of the stars in galaxies in the local volume[2] is critical for testing models, and has served as the main motivation behind many traditional and recent surveys, e.g. the Third Reference Catalog of Bright Galaxies (RC3, de Vaucouleurs et al., 1991), The SIRTF[3] Nearby Galaxies Survey (SINGS, Kennicutt et al., 2003), or the ACS Nearby Galaxy Survey Treasury Program (ANGST, Dalcanton et al., 2009). All of these projects are within the scope of The Spitzer Space Telescope, the final mission in NASA's Great Observatories Program - a family of four space-based observatories, each observing the Universe in a different kind of light. The other missions in the

[1] The NASA/IPAC Extragalactic Database is operated by the Jet Propulsion Laboratory, California Institute of Technology, under contract with the National Aeronautics and Space Administration.

[2] The definition of " local volume" or "nearby universe" varies within different research groups, but we will adopt the definition as the region of space characterized by the distance over which stellar populations in galaxies can be resolved by modern instruments. Currently, this normally includes a distance of roughly $10 - 15$ Mpc.

[3] NASA's Space Infrared Telescope Facility (SIRTF) was the former name of the Spitzer Space Telescope.

program include the visible-light Hubble Space Telescope, Compton Gamma-Ray Observatory, and the Chandra X-Ray Observatory.

RC3 featured data for more than 23000 galaxies, including all galaxies with apparent diameters larger than one arc minute (at the D_{25} isophotal level), magnitudes brighter than about magnitude 15.5, and recessional velocities not larger than 15000 km/s. It was the first attempt to build a robust enough and roughly complete sample of extragalactic data upon many subsequent studies were based upon, containing isophotal diameters and axis ratios, total magnitudes and colors in the UBV system, continuum and 21-cm radio magnitudes, HI index, and redshifts.

RC3 proved to be relevant as the first attempt at dating ancient merger events (Schweizer and Seitzer, 1992), where it was shown that E+S0 galaxies fine-structure content follow a positive correlation with bluer colors. This correspondence also included stellar populations of these E+SO galaxies. Also, the deviations in color and line strength, correlated with fine-structure content, was interpreted as a variation in the mean age of the stellar populations. This allowed age estimations, showing a spread over a range of at least 5 Gyr and up to $\sim$ 10 Gyr. Thus, the UBV colors of E+S0 galaxies are compatible with the hypothesis that these galaxies formed through mergers with significant delays. The correlations between colors, line strengths, and fine structure reported in this work yielded the first quantitative support for the view that there may be a connection between the mean age of stellar populations and dynamical youth in E and S0 galaxies.

SINGS, by the other hand, was an exhaustive imaging and spectroscopic survey at infrared, visible, and ultraviolet wavelengths of 75 nearby galaxies. Its primary goal was to describe the infrared emission of galaxies and their principal infrared-emitting components, across a wide range of galaxy properties and star formation environments. SINGS also aimed to provide insights into the physical processes connecting star formation with the interstellar medium properties of galaxies, providing a vital foundation for understanding infrared observations of the distant universe and ultraluminous and active galaxies.

Additionally, ANGST was a systematic survey that aimed to establish a legacy of uniform multi-color photometry of resolved stars for a volume-limited sample of nearby galaxies, up to 4 Mpc, encompassing 69 galaxies in diverse environments. The galaxies include a nearly complete range of morphological types spanning a factor of $\sim$ 100 in luminosity and star formation rate. The survey data consist of images taken with the Advanced Camera for Surveys (ACS) on the Hubble Space Telescope (HST), supplemented with archival data and Wide Field Planetary Camera 2 (WFPC2) data.

One last relevant data survey to consider when understanding the relevance of S4G is the Local Volume Legacy Survey (LVL; Kennicutt et al., 2008; Lee et al., 2009; Lee et al., 2011; Dale et al., 2009). It includes complete sample of 258 galaxies within 11 Mpc. The broad goal of the LVL was to provide critical insight into two of the primary processes that shape the growth of galaxies: star formation and its interaction with the interstellar medium. This can be achieved by investigating the spatially-resolved star formation, dust, and red stellar populations of galaxies that have been drawn from a statistically robust local sample, in which a full diversity of galaxy properties (e.g., luminosities, surface brightnesses, metallicities) are represented. The LVL sample included some information on the stellar mass, constrained by 3.6 to 4.5 microns luminosities, which are generally dominated by the light from old stellar populations, which in turn tend to dominate the distribution of satellites around galaxies (Johnston, Sackett, and Bullock, 2001).

While these surveys were designed specifically for particular scientific goals, none of them provided an accurate inventory of the stellar mass and the stellar structures in nearby galaxies. The main reason is that infrared surveys, where light from the old stellar population is better measured due to reduced dust extinction and contamination from star formation, are extremely difficult to conduct from the ground. The largest ground-based infrared surveys like 2MASS (Skrutskie et al., 2006), DENIS (Epchtein et al., 1994, only point sources), or Paturel et al. (2003) are rather shallow in depth (reaching $\sim$ 16 mag at 10-σ), restricting studies of nearby galaxies to high surface brightness inner disks. In contrast, deeper infrared surveys like OSUBGS (Eskridge et al., 2002) or NIRSOS (Laurikainen et al., 2010), have imaged only a few hundred galaxies.

In this context, the S4G –built upon SINGS and LVL– was specifically designed to provide over an order of magnitude improvement in the sample size and several magnitudes deeper data than existing surveys at that time. The S4G is a volume-, magnitude-, and size-limited ($d < 40$ Mpc, $|b| > 30°$, $m_{\mathrm{B_{corr}}} < 15.5$, and $D_{25} > 1'$) survey of 2352 galaxies using the Infrared Array Camera (IRAC, Fazio et al., 2004) on the Spitzer Space Telescope (Werner et al., 2004), at 3.6 and 4.5 μm. The azimuthally averaged surface brightness profiles obtained by the S4G are typically robust to isophotes at $\mu_{3.6\ \mu m}(AB) \sim 27$ mag arcsec^{-2}, equivalent to a stellar mass surface density of around 1 M$_\odot$ pc^{-2} (Muñoz-Mateos et al., 2015). The S4G thus provides an appropriate data set for the study of the distribution of stellar mass and structure in the local Universe, and it is complete for galaxies within the volume relevant to our work and for masses greater than $10^{9.2}$ M$_\odot$, allowing us to select a statistically representative sample of galaxies whose stellar masses have been measured in a uniform manner.

Figure 2.1 shows the distribution in stellar mass M in $M_\odot$ and Hubble morphological type t_H of all the galaxies in S4G, as a reference. The left panel shows the distribution of Hubble morphological type in black, compared to the previously available data in blue and green. The right panel does the same for the mass distribution of the galaxies. From elliptical ($t_H \sim -4$) to irregular galaxies ($t_H \sim 8-10$), the distribution peaks within the range $t_H \approx 4-6$ (corresponding to intermediate and barred spirals), and at $\log(M/M_\odot) \approx 9$. The objects of interest to this work tend to live above these ranges, which explains why S4G was chosen as a starting point.

A major area of study for S4G is a quantitative analysis of stellar structures in the faint outer regions of galaxies where the stellar surface density it traces is extremely low and comparable or lower than the atomic gas reservoir. Already, deep optical studies have shown that, in a majority of spiral galaxies, the outer disks exhibit a secondary, exponential component (e.g., Pohlen and Trujillo, 2006; Erwin, Pohlen, and Beckman, 2008). GALEX (Martin et al., 2005) has found extended UV (XUV) disks even farther out, where it was previously assumed only HI gas existed (e.g., Gil de Paz et al., 2005; Thilker et al., 2005; Thilker et al., 2007; Muñoz-Mateos et al., 2007; Zaritsky and Christlein, 2007). The S4G catalog is then providing us with strong quantitative constraints for galaxy evolutionary models. In elliptical galaxies, deep optical observations have revealed the presence of faint tidal tail and shell like structures (e.g., Bennert et al., 2008; Canalizo et al., 2007), already quantifying the frequency and mass of shells and other debris features in the outskirts of ellipticals and lenticulars.

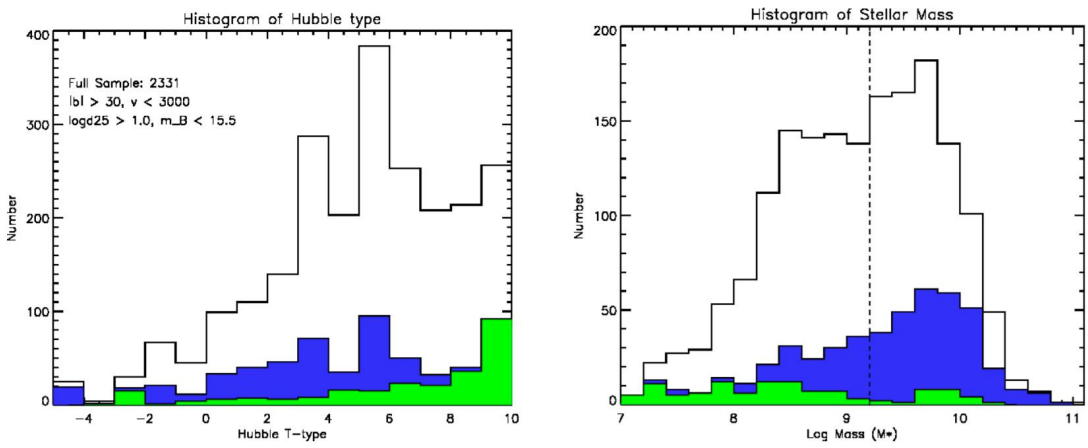

FIGURE 2.1: Left: Histogram of all galaxies in S4G as a function of the Hubble t-type shown in black. The green and blue filled histograms show archival data from the LVL (green) and other GO/GTO data (blue). Right: Histogram of masses for the S4G sample galaxies shown in black, where masses are calculated from the 2MASS photometry assuming the M/L function from Bell et al. (2003). The biggest gains in building a statistically complete sample are for galaxies with $\log(M/M_{\odot}) < 9.2$, marked with a dashed vertical line. Figure taken from Sheth et al. (2010).

u	g	r	i	z
3551 Å	4686 Å	6166 Å	7480 Å	8932 Å

TABLE 2.1: Central wavelengths of the five SDSS imaging filters.

2.2 The Sloan Digital Sky Survey

The SDSS is a major multi-wavelength imaging and spectroscopic survey using a dedicated 2.5-m wide-angle optical telescope at Apache Point Observatory in the United States. The SDSS delivers data in cycles called *Data Releases* (DR) within stages called *phases* (in roman numbers), focusing on different surveys each time. Its current status is therefore referred as the 14$^{\text{th.}}$ Data Release during Phase IV, or SDSS-IV DR14 for short. The final imaging data release covers over 35% of the sky (14555 deg^2), with photometric observations of around 500 million objects and spectra for more than 3 million objects.

SDSS-I imaged 8000 deg^2 of the sky in five broad, optical bandpasses. These filters are called the *ugriz* bands, one letter denoting a single filter; all five spanning the optical part of the electromagnetic spectrum. See Fig. 2.2 and Tables 2.1 and 2.2 for relevant parameters later used in this work.

SDSS-II extended the observations to explore the structure and stellar makeup of the

CCD read noise	< 5 e $-$ /pixel (overall system is sky limited)
Pixel size and scale	24 μm; 0.396 arcsec/pixel
Integration time	54 s
Operating mode	drift scan

TABLE 2.2: SDSS imaging camera parameters relevant for this thesis.

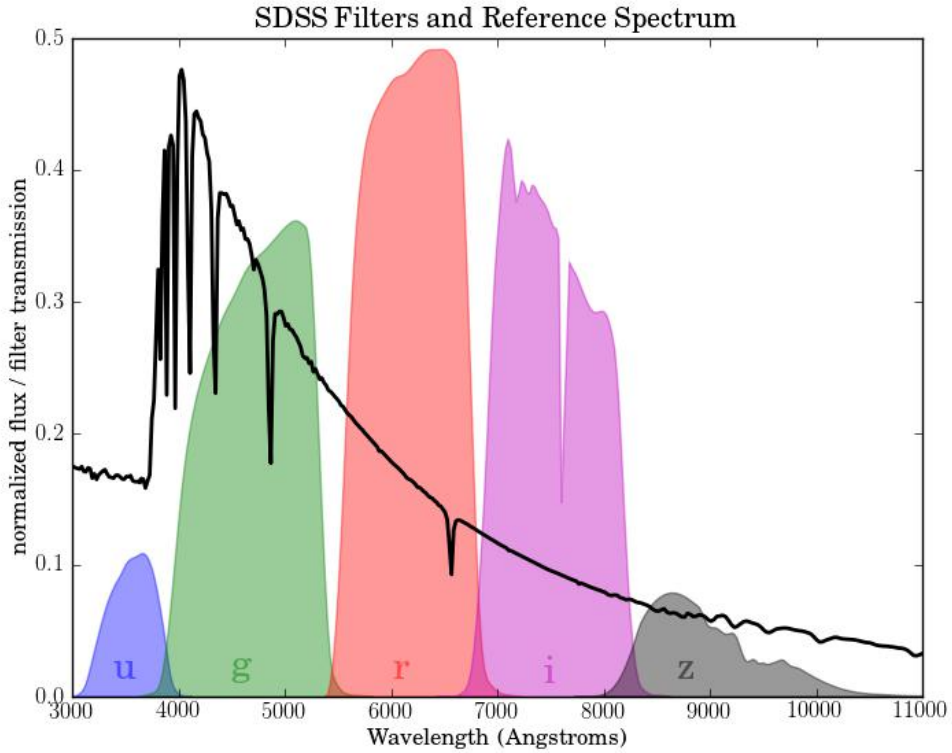

FIGURE 2.2: Transmission curves for the SDSS imaging filters along with the Vega spectrum, as a reference (Doi et al., 2010).

Milky Way, in two separate surveys. The Sloan Extension for Galactic Understanding and Exploration (SEGUE), obtained spectra of 240000 stars, in order to provide evidence for the age, composition and phase space distribution of stars within the various Galactic components. On the other hand, the Sloan Supernova Survey watched for supernova Ia events to measure the distances to far objects.

SDSS-III comprised four independent surveys. The APO Galactic Evolution Experiment, or APOGEE, collected data using high-resolution, high signal-to-noise infrared spectroscopy to penetrate the dust that obscures the inner Galaxy. The Baryon Oscillation Spectroscopic Survey, or BOSS, was designed to measure the expansion rate of the Universe by mapping the spatial distribution of luminous red galaxies and quasars, to detect the characteristic scale imprinted by baryon acoustic oscillations in the early universe. The Multi-object APO Radial Velocity Exoplanet Large-area Survey, or MARVELS, monitored the radial velocities of around 11000 stars, with the precision needed to detect gas giants planets with particular orbital periods. The Sloan Extension for Galactic Understanding and Exploration (extension), or SEGUE-2, obtained spectra of nearly 120000 stars, adding to the 240000 already present in SEGUE. SEGUE-2 focused on the in situ stellar component of the Galactic halo, from distances of 10 to 60 kpc.

Finally, SDSS-IV is currently extending precision cosmological measurements to a critical early phase of cosmic history (eBOSS), expanding its infrared spectroscopic survey of the Galaxy in the northern and southern hemispheres (APOGEE-2), and for the first time using the Sloan spectrographs to make spatially resolved maps of individual galaxies (MaNGA).

This project made use of the imaging dataset exclusively; see Fig. 2.3 for a map of the

SDSS DR10 imaging coverage. The SDSS imaging camera scanned the sky in strips along great circles. Each strip consists of six parallel scanlines, 13 arcmin wide, with gaps of about the same width. Thus two strips together make a single stripe 2.5 degrees wide. Each scanline includes data in all five filters, *ugriz*, which not only can be used to measure color in detected objects, but also are crucial in the method used here to enhance the signal-to-noise ratio of diffuse structures.

SDSS images are comprised by fields into which the scanlines are divided (with some overlap). Each field has a size of 10 by 13 arcminutes, corresponding to 2048 by 1489 pixels. Each field can be uniquely identified by a sequence of three numbers: the `run` number, which identifies the specific scan; the camera column, or `camcol`, a number from 1 to 6 identifying the scanline within the run; and the field number. These numbers will be relevant to understand the mosaic composition algorithm later in Section 2.3, because the run-camcol-field identifier can be useful to download the FITS files for each SDSS filter. Entering that identifier into the Science Archive Server Imaging Fields search will create links to download the individual filter images as FITS files. Finally, there have been multiple reprocessings of the imaging data over the years, with each reprocessing being denoted by an integer. Each rerun consists only in a change to the photometric pipeline, not to the underlying data.

Using the SDSS imaging catalogs requires understanding two important processes: deblending and resolving. Any problem related to these two processes may contribute negatively to the process of identifying diffuse overdensities around the halo, specially if performing photometry in crowded fields. This is why only 'primary' images will be used later in Section 2.3. A survey primary is the main photometric observation of an object, which is the best observation according to some quality measurements. Because many of the survey runs overlap, an object may be observed multiple times, but only one observation is chosen as the primary observation of the object during the resolving process (all the rest are tagged as 'secondary'). These observations are associated to a 'primary' field and a 'primary' run, which can be specified as a contraint when querying the database.

First, the imaging pipeline detects objects in the images by tagging neighboring regions of pixels with a signal exceeding the sky background. These contiguous regions often actually contain multiple astronomical sources, and are thus known as parent objects. Each parent has its properties measured and is tracked into the final catalog, but it is not usually recommended for the user to use them, and they are never considered 'primary' detections. A process called deblending breaks each parent up into individual, distinct astronomical sources, known as the 'child' objects. For the purposes of this work, only children data were used.

Second, there is some overlap between fields within each run, as well as between different runs. Because of these overlaps, any source on the sky can in principle be deblended as a child detection in several different runs. The imaging pipeline's `resolve` procedure determines the "best" observation of every object, which it identifies as the primary object. The resolve algorithm chooses which observation to define as the primary object. Again, only 'primary' fields were used in this work.

Finally, at some point in the data processing, a calibration of the photometry will be needed. Many objects in the SDSS, for various reasons, have defective photometry. The SDSS provides flags to overcome this issue if needed but they were not used, since the calibration process already provides a way to select the best data suited for the specific kind of calibration used in this work. This means that imaging quality

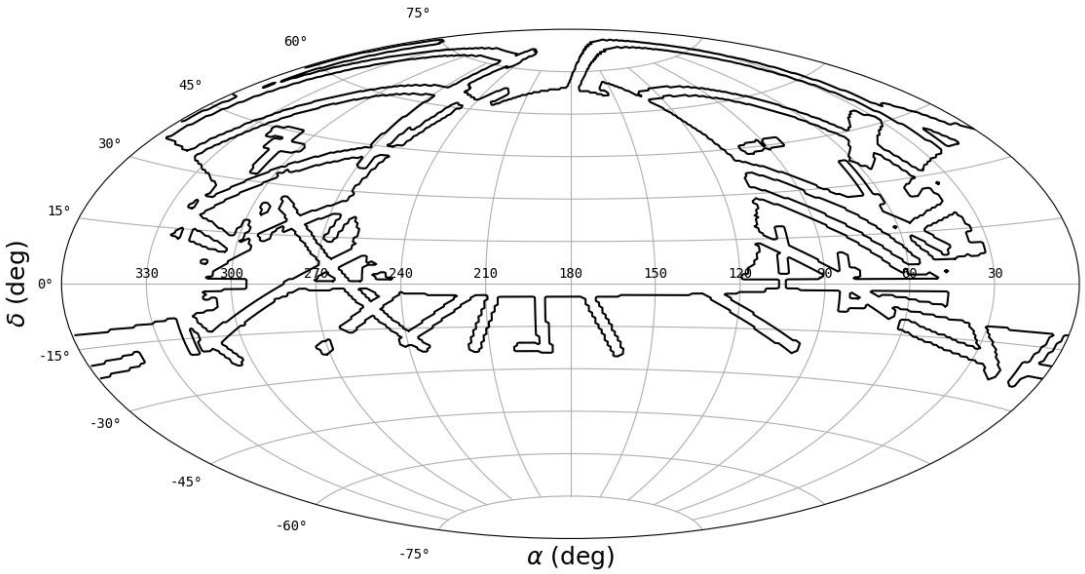

FIGURE 2.3: Full Aitoff projection map for the DR10 imaging coverage. The extent of the SDSS coverage limits the amount of galaxies available. Even if not so deep, it is currently the only public imaging survey available featuring the data needed for this work.

flags associated with saturated pixels, objects too close to the edge of a field, or objects that are possible misclassified cosmic rays will not be considered either way.

2.3 SDSS Data handling and imaging processing

We used SDSS imaging of the target galaxies selected from S4G in order to search for faint features in their surroundings. The SDSS imaging camera worked in drift-scan mode, opening its shutter for extended periods and imaging a continuous strip of the sky (Gunn et al., 1998). This means that, while not very deep, the SDSS imaging survey was able to deliver data with consistently low systematic variations from field to field and excellent flat-fielding. These conditions are critical when searching for extended, diffuse-light features close to the detection limit. The SDSS imaging data also lie in the optical range and have better angular resolution than those of S4G, which is why the latter was used to select the sample, but not for the discovery of stellar substructures. See Laine et al. (2014) for a comprehensive study of surface brightness profiles of disc galaxies in the S4G images.

Our work focuses on the frequency of tidal features around galaxies at and above the stellar mass of the Milky Way, because contemporary cosmological volume simulations can readily resolve these galaxies and their brighter satellites, which give rise to the most conspicuous features. We therefore selected elliptical, spiral, and S0 galaxies (according to the morphological type code T) in the S4G catalog, with a lower stellar mass limit of 10^{10} $M_{\odot}$.

Constraining the sample in stellar mass limits bias when comparing with simulations, because samples can be selected using equivalent criteria in both. We excluded any galaxies in the region of the Virgo cluster from our parent sample, as defined by the Next Generation Virgo Cluster Survey (NGVS) footprint (Muñoz et al., 2014), in both projected position and line-of-sight distance ($15 < d_{\mathrm{L.O.S.}}\ (\mathrm{Mpc}) < 18$). The study of diffuse circumgalactic structure in dense environments such as Virgo is complicated

by additional tidal forces of the cluster potential acting on the host and its satellites. Virgo is a 'rare' system in the context of the volume we study here, and excluding it allowed us to better represent the statistics of lower-mass groups and isolated galaxies. Clusters of mass comparable to Virgo ($\sim 10^{14}$ $M_\odot$) can easily be identified in simulations, so this does not compromise a straightforward model-data comparison. Moreover, 17 known major mergers were removed from the final sample[4]. We note that S4G already excludes targets at low Galactic latitudes ($|b| < 30°$), which is appropriate for our purposes because the detection of features with low surface brightness is severely limited by the presence of extended Galactic cirrus, high extinction, and stellar crowding. Finally, since we used SDSS imaging, we also excluded S4G galaxies outside the SDSS footprint.

In this thesis we present the results for a local volume sub-sample (galaxies selected with a recession velocity lower than 2000 km/s), comprising a total of 297 galaxies. Figure 2.4 shows the distribution of the parent sample across the sky in celestial coordinates. As shown later, the distance distribution peaks around 20 Mpc, roughly at the boundary of the local volume (Karachentsev and Kashibadze, 2006). The stellar mass distribution of the sample is limited to the mass range $10^{10-11}M_\odot$, which follows directly from our selection function. Both mass and distance measurements were taken directly from the S4G catalog. Later figures (Chapter 4) show the sample distribution morphologically and in inclination angle as well.

For each of the 297 target galaxies selected from S4G, we downloaded and processed the available SDSS DR10 imaging archive data. We followed the procedure described by Miskolczi, Bomans, and Dettmar (2011). This consists of four steps: (1) mosaicing of the SDSS images in each bandpass; (2) stacking (adding) images in multiple bands to improve the signal-to-noise ratio (S/N), with no weighting applied; (3) two-stage source extraction, including removal of point sources; and (4) Gaussian filtering to enhance features on the scale of interest.

Square mosaics of 30 arcmin (4595 pixels) per side were created in three filters, g, r, and i, using the automatic script in the SDSS Science Archive Server that can be found online[5] (at 20 Mpc, 30 arcmin corresponds to approximately 176 kpc). We used these three filters because they have the highest reported sensitivity, and because their combined transmission curve closely resembles the luminance filters used by other observational works, such as Martínez-Delgado et al. (2010). The mosaics of each filter were then stacked using the IRAF task `imcombine` with the default parameters, in order to improve the S/N of the image. We call this stacked image $I_{\rm gri}$.

Our analysis relies heavily on visual inspection of extended, diffuse features in moderately crowded stellar fields. We therefore processed the stacked images with SExtractor (Bertin and Arnouts, 1996) using a two-stage procedure (known as "hot and cold run", Caldwell et al. 2008) in order to remove the majority of unsaturated point sources while preserving regions of diffuse emission. In Step 1, we extracted all sources covering an area of at least 5 pixels at a signficance of 1.5σ and saved a FITS file, I_5, containing these detections (including the central galaxy, which covers a significant fraction of the image). In the second run, the minimum source area was set to 800 pixels (≈ 30 kpc^2 at 20 Mpc), so that only the central galaxy and any other large objects were detected. We call the corresponding FITS file I_{800}. A final image was then created by subtracting I_{800} from I_5, that is, the large-scale source(s) from the total detections.

[4] Targets removed as major mergers: NGC 2798, NGC 3166, NGC 3169, NGC 3190, NGC 3227, NGC 3998, NGC 5953, NGC 5954, NGC 4550, NGC 5774, NGC 5775, NGC 3395, NGC 5194, NGC 5195, NGC 4302, NGC 5566, and NGC 5574.

[5] dr10.sdss.org/mosaics

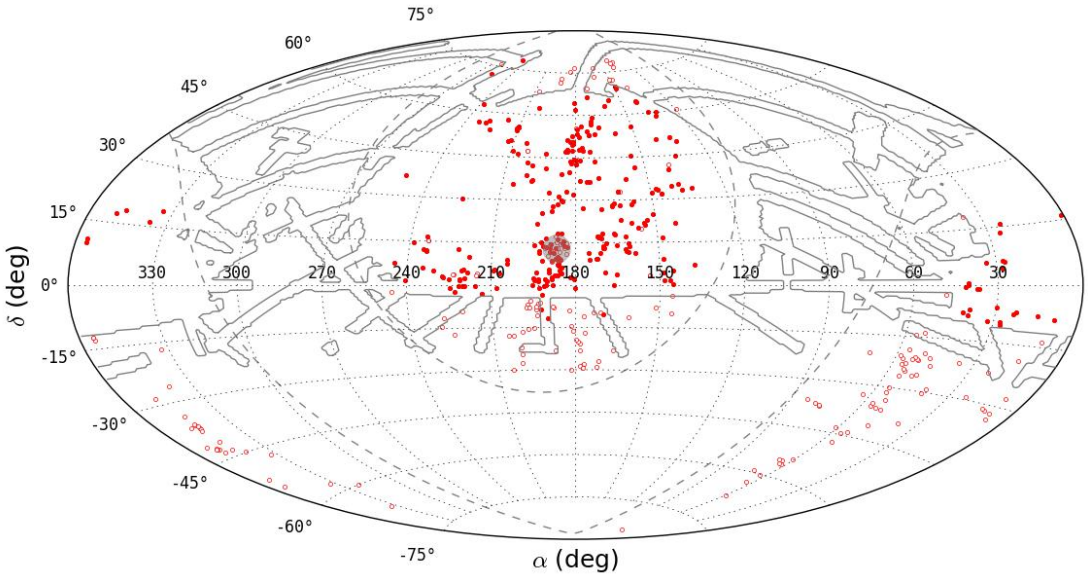

FIGURE 2.4: Aitoff projection of the full S4G catalog (empty and filled red circles). The filled red circles mark our selected parent galaxy sample. The dashed lines enclose the Galactic plane area, the solid gray line encompasses the SDSS DR10 footprint, and the solid gray region encompasses the Virgo Cluster area as defined by the NGVS.

The image resulting from this operation contains only compact sources (mainly stars). We call this image file $I_s = I_5 - I_{800}$. Using the IRAF task `imarith`, the sources previously extracted were subtracted from the original stacked image, that is, $I_* = I_{\rm gri} - I_s$. Thus, I_* is a stacked image with most of the stars in the field masked out, replaced by the average flux of the neighboring pixels.

To enhance the visibility of faint, extended features, we then applied a circularly symmetric Gaussian filter to I_*. MBD11 reported that other possible filter types are available in IRAF, including `adaptive` and `hfilter`, which are both based on the Haar-Transform (Fritze et al., 1977). By testing these filters with different settings, they reported that while both are able to enhance faint features, neither is clearly an improvement over Gaussian filtering. A Gaussian filter is then preferred because it is computationally more efficient than other filters. By experimenting with the parameters of the Gaussian filter, they also reported that the best enhancement of faint extended features is achieved with a kernel scale of $\sigma = 7$. We have carried out our own tests and reached similar conclusions, finding that the best compromise between enhancing diffuse structures and preserving image resolution can be found at a σ of 5 to 7 pixels, which at a distance of 20 Mpc corresponds to roughly 2 to 3 kpc. This works because the diffuse features of interest in this study have scales of a few kiloparsecs, therefore removing fluctuations on smaller scales makes them easier to detect by visual inspection. Convolutions with broader kernels take longer to compute without achieving higher detectability. Figure (2.5) shows an example of the use of this enhancement technique to reveal the giant shell around NGC 4414. Whenever possible, we have added color insets of the central galaxies to the stretched images in order to visualize the relative extent of each galaxy and its low surface brightness halo.

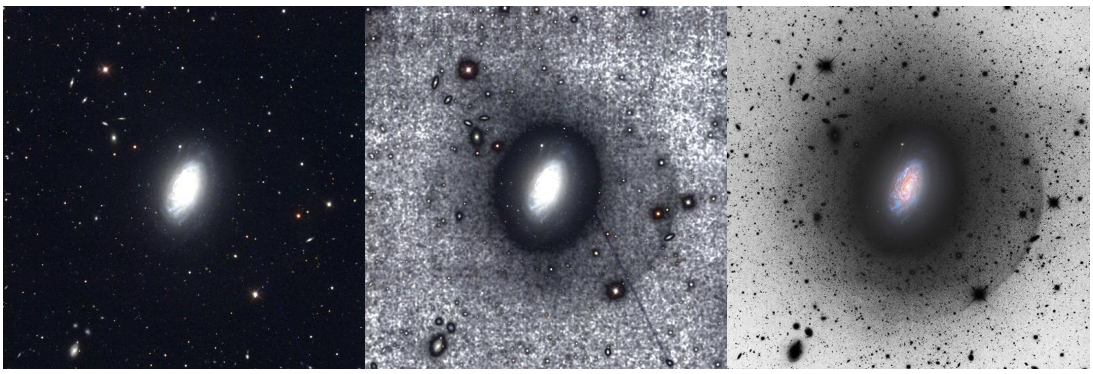

FIGURE 2.5: Example of the enhancement technique described in 2.3 for NGC 4414. The field of view for each panel is $\sim 30 \times 30$ arcminutes (north is up, east to the left). *Left panel*: Original SDSS color-composite image from the public archive. *Middle panel*: Final result of our image processing with an inverted, stretched grayscale showing the extent of a conspicuous shell of debris southwest of the central galaxy. For illustrative purposes, we have added a color inset of the disk of the galaxy and any stars or other objects that are masked in our analysis. *Right panel*: Same field taken from the STSS (Martinez-Delgado et al. in preparation), showing the same overall morphology of this substructure. Credit right panel image: Adam Block.

2.4 Photometric calibration

An important issue for this work is to quantify the depth to which SDSS data allow us to explore faint stellar halo structures. In addition, the mean surface brightness limits of our images must have a narrow distribution to avoid image-to-image variance biasing any statistics we derive from visual inspection. Since the SDSS data were taken over a period of several years, we have to verify that the surface brightness limits of the images of different galaxies do not reflect variations in the quality of flat-fielding and the sky conditions during the observations, such as transparency and lunar phase (we note that SDSS generally observed in dark sky conditions; e.g., Eisenstein et al. 2011; York and SDSS Collaboration 2000; Gunn et al. 2006). Scattered light due to bright stars in the vicinity of a galaxy will also contribute to fluctuations in depth. Large differences in seeing, depth, and the variance of depth across the image can lead to an important bias in the statistics of faint overdensities in our galaxy sample, since in some cases, non-detections of streams could be due to observational effects.

To quantify this, we measured the surface brightness limit of each image in our sample as follows. First, we performed a photometric calibration to the SDSS r band for the coadded images, using the same approach as our previous studies of stellar tidal streams (Chonis et al., 2011) and dwarf satellite galaxy populations (Javanmardi et al., 2016). We chose the SDSS r band to be consistent with other optical studies. All 297 processed images were calibrated using the semi-automatic pipeline developed (and successfully demonstrated) by the DGSAT[6] project (Javanmardi et al., 2016).

Given the similarity between the effective bandpass of the stacked SDSS images and the wide-band luminance filter (used in the DGSAT), the calibration of our stacked images to the r band requires a color correction, taking the form

$$r_{\rm cal} = c_0 \ell_{\rm stacked} + c_1(g-r) + c_2, \tag{2.1}$$

[6]Dwarf Galaxy Survey with Amateur Telescopes

where $r_{\rm cal}$ is the calibrated r magnitude, $\ell_{\rm stacked}$ is the magnitude measured in the 'pseudo-luminance' band of the stacked image, c_0 fixes the linear relation between these two magnitudes, c_1 corrects for a color dependence, and c_2 is the magnitude zero-point correction. The constants c_i are obtained using a set of calibrating stars in each image. These stars are selected using an automated statistical approach (rather than by hand), using the SDSS g and r band as standard magnitudes.

First, SExtractor (Bertin and Arnouts, 1996) was used to detect all the objects in each image. The detected objects were then cross-matched with the most recent SDSS photometric catalog, and only stars with $r \geq 15$, $0.08 < (r-i) < 0.5$ and $0.2 < (g-r) < 1.4$ passed on to the next step (see Chonis and Gaskell, 2008). At this point, very many stars are available for calibration of each image. The SDSS r-band magnitudes of the stars were compared iteratively to $r_{\rm cal}$ calculated from each image and the c_i for each stacked image obtained by a χ^2 minimization.

Next, any star with $\Delta r \equiv r_{SDSS} - r_{cal}$ deviating by more than twice the standard deviation σ from the best-fit relation was discarded and the calibration relation was fit again to obtain new c_i. This clipping was repeated until no 2σ outlier remained, which gave us the final c_i for each image. The standard deviation of Δr provides an estimate of the uncertainty in the calibration and is added in quadrature when we report the uncertainty in magnitudes for each image. See Javanmardi et al. (2016) for further details of this approach to photometric calibration.

2.5 Surface brightness limit

After calibrating the data set to the SDSS r band, the limiting surface brightnesses of our images were determined following the approach described in Martínez-Delgado et al. (2010). In short, to estimate the (residual) sky background, we measured the standard deviation in random sky apertures of 3 arcseconds in diameter and computed the surface brightness corresponding to five times the standard deviation. Figure 2.8 displays the distribution of the surface brightness limit of all images in our sample due to the mean sky background, showing that the data used in this work are sufficiently homogeneous in terms of quality and depth. We conclude that the mean sky surface brightness limit of our sample in the r band is $\mathrm{SB}_{r,lim} \approx 28.1 \pm 0.3$ mag/arcsec^2. This means that for the purposes of the following analysis, we can neglect variations in depth as a significant source of bias in the statistics of low surface brightness features recovered by our visual inspection.

Since we rely on visual detection of stacked imaging, another useful information regarding the surface brightness limit of the sample, is to compute how bright do artificial features have to be in terms of their surface brightness in order to be detectable by eye.

We explored two methods to simulate and measure artificial tidal features in our processed images.

2.5.1 Artificial tidal overdensities

One way to recreate an isolated tidal feature involves using GALFIT to generate multiple realizations of a variety of shapes. GALFIT (Peng et al., 2002; Peng et al., 2010) is a well-known data analysis algorithm that fits 2-D analytic functions to galaxies and

```
0)    sersic                 # Component type
1)    150.0000 50.0000 1 1   # Position x, y
3)    7.0000 1               # Integrated magnitude
4)    15.0000 1              # R_e (effective radius) [pix]
5)    2.0000 1               # Sersic index n (de Vaucouleurs n=4)
9)    0.5000 1               # Axis ratio (b/a)
10)   0.0000 1               # Position angle (PA) [deg:  Up=0, Left=90]
R0)   power                  # PA rotation func.  (power, log, none)
R1)   0.0000 1               # Spiral inner radius [pixels]
R2)   15.0000 1              # Spiral outer radius [pixels]
R3)   180.0000 1             # Cumul.  rot.  out to outer radius [degrees]
R4)   0.3000 1               # Asymptotic spiral powerlaw
R9)   10.0000 1              # Inclination to L.o.S. [degrees]
R10)  45.0000 1              # Sky position angle
F1)   0.3000 45.0000 1 1     # Az.  F. mode 1, ampl., & phase angle
F5)   0.1000 90.0000 1 1     # Az.  F. mode 5, ampl., & phase angle
```

FIGURE 2.6: Base input file for the chosen GALFIT tidal feature model. A Sérsic light profile with Fourier modes $m = 1$ and $m = 5$ is modified by a coordinate rotation function to create a lopsided, multi-armed, spiral structure, resembling a tidal feature.

point sources directly to digital images. By allowing for a wide variety of morphological configurations (e.g. irregular, curved, logarithmic and power-law spirals, ring, and truncated shapes) in otherwise traditional parametric functions like the Sersic, Moffat, King, Ferrer, etc., profiles, one can use GALFIT to an arbitrary number of model components of numerous profile types, so as to produce realistic-looking galaxy model images. In this work, we did not directly used the fitting capabilities mainly due to time contraints, but instead focused on the generation of a mixed-type typical tidal feature on a blank background, spanning a range of surface brightness values. Figure 2.6 summarizes the parameters used and the model generated, which was chosen given its close resemblance with a typical tidal feature, including both size and profile shape.

A second, more straightforward way to generate a fake tidal feature we explored requires the use of IRAF[7] astronomical routines in conjuction with the visualization software DS9[8]. More specifically, the stream can be created as one or more joint DS9 regions resembling a stream of a particular shape. This was done manually by merging two elongated elliptical regions, whose coordinates then enter as an input into the IRAF task `mskregions`, to generate a mask. This mask can then be scaled to any desired surface brightness level and converted into an image file using the IRAF routine `imexpr`. This task evaluates an image expression, in our case of the form $-2.5\log(f) + 2.5\log(A)$ (with f and A being the input flux and area respectively), and writes the result to the output image.

We then coadded these two family of patterns depicted in Figure 2.7 independently to our own processed images in a random place outside of the central galaxy. Thus, for each galaxy image file in our sample:

(a) the whole shape was resized to a scale of 20% of the image size (roughly a few kpc per image), to simulate a tidal feature of an appropriate size;

[7] iraf.noao.edu
[8] http://ds9.si.edu/site/Home.html

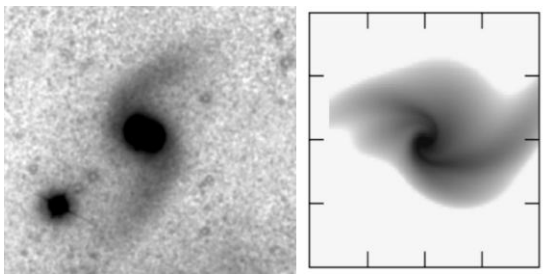

FIGURE 2.7: Base model for the generation of artificial tidal features. *(left)* An arbitrary amount of DS9 regions can be manually added or masked with the help of IRAF tasks to construct a structure similar to an unresolved stream, in this case over a real SDSS stacked image (the central galaxy is not part of the simulated features). *(right)* GALFIT pure model using the input file shown in Figure 2.6.

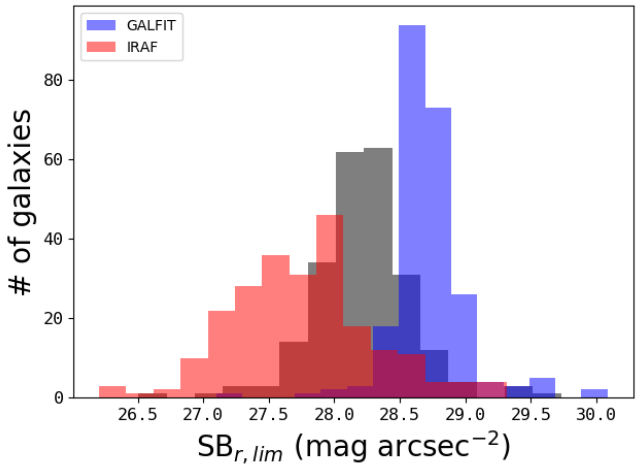

FIGURE 2.8: In grey color: distribution of the surface brightness limit in our sample with a Gaussian fit, using the 232 images in the sample with $N_{\rm star} > 50$ stars after the σ clipping as described in Section 2.4. We obtained an average value of 28.11, with a standard deviation of 0.26. The red histogram shows the surface brightness threshold distribution of detected fake features using IRAF, while the blue histogram corresponds to said limit for a simulated feature generated using GALFIT.

(b) once a position is randomly selected outside of the central galaxy region, the mock tidal feature is coadded to the processed images. We repeated this process 30 times for different peak surface brightnesses; from 27.0 to 30.0 maga $<$ rcsec^{-2} with a step of 0.1 magarcsec^{-2}. Taking into account the gray histogram shown in Figure 2.8, this means we are exploring how much the visual inspection differs in practice from the *nominal* surface brightness limit of the sample.

From Figure 2.8, we can see how the choice of the mock tidal feature affects visual inspection. As expected, detection by eye tends to be more efficient with a more coherent and distinct GALFIT overdensity, when compared to the more spread but regular tidal structure based on ellipsoids created with IRAF. From here on, we will adopt the Gaussian fit to the surface brightness distribution computed in Section 2.4 as its formal value for this thesis, noting that there is room for it to change within a reasonable amount depending on its definition and estimation methodology.

Chapter 3

Simulations

> The most that can be expected from any model is that it can supply a useful approximation to reality: All models are wrong; some models are useful.
>
> George Box

The main idea of this project is to make a strong comparison of data and simulations, focusing on galactic substructures in the tidal field and haloes around nearby galaxies. This implies to have a clear understanding on the limitations of a comparability between the available observable evidence, and the models used to simulate the observations. Since stellar mass plays a major role in galaxy formation theory –in particular by influencing the frequency of observable tidal streams– the stellar mass of galaxies hosting observable satellites plays a key role in the data selection. Thus, for any comparison to make sense, constraining the data by stellar mass to a range where models are currently able to reproduce useful results dominates the main reasoning behind this work, meaning that an statistically strong survey of galaxies for which stellar masses are available is needed as a basis. Such survey was covered in Chapter 2, while here the modelling part is addressed.

A well known high-resolution, full phase-space models of a statistical sample of stellar halos will be described, Bullock and Johnston (2005) and Johnston et al. (2008) (here after J&B), as it gives insights later useful when dealing with the primary set of models used in this thesis. Cooper et al. (2010) (here after *C*10) also worked on simulations of galactic stellar haloes formed by the tidal disruption of accreted dwarf galaxies in a fully cosmological setting, using a method called 'particle-tagging', which will also be characterized here. This is the same technique used later by the *Copernicus Complexio* simulation (the Copernicus Conundrum; hereafter COCO, Hellwing et al. 2016), which is a DM-only simulation specifically fit for the study of a statistically significant sample of well resolved MW-size haloes and their satellites.

3.1 The Bullock & Johnston (2005, 2008) models

Searching the stellar halo for hints about galaxy formation has been useful because stars in there have long orbital time periods, probably experienced not much dissipation, and have the tendency to populate the outer regions of the Galaxy, where

the gravitational potential is more or less smooth, and evolves more gradually. As described in Chapter 1, the currently preferred cosmological model (ΛCDM) of structure formation specifically predicts that galaxies like the Milky Way form hierarchically, from a series of accretion events involving lower mass systems. This leads naturally to the expectation that the stellar halo should be formed, at least partially, from disrupted, accreted systems.

In this context, J&B developed an explicit, cosmologically motivated model for stellar halo formation using a hybrid N-body plus semi-analytic approach.

Cosmological N-body simulations are the numerical solutions of the equations of motions for N particles interacting gravitationally, widely used to study galaxy collisions and also the formation of large scale structure in the universe. In this case, the authors assumed a ΛCDM cosmology with $\Omega_m = 0.3$, $\Omega_\Lambda = 0.7$, $\Omega_b h^2 = 0.024$, $h = 0.7$, and $\sigma_8 = 0.9$, and focused on the formation of stellar halos in MW-type galaxies. Their $z = 0$ host DM halo have virial masses $M_{\rm vir} = 1.4 \times 10^{12}\ M_\odot$, corresponding to virial radii $R_{\rm vir} = 282$ kpc, and virial velocities $v_{\rm vir} = 144$ km s^{-1}.

Normally, studying the phase-space structure of debris in galaxy formation requires very high resolution simulations, which in turn are computationally expensive enough to make statistically robust descriptions a challenge (Helmi, White, and Springel, 2003). One alternative is to approach halo building semi-analytically, which includes the use of pre-calculated dark matter merger trees, and follow the formation of galaxies with simplified, physically and observationally motivated, analytic recipes. The computational costs of this approach are generally lower, and the influence of different physical mechanisms can be investigated separately in a straightforward way (see Bullock and Johnston (2005) for more details).

Within this framework, 11 random realizations of stellar halos were generated by J&B (also recovered by our work), whose phase-space structure variations are determined by differences in their accretion histories. Figure 3.1 show 2D cuts of these models, that we generated at $z = 0$. Three main conclusions specially relevant for this thesis are:

1. Stellar halos (like DM halos) are expected to form gradually towards increasing radii, with the majority of mass being deposited from the $\sim$ 15 most massive accretion events, typically dwarf-irregular size halos with mass $\sim 10^{10}\ M_\odot$ and luminosities of order $\sim 10^7 - 10^9\ L_\odot$. This is essential to establish a mass cut in galaxy surveys when comparing the frequency of observable tidal features.

2. Destroyed satellites contributing mass to the stellar halo tend to be accreted earlier than satellites that survive as present-day dwarf satellites. This means that low-surface-brightness lumps with predominantly old populations ($>$ 8 Gyr old) are more likely to be disrupted satellites.

3. Substructure, visible both spatially and in phase-space diagrams, should be abundant in the outer parts of galaxies. Proper counts of this structure, both in our galaxy and external systems, should provide important constraints on the late-time accretion histories of galaxies and a test of hierarchical structure formation.

Note that, together, the last two points imply that most of the stars in the inner halo are associated with massive satellites that were accreted $\sim$ 9 Gyr ago. Dwarf satellites, on the other hand, tend to be lower mass and are associated with later time accretion events. This suggests that classic stellar halo stars should be quite distinct chemically from stars in surviving dwarf satellites.

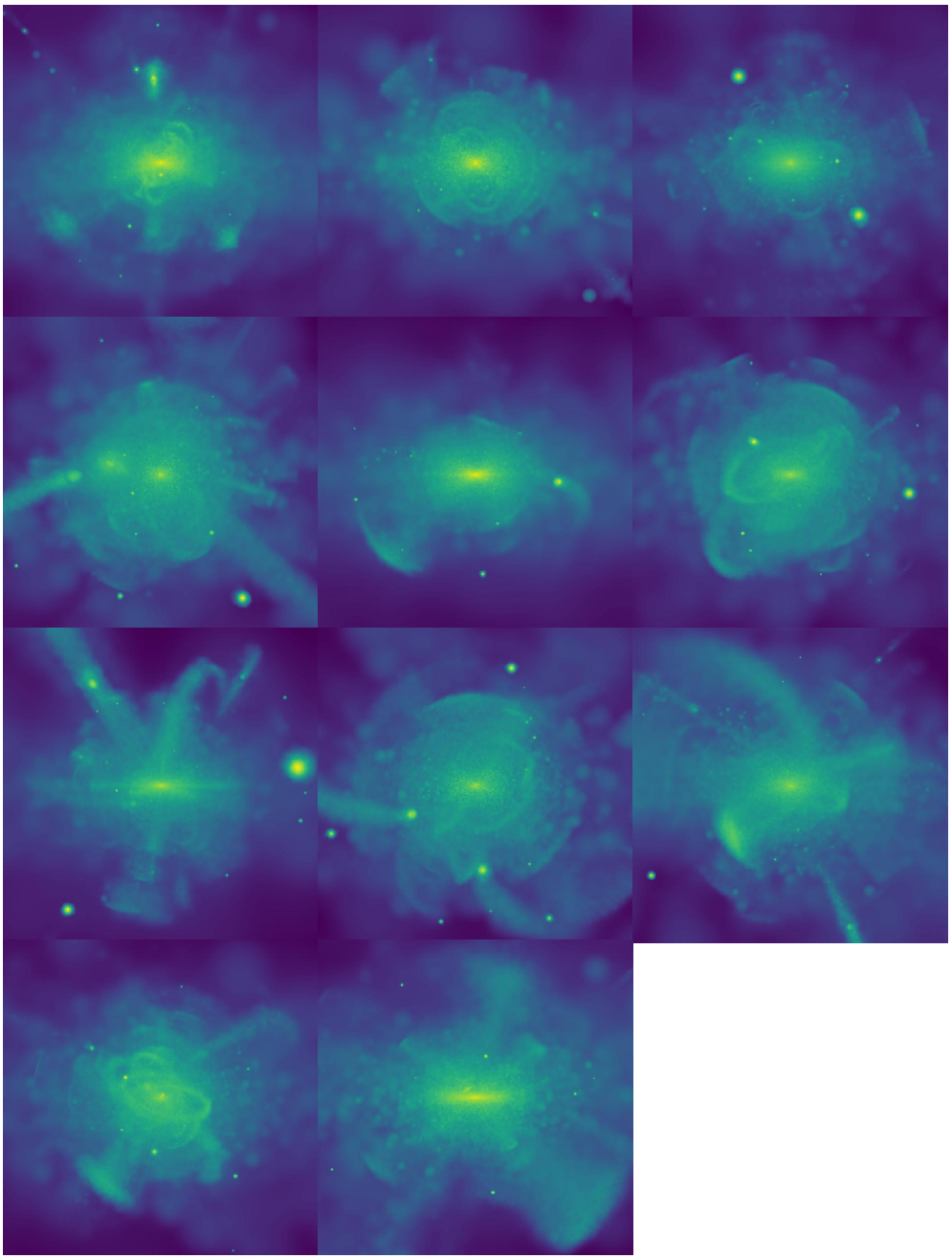

FIGURE 3.1: External, smoothed views for the 11 halo realizations, representing 11 different merging histories. The boxes are 300 kpc by 300 kpc. The color scale indicates surface brightness: 20 mag arcsec^{-2} (yellow) to 40 mag arcsec^{-2} (dark blue), assuming a stellar mass-to-light ratio of 2.

Observable Property	Interpretation	Implication
Fraction in substructure	Recent accretions	High fraction ⇒ many recent events Low fraction ⇒ few recent events
Scales in substructure	Luminosity function and orbit type of recent events	Large high-luminosity ⇒ events Small low-luminosity ⇒ events
Number of features	Number of recent events	Large ⇒ many events Small ⇒ few events
Morphology of substructure	Orbit distribution	Clouds/plumes/shells ⇒ radial orbits Great circles ⇒ circular orbits
$[Fe/H]$	Luminosity function	Metal-rich ⇒ high-luminosity events Metal-poor ⇒ low-luminosity events
$[\alpha/Fe]$	Accretion epoch	α-rich ⇒ early accretion epoch α-poor ⇒ late accretion epoch

TABLE 3.1: Summary of general trends for stellar halo interpretation, taken from Johnston et al. (2008).

When characterizing the morphologies of debris from individual accretion events, three basic shapes can be identified from simulations: arcs, clouds, and mixed configurations. These correlate broadly with the morphologies observed in extragalactic halos (e.g. Martínez-Delgado et al., 2010; Miskolczi, Bomans, and Dettmar, 2011). Moreover, mixed morphologies emerge from events accreted more than 10 Gyr ago that have had time to fully mix along their orbits; clouds are from events accreted less than 8 Gyr ago on eccentric orbits; while great circles are from events accreted $6-10$ Gyr ago on near circular orbits. The transition types mixed clouds and mixed great circles correspond to events that are partially, but not yet fully mixed along their orbits; and cloudy great circle morphologies correspond to recent events on moderately eccentric orbits.

Also noteworthy is Table 3.1, showing a summary of the interpretation of the observable phenomena extracted from J&B simulations. While the frequency of substructure around a host galaxy is sensitive to the amount of recent accretion events, the different scales in substructure tells about the luminosity function and orbit type of such events. The number of features is clearly correlated with the frequency of merging events, and the morphology of tidal substructure traces orbit distribution. Metallicity and α-elements abundance of satellites and substructure are linked to the luminosity function and accretion epoch respectively.

Finally, their analysis of number of features show that distinct debris features brighter than 26 mag arcsec^{-2} should be unusual, while surveys reaching to $30-35$ mag arcsec^{-2} can be expected to see of order a few to a dozen features around Milky Way–type galaxies. Generally speaking, there is a correlation beetween stream detectability and the surface brightness limit of the sample used. Also note that, by one hand, the simplified nature of this modeling is likely to prolong the prominence of substructure. However, this analysis considers only the brightest point of each event's debris, while in reality debris from a satellite might contribute several distinct observable features. Hence these numbers are best thought of as order-of-magnitude estimates for what surveys might be able to detect.

3.2 Cooper et al. (2010)

As explained before (see Chapter 1), stellar halos formed by the remains of gravitationally disrupted satellite galaxies are a natural consequence of hierarchical galaxy formation in the ΛCDM theory. The properties of stars in the halo encode, in principle, the entire aggregation history of a galaxy, including its kinematics, metallicities, ages and spatial distributions. So, stellar halo simulations in realistic cosmological settings are thought to be essential for a comparison at the level attempted by this thesis project.

Nevertheless, as mentioned before in Section 3.1, the computational cost of hydrodynamical simulations are still very high even today. This limits the freedom to explore different parameter choices or alternative assumptions for each model, and motivated the development of new techniques. In the context of modeling a statistically representative population of galaxies in cosmological volumes, two distinct approaches have been worked on: high-resolution N-body simulations of large-scale structure evolved self-consistently from ΛCDM initial conditions, and fast, low-cost, adaptable semi-analytic models of galaxy formation (Cooper et al., 2010, and references therein).

In particular, *C*10 presented a method called particle-tagging, where sets of individual particles in the N-body component of the simulation are dynamically associated with stellar populations. These stellar populations can come from different semi-analytical models, as later shown in Cooper et al. (2013) and Hellwing et al. (2016), etc.. It is important to note that before the publication of this work, preceding applications of this method had so far relied on cosmological simulations that were first limited by resolution, or else physically simplified higher resolution N-body models, as in J&B. *C*10 applies particle-tagging to a fully cosmological simulation instead, where larg-scale structures interact with each other self-consistently. The achieved resolution of these simulations reach considerable scale that is enough to resolve stellar halo substructure (down to $\sim 10^6\ M_\odot$, comparable to the least massive DM halos predicted for Milky Way-satellites).

3.2.1 Aquarius and GALFORM

GALFORM (Cole et al., 2015) is a semi-analytic model for calculating the formation and evolution of galaxies in hierarchical clustering cosmologies. Using a Monte Carlo algorithm to follow the merging evolution of DM haloes with arbitrary mass resolution, it makes use of realistic characterization of the density profiles of dark matter haloes and the gas they contain. It describes the chemical evolution of gas and stars together with their production of dust, and includes a calculation of the sizes of disks and spheroids.

Aquarius, by the other hand, is a set of cosmological (ΛCDM) N-body simulations consisting of six cases of an isolated DM halo, comparable in mass to that of the Milky Way. These simulations have been used to explore the fine-scale structure predicted around the Milky Way by the standard structure formation model, and constitute the basis to delve into many techniques of researching growth of the stellar components of our Galaxy (Springel et al., 2008).

*C*10 basically applied a semi-analytic model of galaxy formation (GALFORM) to the Aquarius suite of high-resolution N-body simulations of Milky Way-like DM haloes. Here, in the post-processing of the N-body simulation, the stellar populations predicted by GALFORM to form in each halo are also associated with 'tagged' subsets

of DM particles. By following these tagged DM particles, *C*10 tracked the evolving spatial distribution and kinematics of their associated stars, in particular those that are stripped from satellites to build the stellar halo. This level of detail regarding the distribution of halo stars was at the time unavailable to a standard semi-analytic approach, in which the structure of each galaxy is represented by a combination of analytic density profiles.

3.2.2 The Particle-tagging technique

The particle-tagging approach is perhaps the main novelty of the simulations used in this thesis, and we will refer generally to Cooper et al. (2010) and Cooper et al. (2013). Firstly, it is assumed that stars in dwarf spheroidal satellites are formed intrinsically connected to the dynamics of a bound fraction of their dominant DM component, which is traced along the whole simulation. It is also assumed that the total mass of the halo determines the mass scale at which stars are formed in their potential well. It is shown that even with these simplistic hypotheses, these simulations achieve good concordance in terms of the phase-space structure with those of Milky Way dwarf spheroidals. This is why disruptions of these satellites are able to reproduce stellar tidal streams, but are not intended as predictions of satellite populations.

In order to assign stellar content to DM halos and follow them through, stars in galaxies can be understood as the combination of many different stellar populations, each defined by a particular formation time and metallicity, and worked out by a particular galaxy formation simulation. The model used for galaxy formation in the case of *C*10 is a modified version of the Bower et al. (2006) GALFORM (Cole et al., 2015) model. Since this technique assumes that star motions can be characterized by DM particles, the objective is to select a representative set of particles from the original *N*-body simulation to track each such stellar population within a galaxy.

For the case of an isolated semi-analytic galaxy, the stellar mass difference $\Delta M_\star$ between two snapshots is identified with the total mass of new stars formed in that period. This $\Delta M_\star$ then correlates with a single stellar population within the galaxy. From the list of particles in the simulation identified with the DM halo of the galaxy at the later point in said time window (simulation step), a subset of particles are selected as the tracers of $\Delta M_\star$, which are the tagged particles of this method. Then, each time new stars are formed in the galaxy, a new set of DM tracers are selected. This means that a given DM particle aggregates its own individual star formation history through out the simulation.

In practice, this idea is applied to a merger tree instead of a galaxy alone, where galaxies grow not only by *in situ* star formation, but also by accretion of satellites. In this case, the total stellar mass of newly formed stars also includes the substraction of its immediate progenitor galaxies.

Thus, in the whole simulation with tagged particles, there is a one-to-one correspondence between a semi-analytic galaxy and a DM halo or subhalo from which particles as chosen of tracers of new stars. This method differs significantly from J&B models, where initial conditions of accretion events are simplified. In *C*10 instead, the cosmological, self-consistent *N*-body simulation is post-processed, where the most-bound fraction of particles are tagged with newly formed star content. It also must be noted that the central potential of these galaxies is non-spherical, without disk component included in their dynamical model. This implies that while the dynamical modeling

of star satellites is somehow streamlined, the satellites themselves are not as crucial as the debris of objects that build the stellar halo.

3.2.3 Main results

Partial results regarding modeled halos with surviving satellites are depicted in Figure 3.2. The brightest and most tight structures visible in said figure are related to the most recent accretion events. Stars stripped from surviving satellites constitute $\sim 60-70\%$ of the halo for cases *C* and *D*, while in the rest of the halos their contribution is less than 10%. Not all the recently infalling satellites responsible for bright halo features survive

Figure 3.2 also shows that all of these halos are notably flattened, particularly in the central regions where most of their light is concentrated. Most of these haloes are strongly prolate within 10 kpc. Beyond $10-30$ kpc, the stellar mass in these haloes is not smoothly distributed but instead consists of a number of discrete streams, plumes and other irregular structures.

In summary, *C*10 found that:

1. Their six stellar halos are mainly built by satellite accretion events occurring between $1 < z < 3$, spanning a range of assembly histories, from a more smooth growth to a rather episodic, discrete set of a few events.
2. Typically, the most massive halo contributor is accreted at a lookback time of between 7 and 11 Gyr, with tidal debris covering a wide radial range, dominating the contribution at large radii. Stars stripped from progenitors accreted at even earlier times usually dominate closer to the center of the halo.
3. Contrary to the expectations from J&B studies as described in 3.1, an important fraction of the stellar halo consists of stars stripped from single surviving galaxies. It is the most recent (and significant) contributors that are likely to be identifiable as surviving bound cores, and so with observable tidal features.

Regarding this thesis project, *C*10 showed that the particle-tagging technique can be used to extract information on the spatial and kinematic properties of galactic stellar halos, by combining a very high resolution, fully ΛCDM cosmological simulation, with a semi-analytic model of galaxy formation. While differencies in predicted halo masses are recognized, satellite populations and stellar haloes are in broad agreement with observations of the Milky Way and Andromeda. This is crucial for actual set of models used in this thesis: the Copernicus Complexio simulation.

3.3 The Copernicus Complexio (2016) simulation

The COCO simulation is a high-resolution cosmological *N*-body simulation of structure formation in the ΛCDM model. It is specially appropriate for statistical studies of a sample of well resolved MW-size halos and its satellites. Similar to *C*10, it features a hybrid approach, following a high-resolution region embedded within a much larger box resolved at low-resolution. The larger-resolution region, of size $\sim 17h^{-1}$ Mpc, contains around 60 MW-size halos with their satellite populations.

The idea behind this 'zoom-in' technique (Katz and White, 1993; Frenk, Baugh, and Cole, 1996) is to be able to follow the evolution of galaxy formation at a resolution

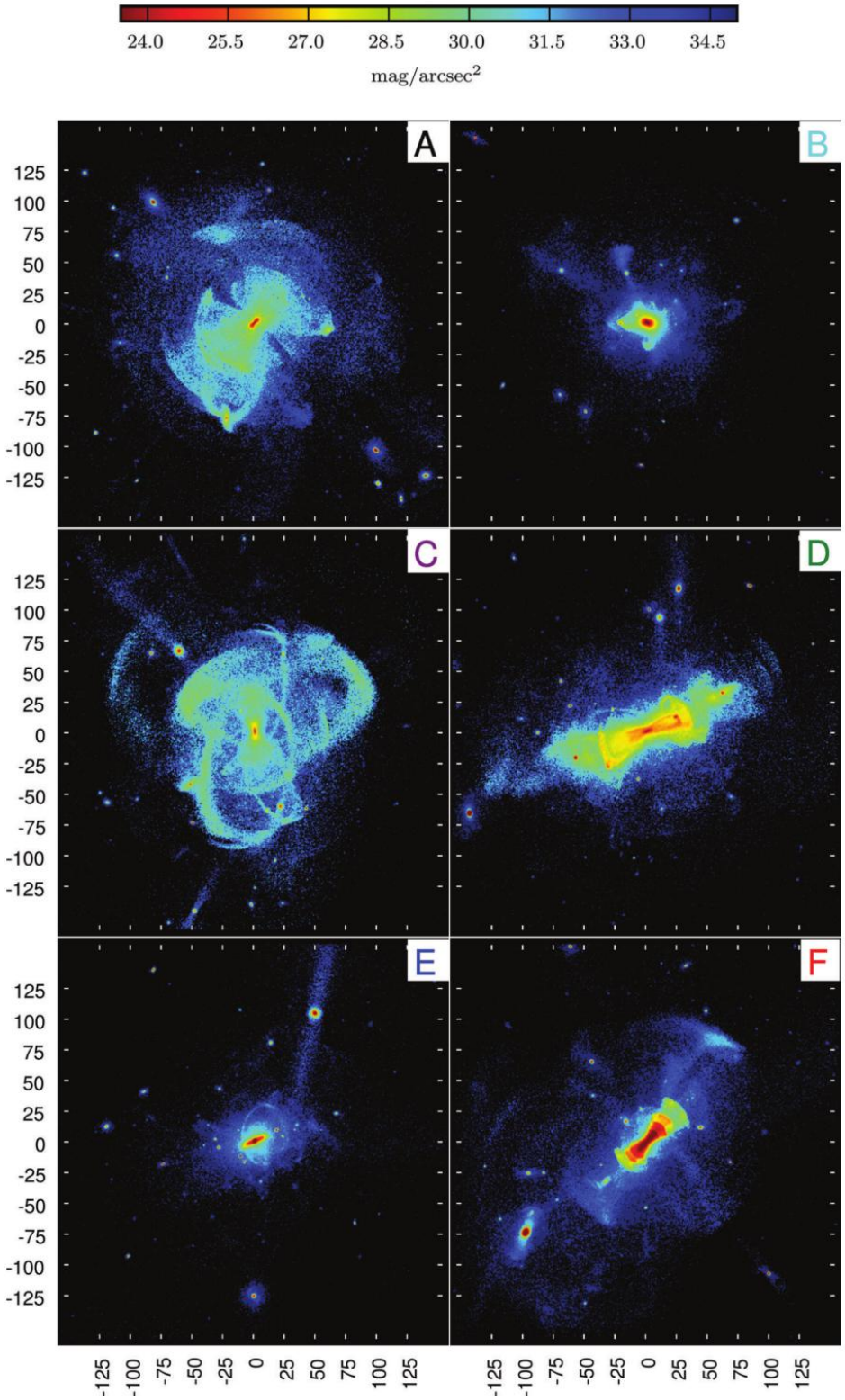

FIGURE 3.2: V-band surface brightness of model halos with satellites, taken directly from Cooper et al. (2010), to a limiting depth of 35 mag arcsec^{-2}. The axis scales are in kiloparsec. Only stars formed in satellites are present in these models; there is no contribution to these maps from a central galactic disc or bulge formed in situ.

high enough to resolve the objects of interest in a small volume, but embedded in a region that correctly reproduces the large-scale gravitational effects within said high-resolution box, so that the computational costs are lower. In this context, three simplifications are in order:

1. No cluster-mass halos ($M > 5 \times 10^{13} h^{-1}\ M_{\odot}$) inside the zoom-in volume.
2. No massive cluster halos ($M > 5 \times 10^{14} h^{-1}\ M_{\odot}$) within $5h^{-1}$ Mpc of the zoom-in boundary.
3. The mass function of MW-mass halos ($M \sim 10^{12} h^{-1}\ M_{\odot}$ has to be as close as possible to the universal mass function.

The basic properties of the COCO cosmological component are summarized in Table 3.2, based on the Wilkinson Microwave Anisotropy Probe (WMAP) - seventh year result cosmogony (Komatsu et al., 2011).

TABLE 3.2: COCO (Hellwing et al., 2016) basic properties.

Zoom-in volume	Periodic box volume	Number of particles	Mass per particle	Ω_{m0}	$\Omega_{\Lambda 0}$	Ω_b	Ω_k	h	σ_8	n_s
$17.4h^{-1}$ Mpc	$70.4h^{-1}$ Mpc	12.9 billion	$1.135 \times 10^{-5} h^{-1}\ M_{\odot}$	0.272	0.728	0.04455	0	0.704	0.81	0.967

The COCO (and its low-resolution version) simulations were run with GADGET-3 Tree-PM N-body code, which is an updated version of the publicly available GADGET-2[1] code (Springel, 2005). This particular version of the GADGET-2 code is a hybrid code in which the long-range forces are computed using a particle-mesh method[2], while short-range forces are obtained by using a hierarchical oct-tree[3] algorithm. This allows for an easier follow-up of nested grids placed with increasing accuracy around the high-resolution volume, while also permitting a long-range force accuracy throughout the whole low-resolution region, but focusing most of the computational effort inside the high-resolution one.

The full description of the COCO simulation, including halo finding, merger trees and Friends-of-Friends[4] (FoF) prescriptions, the DM halos mass function, their density and radial profiles and mass-concentration relations are fully detailed in Hellwing et al. (2016), and is relatively similar to the work of Cooper et al. (2010) and Cooper et al. (2013). The main difference with C10 is that uses a different galaxy formation model, described in (Gonzalez-Perez et al., 2014). Here in this work, 100 galaxies were selected from the final results and snapshots were generated mimicking images with observational effects applied, for three different perpendicular projections that later are compared to the processed SDSS data (see Section 4.2).

3.3.1 Main results

The following summarizes the central points of Hellwing et al. (2016):

[1] GADGET-2 is an improved version of the GADGET-1 code, the first public release of a set of cosmological N-body/SPH simulations that can run with parallelization and distributed databases in mind.

[2] A particle-mesh method, or PM or P^{3}M, is a summation method used to calculate potentials in N-body simulations.

[3] An octree is a tree data structure in which each internal node has exactly eight children, typically used to partition a three-dimensional space by recursively subdividing it into eight octants.

[4] In the FoF halo finding algorithm, particles are associated together if their distance lies below a certain threshold.

1. The FoF mass function used matches previous halo abundance predictions made with N-body simulations at $z = 0$ (although underestimates the number of collapsed objects in the range $2.0 < z < 0.5$).
2. The concentration–halo-mass relation breaks apart from a single power-law function at lower halo masses, consistent with previous studies. This relation is monotonic for small halo masses in the range $9 < z < 0$.
3. The gradual nature of halo formation processes is confirmed for seven orders of magnitude in mass. There is an object-to-object scatter of halo formation time that depends on this halo mass that is larger for low mass halos, interpreted to be the result of the many different external conditions in which these low mass halos form and evolve.
4. There is a power-law function governing the subhalo mass function, with its power-law exponent depending on the host halo mass.
5. The spatial distribution of low mass satellites has a universal shape across hosts of different masses.
6. Finally, and of more relevance to this thesis: the relation between the maximum circular velocity of subhalos, $V_{\rm max}$, and the radius corresponding to this maximum value, $R_{\rm max}$ is found to depend on the host halo mass, with lower mass hosts having subhalos with higher $R_{\rm max}$ values. This would reflect the fact that at some fixed subhalo size, the tidal stripping mechanisms are more efficient in more massive hosts, leaving lower mass hosts with faster orbits at larger radii.

Finally, it must be noted that COCO has been already used to study systematically and statistically the presence of uncommon plannar satellite structures in the ΛCDM paradigm (Cautun et al., 2015), and has extended use beyond the testing of hierarchical growth in galaxies that will be published in forthcoming publications.

3.3.2 Applying observational effects

As mentioned before, 100 galaxies were identified using the COCO simulation, described in Table 4.3 in Appendix B. These models are selected in terms of their halo (virial) mass M_{200}, defined as the mass enclosing a mean density 200 times the critical density of the Universe[5]. For the purposes of this thesis, their internal tags have been conserved, and only spatial coordinates (x, y, z) in kiloparsecs and masses in solar masses for every particle are available in the data files.

Before continuing, it must be noted that while the fundamental attribute to look for from a modeler point of view is the virial mass, and the observable property are the stellar mass (and fluxes) instead, the relationship between both is not exactly one-to-one. In other words, there is a substantial scatter around the $M_{\rm star} - M_{200}$ relation, and there is not some single underlying physical function that maps one to the other. To overcome this, several papers have given functional forms for fitting relations using mainly observational data (e.g. Moster et al., 2010; Guo et al., 2010; Behroozi, Wechsler, and Conroy, 2013; Moster, Naab, and White, 2017). This scatter cannot be overlooked when interpreting the mass range at which data and models will be compared.

The algorithm to apply observational effects and create mock images to compare to the SDSS processed data works as follows:

[5] In an Einstein-de Sitter model, the critical density equals $18\pi^2 \approx 178$. As a convention, the value 200 is often used in cosmological studies.

1. Loads the COCO data file and applies a 3D rotation if supplied to the coordinate vector $\vec{v}$. This rotation $\vec{T}$ accepts any degree of rotation θ about an arbitrary (unitary) axis $\hat{r}$, and is given by an Euler transformation matrix (Luo and Hou, 2014):

$$\vec{T}(\vec{v}) = \begin{bmatrix} tu_x^2 + C & tu_x\,u_y - Su_z & tu_x\,u_z + Su_y \\ tu_x\,u_y + Su_z & tu_y^2 + C & tu_y\,u_z - Su_x \\ tu_x\,u_z - Su_y & tu_y\,u_z + Su_x & tu_z^2 + C \end{bmatrix} \vec{v} \tag{3.1}$$

   where

$$\begin{aligned} \hat{r} &= (u_x, u_y, u_z), \\ C &= \cos\theta, \\ S &= \sin\theta, \\ t &= 1 - \cos\theta. \end{aligned}$$

2. Given a distance, a pixel scale, a map size in pixels, a smoothing scale, and a projection axis, it smooths the density field represented by the set of particles $\vec{v}$ onto a regular grid in projection. If smoothing lengths are not given, they are calculated from the particles themselves. The pixel scale $\eta = 0.396$ arcsec/pixel and map size $s = 4595 \times 4595$ sq. pixels were set to that of the processed SDSS images (recall Section 2.3). The distance is somehow arbitrary, and was set to cover 300 kpc in said map size. The smoothing scale was left fixed in $n = 32$[6], which was found to be a good enough compromise between precision with high computational cost and timely analysis. Thus, the projection axis and rotation angles are left free for study.

   Do note that the computation and application of the smoothing scale is important because it spreads the particles weight (given by their luminosity, set in turn by the mass) before adding their contribution to each and every pixel in the grid, instead of just creating a normal scatter plot. This smoothing process takes into account the n-nearest neighbors by mapping the most crowded areas with higher resolution than the less populated ones, giving the mock images their characteristic look.

3. Optionally, a convolution with a Gaussian kernel is applied if needed. Gaussian kernels with the right size ($\sim 5 - 7$ pixels at the distance range of this work, as explained in Section 2.4) have the potential to enhance diffuse structures at galactic scales.

Fluxes were coadded accordingly. Every SDSS image was coadded in the 'natural' unit of the SDSS photometry, nanomaggies, or 1×10^{-9} Mgy. This is a conveniently linear unit, where 1 nMgy $\approx 3.631 \times 10^{-6}$ Jy. To interpret results for both data and mock images in a more commonly used logarithmic scale, like the AB-system, the following conversion from flux f in Jy to m_{AB} can be used (Currie et al., 2014):

$$m_{\mathrm{AB}} = 2.5[23 - \log(f)] - 48.6 \tag{3.2}$$

[6] In J&B models, the smoothing scale is set to 64

TABLE 3.3: Summary of general sources of background in imaging. Note that not all of them contribute equally in the case of the SDSS processed images.

Categories	Examples of contamination
Instrumental effects	Ghost effects, LEDs in CCD encoders, software artifacts.
Diffuse light	Extragalactic background, zodiacal light, scattered starlight, airglow, moonlight.
Astrophysics	Wings of foreground stars and galaxies, intracluster light, infrarred cirrus.

More importantly, due to time constraints, two fairly significant simplifications have been made at this point, and currently constitute the most important caveats of this work. While the full script to apply observational effects was proved succesfully with J&B models, COCO data files needed more work. Unlike with J&B data files, information on the luminosity is currently lacking, so a mass-to-light ratio (M/L) of ~ 2 was assumed, consistent with the previous studies cited here. Consequently, there is also no information on the corresponding optical SDSS bands (*ugriz*) at which these luminosities would correspond, which is important when reporting to which SDSS band the images are calibrated to (as seen in Section 2.4), so for now it is assumed that all light correspond to the SDSS$-r$ band. While these issues do not prevent testing the images by visual inspection, it does leave considerable room for improvement.

In this way, 300 models were generated in total, with three different perpendicular projections for each model in Table 4.3 in Appendix B.

Finally, in order to add all of the possible phenomena that contribute as sources of background to imaging (see Table 3.3 –that may or may not have been sucessfully eliminated by background substraction— which in turn have the potential to contribute to the detectability of diffuse structures around galaxies, three different SDSS backgrounds (*gri*-stacked) have been randomly coadded (i.e. summed in linear flux units) to the model only images. These background SDSS images have the same characteristics as the science ones processed in Section 2.3 except for the gaussian filtering, which is applied after coadding the models. These fields are centered in the following J2000 celestial coordinates:

$$\begin{aligned}\alpha_1, \delta_1 &= 08:03:07.99, +34:03:07.9,\\ \alpha_2, \delta_2 &= 11:58:52:00, -00:26:44.0,\\ \alpha_3, \delta_3 &= 12:10:23:00, +01:41:19.0,\end{aligned}$$

and have been chosen to span a wide variety of effects already observed in the SDSS processed images, except for strong galactic cirrus.

Chapter 4

Results

> Facts are stubborn, but statistics are more pliable.
>
> Mark Twain

The results of this thesis can be divided in two sections, that later are compared together: results from the processing of SDSS imaging data, and the outcome of simulations with applied observational effects.

4.1 Tidal features around galaxies in the SDSS

The aim of this thesis was to study systematically the frequency of occurrence and other observational properties of tidal features around nearby galaxies. The constructed sample will act as a foundational dataset for statistical comparison with cosmological models of galaxy formation. The approach is based on a visual classification of diffuse features around a volume-limited sample of nearby galaxies, using a post-processing of SDSS imaging optimized for the detection of low-surface-brightness stellar structure.

At a limiting surface brightness of 28 mag arcsec^{-2}, 14% of the galaxies in this sample exhibit evidence of diffuse features likely to have arisen from minor merging events. The technique used recovers all previously known streams in the galaxy sample and yields a number of new candidates. Consistent with previous studies, coherent arc-like features and shells are the most common type of tidal structures found in this study. In conclusion, although some detections are ambiguous and could be strengthened or refuted with deeper imaging, this methodology provides a reliable foundation for the statistical analysis of diffuse circumgalactic features in wide-area imaging surveys, and for the identification of targets for follow-up studies.

4.1.1 Deeper follow-up of tidal features

Although our processed SDSS images reach a surface brightness limit in the r band ($SB_{r,lim}$) that would conventionally be considered 'deep', they are still only deep enough to reveal the brightest structures (if any) in the halos of our target galaxies. In some cases, the low S/N detection of a particular feature and artifacts in the image significantly reduce our confidence in the nature of the detection and/or its interpretation

as a signature of tidal disruption. Better (i.e., deeper) data are necessary to improve confidence in these detections.

Figure 4.1 shows some examples of different types of overdensities found in our search. These illustrate cases in which it is ambiguous whether well-detected overdensities are the result of minor mergers or perturbations of the central galaxy, such as extended stellar warps (e.g., NGC 5506), rings (e.g., NGC 2859) or other tidal distortions (e.g., Trujillo et al., 2009). Significant sky background fluctuations or extended Galactic cirrus (e.g., NGC 7497) are also a well-known problem for the detection of tidal streams (e.g., Duc et al., 2015). Finally, NGC 3489 is a clear example of a typical artifact in the SDSS images, a reflection from a bright star that resembles a diffuse satellite interacting with the central galaxy.

We have explored the availability of deep images for our stream candidates in two separate sources of additional optical data described below. Unfortunately, these additional surveys currently cover a smaller sky area and have fewer bandpasses than the SDSS, and hence are not suitable for the statistical analysis we attempt with SDSS data in this thesis.

The Stellar Tidal Stream Survey

Figure 4.2 shows a comparison of our results to the ultra-deep observations of the STSS (Martínez-Delgado et al., 2010) for a set of well-known diffuse features. As found by Miskolczi, Bomans, and Dettmar (2011), the filtering technique we used renders visible in SDSS images the majority of features reported so far by the robotic amateur telescope observations in the STSS pilot survey, although with a lower S/N because of the brighter surface brightness limit of the SDSS. The lower quality of our SDSS data compared to those of Martínez-Delgado et al. (2010) is mainly explained by the short effective exposure times of the individual broadband SDSS observations. This complicates the classification of very faint overdensities, since the lower S/N makes it harder to distinguish actual tidal features from overdensities related to Galactic cirrus, perturbations to the structure of the central galaxy, or image artifacts (see Fig. 4.1). Deeper follow-up observations are necessary to classify these ambiguous detections.

Figure 4.3 illustrates the benefits of deeper follow-up with observations like those of the STSS for three galaxies in our sample. The first column presents NGC 7743, a galaxy with an apparently clear stellar tidal stream candidate in its outskirts; however, with STSS observations this feature is shown to be (at least predominantly) Galactic cirrus. The second column presents NGC 5750, which shows a remarkable irregular substructure apparently emerging from its disk; deeper STSS observations reveal an additional overdensity on the other side of the galaxy, which is only barely visible at the detection limit of our processed SDSS images. Finally, the third column presents NGC 3041, in which an arc-like feature is apparent to the north of the galaxy. The amateur telescope data strongly support the interpretation of this feature as a great-circle stream.

The Dark Energy Camera Legacy Survey

We have also searched for images of galaxies with visible low surface brightness features (Table 4.1) in the optical images from the third data release (DR3) of the Dark Energy Camera Legacy Survey (DECaLS, Blum et al., 2016b). This survey uses the

Dark Energy Camera (DECam), a wide-field CCD imager at the CTIO Blanco 4 m telescope, to obtain optical imaging covering 14,000 deg^2 in three optical bands (g,r,z). Since the footprint is mostly in the equatorial and southern sky and only a fraction of the DECaLS data have been publicly released, only a few targets have been imaged with sufficient quality and depth to aid in the interpretation of our SDSS images. In the publicly available DECaLS data, we found that three of our targets were imaged in the g, r, and z bands, confirming the detected streams or diffuse-light substructure in the halo from our analysis. Although some sky regions have been imaged in just one DECaLS band so far, we are able to improve our confidence in some low surface brightness features with even these data. Regarding background subtraction around large objects, it must also be noted that the DECaLS data reduction for large sources has not yet been optimized to the same extent as in the SDSS (Blanton et al., 2011). This explains the rectangular patches in DECaLS images with poor subtraction around large galaxies, which sometimes mimic diffuse galactic structure.

4.1.2 Confidence of detections and morphologies

For all of the galaxies listed in Table 4.1, we estimated our confidence in the detection of faint tidal features on a five-point scale, similar to the scheme used by Atkinson, Abraham, and Ferguson (2013). We refer to it as the detection confidence level (DCL), reflecting our certainty that a tidal feature with low surface brightness that is associated with the target galaxy was detected in an image, as follows:

0: No detection of any sort, or high confidence that any candidates are perturbations of the central object (spiral arms, cirrus, etc.).

1: Very uncertain detection of a feature at a S/N too low to judge either the quality of the detection or its tidal nature.

2: Possible detection of a low surface brightness feature, but with low confidence in a tidal origin ($\sim$ 50% certain).

3: Strong detection judged highly likely to be of tidal origin, but without support from any data other than our own.

4: Strong detection where a tidal origin is supported by other data.

In the same table, we also provide an approximate visual classification system for the morphology of the most common features we detect using the following categories, which are not mutually exclusive:

S for classic shells. Disconnected, coherent arcs of material usually concentric with the central galaxy.

C for any coherent, curvilinear features seen in the image (that are not shells). This includes arcs, plumes of debris, and looped structures of gas or stars surrounding their host.

Sph for spheroids and diffuse satellites in the process of disruption, suggestive of very low surface brightness galaxies.

E for extensions of the central galaxy, including but not limited to warps and spiral arms, and some unclassifiable overdensities clearly connected to the disk.

O for any other less common type of features not included above, but suggestive of tidal interactions: fuzzy clouds, spikes, wedges, irregular filaments, etc.

These categories are intended as an simple indication of the appearance of the features we detect. Stronger conclusions about the true physical nature of these features are beyond the scope of this work, and in most cases would require support from techniques other than photometry.

4.1.3 Sample statistics

By visual inspection of the processed images, we determine that 51 of the 297 galaxies in our sample show either clear or potential signatures of diffuse overdensities in their outskirts above our surface brightness limit (28.1 mag arcsec^{-2}). Table 4.1 describe these galaxies and their associated low surface brightness features. Of these 51 targets, 28 show overdensities that we judge to be either stellar or gaseous tidal features on the basis of other, deeper observations. A further 23 objects for which we currently lack deeper observations show overdensities that are likely tidal feature candidates (listed in Table 4.1 as features with DCL 1 and 2; see Sec. 4.1.2). Hence a conservative estimate for the frequency with which such features occur in our volume- and mass-limited sample of the local Universe is $\approx$ 9%. This would rise to $\approx$ 17% if all candidates were confirmed by deeper follow-up observations. Considering only previoumasly published features together with the new discoveries reported in this paper, we estimate that $\approx$ 14% of galaxies in the local Universe exhibit diffuse tidal features brighter than 28.1 mag arcsec^{-2} in the SDSS *r* band. As a reference, all galaxies in our sample that do not show any evidence of diffuse-light structures are listed in Table B.1.

ID	Galaxy morphology	Distance (Mpc)	log(Stellar Mass) ($M_\odot$)	DCL	Tags	Comments
NGC 681	SAB	33.600	10.752	4	S C	This work
NGC 718	SAB	21.400	10.283	3	C E	Very faint arc-like feature to the north plus possible overdensity to the south
NGC 936	SB0	20.683	10.926	3	C E	Double arc-like feature; hints of warped disk
NGC 1055	SBb	16.630	10.739	4	O	Martínez-Delgado et al. (2010)
NGC 1084	SAc	21.225	10.619	4	C	Martínez-Delgado et al. (2010)
NGC 2775	SAab	17.000	10.870	4	S	This work; MD+
NGC 2859	(R)SB0	27.333	10.882	3	C Sph	Two possible partially disrupted satellites within a ring, with leading and trailing tails
NGC 3034	I0	3.777	10.449	2	E O	Possible spike features
NGC 3041	SAB	26.350	10.437	4	C	This work
NGC 3049	SBab	30.775	10.132	4	S C E	This work; MD+
NGC 3185	(R)SBa	24.725	10.215	3	C E O	Very faint loop connected to the disk, with a compact object embedded on it
NGC 3277	SA	25.000	10.375	1	S	Possible shells very close to the halo
NGC 3521	SABbc	12.078	11.030	4	S C E O	Martínez-Delgado et al. (2010)
NGC 3611	SAa	33.300	10.462	4	C	Schweizer and Seitzer (1990); This work
NGC 3628	Sb	11.300	10.805	4	Sph	Martínez-Delgado et al. (2010)
NGC 3631	SAc	13.102	10.163	4	E O	This work; MD+
NGC 3675	SA	17.200	10.919	1	E	Candidate tidal overdensities, not clearly distinguishable from disk warping
NGC 3682	SA0	ND	10.230	4	S	This work
NGC 3729	SB	20.183	10.233	3	Sph E	Possible satellite being disrupted
NGC 3877	SA	15.612	10.445	1	E O	Asymmetrical and coplanar spike extending from the disk
NGC 3949	SA	18.341	10.246	3	S E	Possible shell very close to the outer disk
NGC 4013	Sb	18.600	10.630	4	E O	Martínez-Delgado et al. (2010)
NGC 4051	SAB	14.575	10.359	3	Sph E O	Possible compact object with halo and tail, plus an overdensity south of the galaxy
NGC 4111	SA0	15.550	10.452	4	Sph O	Brodie et al. (2014)
NGC 4203	SAB0	14.940	10.528	4	Sph	This work
NGC 4262	SB0	20.510	10.377	2	E	Two overdensities not clearly related to tidal features, perhaps part of the disk
NGC 4293	(R)SB0	14.320	10.418	3	E O	Clear substructure in the inner halo, very close to the disk
NGC 4394	(R)SB	16.800	10.440	3	E	Possible extended disk features, or tidal arcs surrounding the galaxy
NGC 4414	SAc	18.312	10.883	4	S	de Blok et al. (2014)
NGC 4494	E	13.841	10.542	2	O	Possible diffuse substructure, resembling symmetric spikes in an elliptical galaxy
NGC 4519	SB	28.411	10.191	3	C E	Filamentary feature with two components, likely related to either the halo or the disk
NGC 4569	SABab	12.352	10.638	4	E O	Martínez-Delgado et al. (2010)
NGC 4594	SAa	10.390	11.253	4	C	Malin and Hadley (1997)
NGC 4631	SBd	6.050	10.127	4	E O	Martínez-Delgado et al. (2015a)
NGC 4643	SB0	25.700	11.028	4	C Sph	This work
NGC 4651	SAc	26.708	10.844	4	S C E O	Martínez-Delgado et al. (2010)
NGC 4691	(R)SB0	22.500	10.479	2	E O	Possible outer halo overdensity with the appearance of a dense stellar cloud
NGC 4753	I0	16.869	10.930	4	E	Steiman-Cameron (1992)
NGC 4762	SB0	22.460	10.848	2	E O	An interesting case of disk warping with mixed tidal features
NGC 4772	SAa	30.475	10.747	4	E	Haynes et al. (2000)
NGC 4866	SA0	23.800	10.689	1	E O	Unclassifiable disk feature to the right of the galaxy, possibly with tidal origin
NGC 5055	SAbc	8.333	10.778	4	C O	Martínez-Delgado et al. (2010)
NGC 5364	SA	19.513	10.614	3	E O	Giant tidal structure west of the galaxy
NGC 5506	S pec	23.833	10.122	3	C O	Distorted, asymmetric tidal features connected to each side of the disk
NGC 5576	E	23.930	10.770	1	S	Possible diffuse shells
NGC 5750	SB0	33.633	10.741	4	E O	This work
NGC 5806	SAB	25.541	10.585	3	C S E	Diffuse extended overdensity, with a shell or arc-like feature very close to the disk
NGC 5907	SAc	16.636	10.871	4	C	Martínez-Delgado et al. (2010)
NGC 7241	SB	ND	10.263	4	E O	Leaman et al. (2015)
NGC 7742	SAb	22.200	10.343	4	S C	This work
NGC 7743	(R)SB0	21.433	10.447	4	C E	This work; MD+

TABLE 4.1: Tidal streams found in this work, including previously known features and new discoveries (28 host galaxies), with detection confidence levels (DCL) 3 and 4. Diffuse-light overdensities, with their physical nature yet to be confirmed (23 host galaxies) are also included, with DCL 1 and 2. This implies a total of 51 galaxies with any type of tidal features related to them. Distances and stellar masses were taken from S4G, while their morphology was extracted from NED database. Additionally, substructures we found have been tagged: *S* for shells; *C* for curved, arcuated features, including anything coherent and stream like; *Sph* for spheroidal satellites and partially disrupted cores; *E* for extensions of the central galaxy (e.g. warps and spiral arms); and *O* for any other type of less common features (wedges, radial spikes, fuzzy clouds of debris, etc.). For known substructures, references of previous studies have been supplied. MD+ refers to Martínez-Delgado et al. (in prep.), a forthcoming paper.

Figure 4.4 shows histograms of our galaxy samples, including the parent sample and subsets of targets that show evidence of tidal streams[1]. Furthermore, it shows that above the surface brightness limit of our sample there are no significant selection effects arising from either morphology or inclination angle, consistent with a roughly isotropic distribution of features. There are some hints of an excess of low surface brightness features at short distance and high stellar mass. The latter is compatible with the expectation of ΛCDM, where more massive galaxies are hosted by more massive DM haloes and are therefore more likely to accrete brighter satellites. Any selection effect with distance is likely to reflect the balance between this effect (large volumes include more bright galaxies) and the increasing difficulty of detecting low surface brightness substructures at larger distances.

We also computed a two-sample Kolmogorov-Smirnov (KS) test to provide a quantitative comparison between the distance, mass, morphology, and inclination angle distributions of the 297 galaxies in our parent sample and those of the hosts of high-confidence tidal feature candidates from Table 4.1 (this means a DCL equal to 3 or 4, i.e., a comparison of the black and solid green histograms in Fig. 4.4). The p-values obtained are shown in Table 4.2. At a significance of $p = 0.05$, on the basis of any one of these four distributions, we cannot reject the null hypothesis that our sample of galaxies with overdensities is drawn from the same underlying population as the parent sample we selected from S4G. In other words, random sampling from our parent sample has a high probability of yielding distributions similar to those of our sample of galaxies with overdensities.

4.1.4 Confirmed low-surface-brightness stellar structures

Table 4.1 lists, among others, the 28 tidal streams that we have confirmed. This list contains 12 unpublished detections, including those found recently in the STSS (Martinez-Delgado et al., in preparation). Figure A.1 in Appendix A shows the corresponding image for each galaxy. In these images, the disks of galaxies tend to dominate the field of view because the images have been significantly contrast-stretched to render the low surface brightness structures visible. These new streams are briefly described below. The estimated physical extent of these substructures has been calculated assuming the distance to the target taken from the NASA/IPAC Extragalactic Database

[1] Instead of using the mean redshift-independent distances from NED, we here used the Hubble flow distances, cz/H_0, where cz is the recessional velocity, and $H_0 = 75$ km/s/Mpc.

Variable	p-value
Distance	0.113
Stellar Mass	0.067
Hubble Stage	0.241
Inclination	0.654

TABLE 4.2: p-values obtained from a two-sample KS test applied to the histograms depicted in Fig. 4.4; specifically, the distribution of confirmed tidal streams plus strong candidates, versus the whole sample of 297 galaxies. We cannot reject the hypothesis that the distributions of the two samples are the same.

(NED). It must be noted that the NED uses the mean value of redshift-independent distances. When no mean distance is reported, the Hubble flow distance is used instead.

NGC 681 is an edge-on disk galaxy with a prominent spheroid surrounded by two clear shells along the major axis, extending to $R = 25$ kpc southwest and $R = 39$ kpc northeast. Other possible arc-like features (concentric around the galaxy $R = 10$ kpc to the south and extending northeast from the south edge of image) are not apparent in DECaLS images (see Fig. A.3).

NGC 2775 is an unbarred spiral galaxy showing a prominent ~ 29 kpc cloudy structure in its halo, reminiscent of a classical shell from Martínez-Delgado et al. (2010).

NGC 3041 shows an arc-like stream with an extent along its longest dimension of ~ 4 kpc, northeast of the central galaxy. STSS and DECaLS data (Fig. 4.3) show this feature clearly, but they do not reveal any further detail. This may be the brighter part of a great circle structure similar to the Milky Way Sagittarius stream, but no surviving progenitor is apparent.

NGC 3049 shows an arc-like feature east of the central galaxy, with a size of ~ 3 kpc. Another very diffuse substructure can be identified to the west, suggestive of a shell formed by tidal disruption. More definitive statements require deeper observations.

NGC 3611 is well known for the peculiar ~ 30 kpc bright off-center ring-like structure previously noted by Schweizer and Seitzer (1990). These authors favored merging as the origin of this feature, excluding the possibility of a disturbed polar ring. DECaLS data (Fig. A.3) show two distinct features: a clear umbrella-like stream with shells on both sides of the galaxy (the most prominent to the east), and an incomplete blue ring or arc encircling the disk. The colors of both structures are clearly different, and it is unclear whether they have a common origin (e.g., the tidal disruption of a Magellanic-type dwarf galaxy).

NGC 3631 shows a giant cloud at a galactocentric distance of ~ 19 kpc. This is very similar to the M83 stream (Malin and Hadley, 1997). It is not clear whether the structure is part of a very faint outer disk or a tidal structure in the galactic halo. This overdensity has also been observed by the STSS (Martinez-Delgado et al., in preparation), indicating that it is not an artifact in the SDSS image.

NGC 3682 shows two classical shells on both sides of the central galaxy, with diameters of ~ 2 kpc.

NGC 4203 shows a bright, partially disrupted and nucleated satellite southwest of the galaxy, with both a leading and a trailing tail of total length $\sim$ 13 kpc.

NGC 4569 is a spiral galaxy with a dIrr satellite (IC 3583) to the north, with an apparent interaction between the two[2]. There is evidence of a shell-like overdensity on the northern side of the galaxy, although we cannot reject the possibility that this is an extended warp of the stellar disk.

NGC 4643 shows a clear stellar tidal stream apparently perpendicular to the plane of the galaxy. DECaLS data show evidence for a progenitor in the northern tail. Assuming that both structures apparent in the image are part of the same feature (for example, an arc viewed edge-on), this feature has an extent of $\sim$ 73 kpc. Whitmore et al. (1990) reported an inner, edge-on arc structure in the main body of the galaxy that is also visible in our images, but not related to the giant tidal structure we report here.

NGC 5750 Both images from our analysis and the STSS deeper images (see Fig. 4.3) show a truncated overdensity west of the central galaxy, which resembles a faint, distorted satellite galaxy. In addition, an elongated, irregular feature east of the disk (clearly visible in the STSS image) could be part of a tidal stream associated with that satellite.

NGC 7742 is a face-on unbarred Seyfert spiral galaxy, which shows three very distinct stellar arcs, possibly sections of a shell (or shells), each $16 - 17$ kpc in diameter.

NGC 7743 is a barred Seyfert spiral galaxy showing a giant, 18 kpc loop structure to the northeast. Galactic dust clouds dominate the field of view in longer exposures, as shown in the first column of Fig. 4.3.

4.1.5 Tidal stream candidates for follow-up studies

Table 4.1 lists the galaxies of our sample with detected structures for which a tidal origin cannot be confirmed in this work because we lack deeper data; 23 in total, with a DCL equal to 1 or 2. Follow-up observations of these galaxies are currently being carried out by the STSS and will be published in a forthcoming companion contribution (Martínez-Delgado et al., in preparation). These signatures define those that are very probably stellar tidal streams, that is, tracing orbits of satellites in the tidal field of the host galaxy, and features that are probably linked to disk warping, polar rings, and other types of signatures. In general, any features more likely related to galactic perturbations of the central galaxy disk due to dynamical interaction with other massive galaxies were tagged accordingly. Some examples of these structures of different types are displayed in Fig. A.2. Figure A.3 shows the images used to confirm the faint tidal debris detected around six of the galaxies listed in Table 4.1.

4.2 Mock images from simulations

The outcome of Section 3.3.2 can be seen in Figures A.4, A.5 and A.6 in Appendix A, for the case of pure models. Once the random background is coadded, this generates the mock images shown in Figures A.7, A.8 and A.9 also in Appendix A. Every analysis from now on relies purely on visual inspection, which is the same method used on Section 2.3.

[2]Although gravitational interaction has been ruled out by some authors (e.g., Boselli et al., 2016).

First, a qualitative comparison of these images reveal the two most conspicuous effects of adding realistic observational effects to models. As expected, most of the tidal streams tend to go below the detection limit –specially arcs, plumes and umbrellas– with only the brightest components observable, particularly shells and disrupted cores or dwarf galaxies (see Figure 4.5). This is specially true for galaxies closer to the mass range of the Milky Way[3], namely the last half of models from Table 4.3 (within an order of magnitude).

Secondly, also immediately noticeable is how the presence of streams not only depends on the surface brightness limit of the image, but also on the mass: the most massive objects tend to aggregate more features, as expected by hierarchical growth, and confirmed also in 4.4, where the same trend for the mass histograms is observed.

The effect of changing the orientation angle can also alter the visual detection of streams in the simulated images. While not particularly significant for the most and less massive galaxies, it has the potential to be relevant for MW-mass galaxies. Figure 4.6 shows three galaxies viewed from three different perspectives. Note how one of the projections changes the morphology interpretation.

To somehow quantify the frequency of tidal streams (recall the limitations stated in Section 3.3.2), Table 4.3 presents a a summary of the most prominent tidal feature detected by visual inspection. The tidal classifications are fully consistent with Section 2.3. Note that uncertain features in here are not truly uncertain, since it is known that the backgrounds used have no diffuse light from galaxies at all. In an attempt to reduce the bias given by simulations, the mock images were visually inspected before the actual models, to emulate what can be done with SDSS processed images. This small experiment can be greatly improved by increasing the amount of background images used to at least 100, in a fully random fashion.

TABLE 4.3: Predominant diffuse tidal features detected by visual inspection using COCO galaxies with observational effects applied, sorted by decreasing halo mass ($M_{200}/10^{10}\ M_\odot$) for three perpendicular orientations. See Section 4.2 for more.

Tag	Halo Mass	x-projection	y-projection	z-projection
cdm-000000	1540.727661	Major Merger	Major Merger	Major Merger
cdm-037906	1526.037109	Shell	Shell	Shell
cdm-070785	1456.970703	Major Merger	Shell	Shell
cdm-098766	1176.434937	dG	dG	dG
cdm-129597	1166.193726	Major Merger	Major Merger	Major Merger
cdm-157734	1024.982300	Major Merger	Major Merger	Major Merger
cdm-175602	851.2978516	Shell, dG	Shell	Shell, dG
cdm-202269	840.2289429	dG	dG	dG
cdm-226523	585.4128418	dG, Arc	dG	dG
cdm-242754	428.2441711	Shell	Shell	-
cdm-257060	440.8923645	Umbrella	Arc	Shell
cdm-270031	418.9203491	Shell	Shell	Shell
cdm-279859	409.6905518	Shell	Shell	Shell
cdm-287449	403.1407471	Arc	Arc	Arc
cdm-296558	400.8192749	Shell	-	Shell
cdm-303625	393.0110779	-	-	-

[3]The mass of the MW halo has been measured to be $\sim 10^{12}\ M_\odot$, see Xue et al. (2008), McMillan (2011), McMillan (2017), and Ninković (2017).

Table 4.3 continued from previous page

Tag	Halo Mass	x-projection	y-projection	z-projection
cdm-319291	384.8261719	Shell, Umbrella	Shell, Umbrella	Shell
cdm-326326	346.9300232	uncertain	uncertain	Shell
cdm-331344	341.2802429	dG	dG	dG
cdm-337587	286.4193420	Shell	-	-
cdm-350462	242.2131958	-	-	-
cdm-354563	230.1257324	Shell	-	Shell
cdm-360072	200.9082031	uncertain	-	uncertain
cdm-366117	196.1129456	dG	dG	dG
cdm-375907	193.1515808	Shell	Shell, dG	Shell, dG
cdm-381188	178.5150604	Shell	uncertain	Umbrella
cdm-386970	173.0773468	-	-	Shell
cdm-399930	167.8917542	Umbrella	uncertain	Umbrella
cdm-403717	166.9986420	Shell	-	Shell
cdm-407643	156.4916077	uncertain	Umbrella	Umbrella
cdm-410049	155.4548340	dG	dG	Shell, dG
cdm-421034	148.2039490	-	-	-
cdm-424148	147.2010040	Umbrella	Umbrella	Umbrella
cdm-427222	144.3229065	uncertain	Shell	-
cdm-431047	139.5342712	dG	dG	dG
cdm-437876	137.9163818	uncertain	uncertain	-
cdm-441439	137.0555115	-	-	-
cdm-444756	135.2365265	uncertain	Shell	Shell
cdm-452986	133.5937347	-	-	-
cdm-460585	130.0959930	Shell	uncertain	Shell
cdm-462710	129.1551971	-	-	-
cdm-467970	118.1932907	dG	Shell, dG	Shell, dG
cdm-479959	121.3956757	-	-	-
cdm-482306	117.0206223	dG	dG	dG
cdm-486990	115.9994507	uncertain	-	-
cdm-489418	99.64174652	dG	dG	dG
cdm-493928	98.66640472	dG	dG	dG
cdm-496706	93.87747192	Shell	Shell	Shell
cdm-503430	93.64327240	-	-	-
cdm-507911	92.47998047	-	-	-
cdm-518575	86.84859467	-	-	-
cdm-523429	86.66194153	-	Shell	Shell
cdm-525089	86.54150391	-	-	-
cdm-528703	77.84540558	Shell	Shell	Shell
cdm-530810	75.09019470	-	-	-
cdm-534617	74.84310913	-	-	-
cdm-536606	74.44625854	-	-	-
cdm-539188	73.89627075	dG	dG	dG
cdm-542496	68.00929260	-	-	-
cdm-543950	66.76550293	-	-	-
cdm-545227	66.17815399	Shell	Shell	Shell
cdm-547722	66.12858582	uncertain	uncertain	-
cdm-559403	61.45307159	-	-	-
cdm-560813	59.25858307	-	-	-
cdm-562409	59.21010208	-	-	-

Table 4.3 continued from previous page

Tag	Halo Mass	x-projection	y-projection	z-projection
cdm-563544	57.69398117	Shell	Shell	Shell
cdm-564914	57.58187485	-	-	-
cdm-566166	57.05669022	Shell	Shell	Shell
cdm-567390	56.66251373	-	-	-
cdm-568888	56.43365479	-	-	-
cdm-572956	55.52494431	-	-	-
cdm-574232	55.14844131	Shell	-	-
cdm-577844	54.76765442	-	-	-
cdm-579199	50.50572968	-	-	-
cdm-584355	49.53644180	-	-	-
cdm-590068	47.82743073	dG	-	dG
cdm-591010	46.21907043	-	-	-
cdm-593364	45.88446045	-	-	-
cdm-595376	45.05766296	-	-	-
cdm-598850	44.40703964	Shell	Shell	Shell
cdm-599897	43.26707458	-	dG	dG
cdm-606999	42.96558380	-	-	-
cdm-608984	41.60479736	-	Shell	uncertain
cdm-614033	41.52002716	-	-	-
cdm-622655	41.43123627	-	-	-
cdm-624281	41.30025482	-	-	-
cdm-624984	41.22692108	-	-	-
cdm-630525	39.39570618	-	-	-
cdm-631272	38.02096176	-	-	-
cdm-632038	36.55353165	-	-	-
cdm-632814	36.21188354	-	-	-
cdm-641891	35.15205383	-	-	-
cdm-647880	34.85165405	-	-	-
cdm-649510	34.16174698	-	-	-
cdm-662791	32.85768127	-	-	-
cdm-664093	30.94861031	-	-	-
cdm-668361	30.92017174	-	-	-
cdm-674619	27.31340599	-	-	-
cdm-681661	26.95627594	-	-	-
cdm-702124	21.47602272	-	-	-

By simply counting only the features surely to be tidal streams (i.e. leaving aside structures with DCL 1 or 2, tagged as uncertain in Table 4.3), and considering realizations no more than $M_{200} \sim 150\ M_{\odot}$ (to not go farther than one order of magnitude from MW-mass galaxies), it is found that the frequencies of tidal features from simulations with observational effects are: 16%, 19% and 18% for each projection, x, y and z. While these numbers are not far off from the range reported in Section 2.3, some degree of excess in the amount of dwarf galaxies and partially disrupted cores can be inferred from the mock images, when compared to the processed SDSS images. It remains to be seen whether they are over-produced in the COCO simulations (recall the missing satellites problem), or are simply still too bright in the mock catalogue generated by this work.

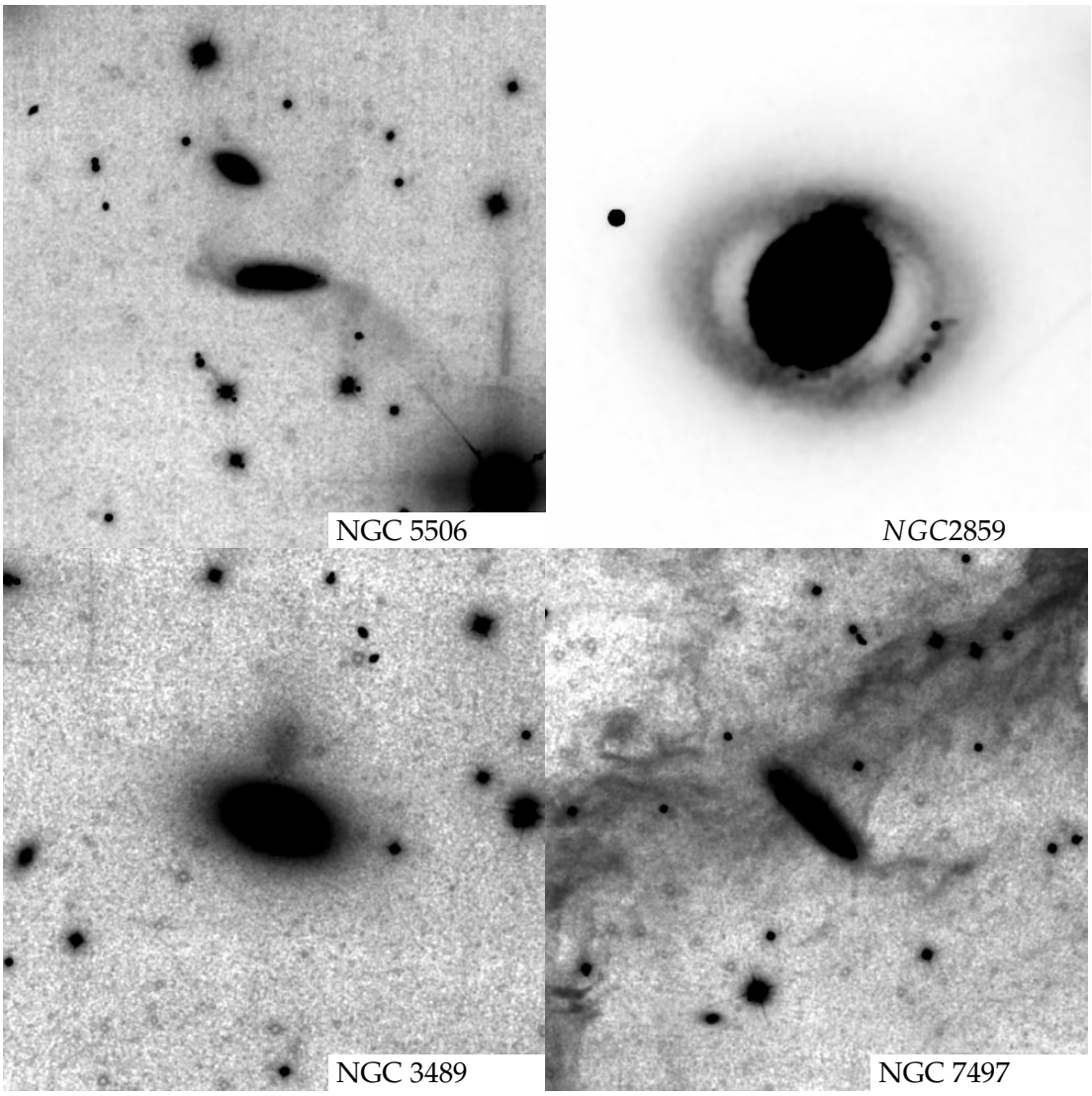

FIGURE 4.1: Examples of very faint diffuse overdensities of different types found during our analysis: i) giant stellar warps of a galactic disk (NGC 5506); ii) a stellar ring with two seemingly interacting, partially disrupted cores embedded in it (NGC 2859); iii) an image artifact resembling a giant satellite (NGC 3489); and iv) extensive Galactic cirrus around NGC 7497. All these images have been processed with our technique, adapted from Miskolczi, Bomans, and Dettmar (2011), using stacked SDSS *g*, *r*, an *i* band images, with a field of view of 30 arcminutes. North is up, east to the left.

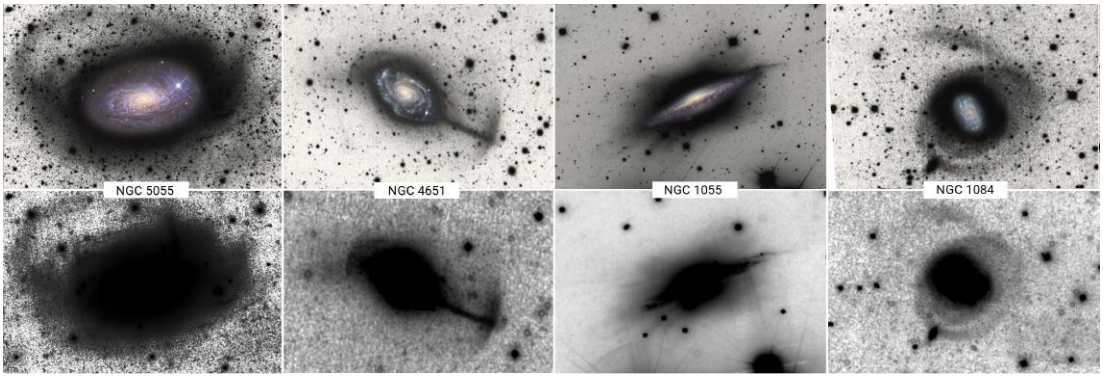

FIGURE 4.2: Comparison between our processed SDSS images and the deep images from the STSS (see Sec. 2.2) for the spiral galaxies (from left to right) NGC 5055, NGC 4651, NGC 1055, and NGC 1084. Top row: Images taken from Martínez-Delgado et al. (2010). Bottom row: This work, using SDSS data, after processing as described in Miskolczi, Bomans, and Dettmar (2011), stacking *g*, *r* and *i* band images. Even at the shallower depth reached by the SDSS, high-confidence detections can be made with our technique. North is up, east to the left.

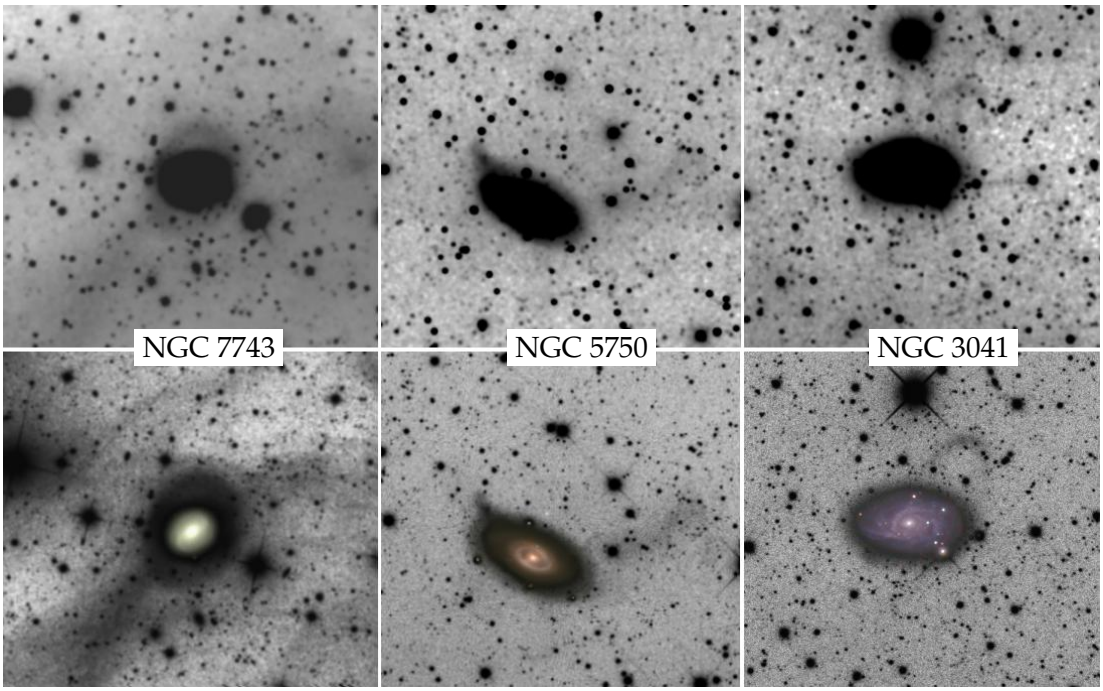

FIGURE 4.3: Examples of some follow-up images used to confirm stellar tidal stream candidates in our sample. The top row shows the SDSS *g*-*r*-*i* stacked images for NGC 7743, NGC 5750, and NGC 3041 (see Chapter 4) processed as described in Sec. 2.3, and kindly provided by A. Miskolczi. The bottom row shows the deep images obtained by the STSS (Martínez-Delgado et al., in prep.) for the same objects, but with a luminance filter. In all cases, the deeper images detect additional features or reveal a more detailed morphology of the features detected in the SDSS images.

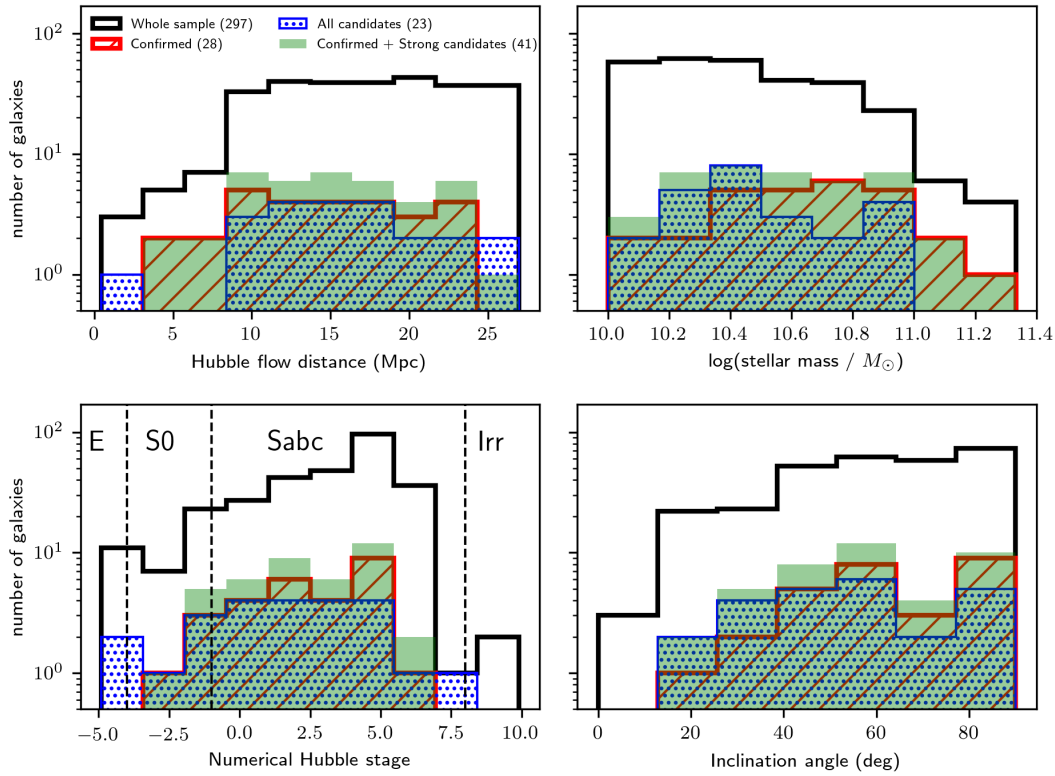

FIGURE 4.4: Histograms of the diffuse-light features found in our whole sample, with or without overdensities, as a function of target distance, stellar mass, morphology and inclination angle. The distribution of all 297 galaxies in our sample is shown in black, while histograms in color correspond to the galaxies listed in Table 4.1, our main results. The red distributions represent 28 confirmed features, previously known and new (with a DCL of 4; see Sec. 4.1.2). Unconfirmed feature candidates (with a DCL of 1 and 2) are represented by blue dotted histograms. Confirmed streams and strong candidates (i.e., every feature with a DLC of 3 or 4) are grouped together in the solid green histogram (41 targets). For our limiting sky surface brightness of 28.1 $\pm$ 0.3 mag arcsec^{-2}, this implies that $\approx$ 14% of the galaxies in the mass and volume limits our parent sample have detectable stellar overdensities in their outskirts. No significant biases are apparent in our sample of galaxies with diffuse overdensities (with respect to the S4G parent sample, black solid line) except for a somewhat flatter distribution of stellar mass and the lack of overdensities for galaxies more distant than 35 Mpc.

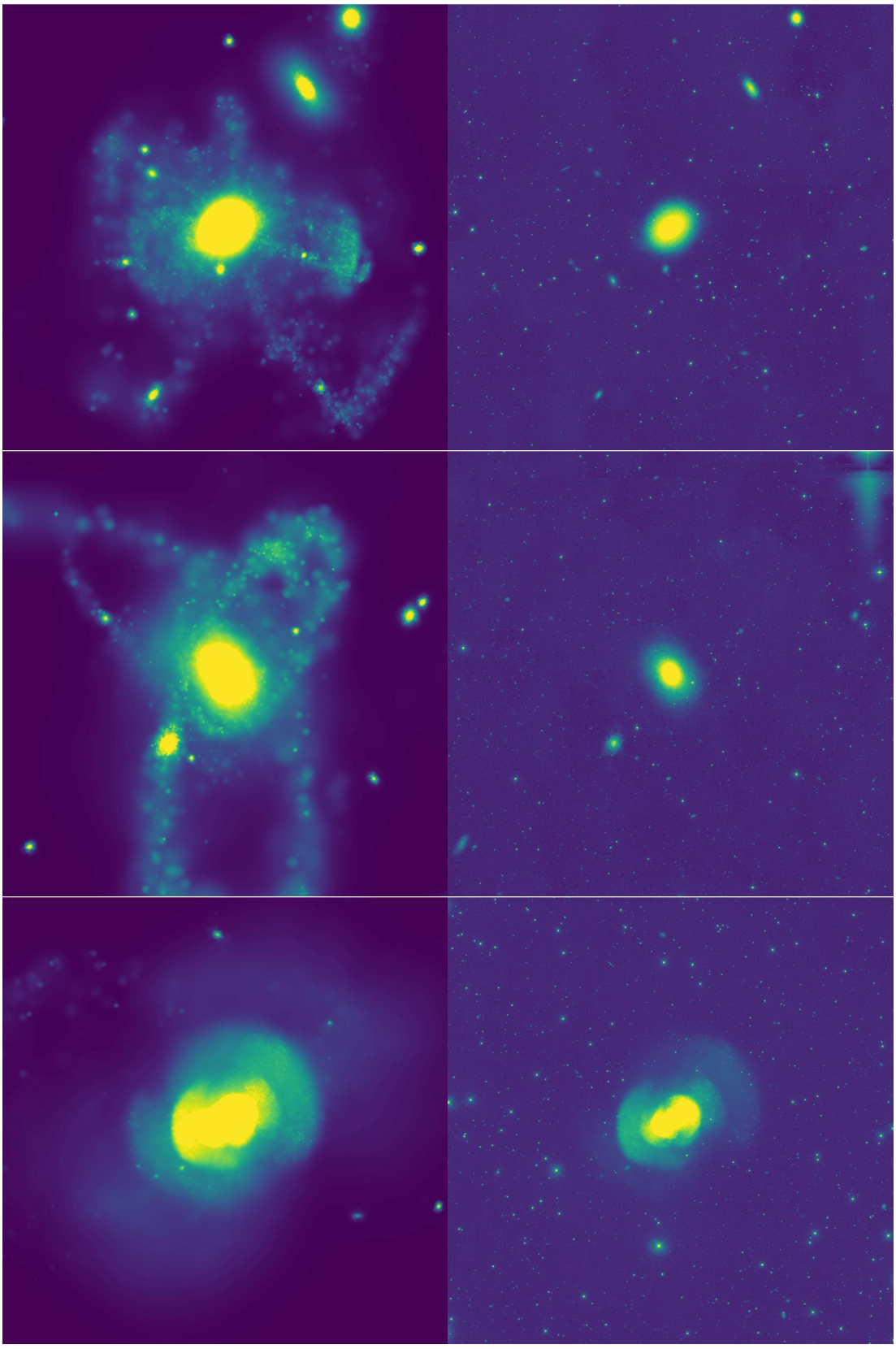

FIGURE 4.5: Three different examples of how observational effects lowers the detectability of tidal streams in the models. Model to the left, mock image to the right. Tags from Table 4.3: cdm-507911, cdm-560813, cdm-566166.

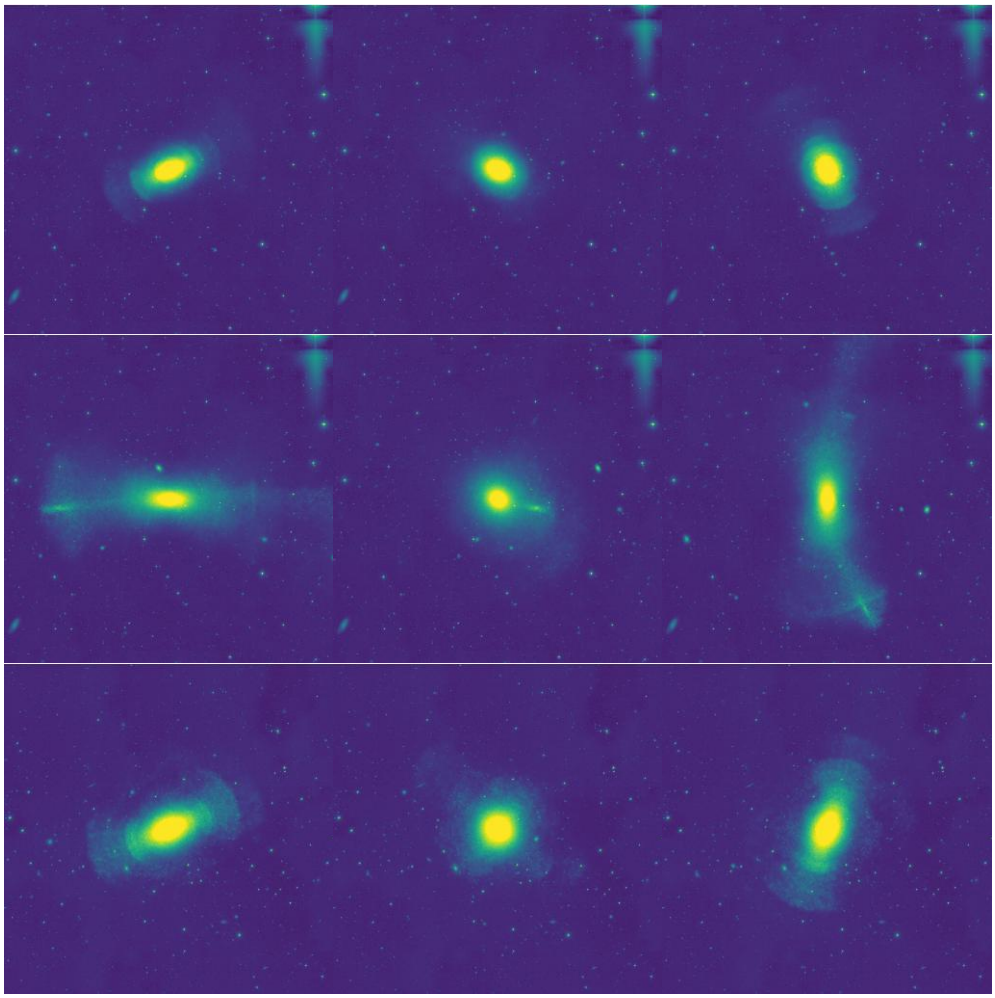

FIGURE 4.6: Examples on the effect of orientation in the visual interpretation of stream morphologies. Each row is one MW-mass halo seen from three different axes, one per column. Tags from Table 4.3: cdm-354563, cdm-399930, cdm-460585.

Chapter 5

Conclusions

We have estimated the frequency of stellar tidal streams in the halos of massive galaxies in the local Universe by processing SDSS images to reveal low surface brigthness features, using a technique similar to that of Miskolczi, Bomans, and Dettmar (2011). Our results are summarized in Table 4.1. To facilitate statistical comparisons with cosmological simulations of galaxy formation, we have defined a volume-, mass-, and size-limited parent sample of galaxies with stellar masses similar to that of the Milky Way based on the S4G catalog. From the 2331 galaxies listed by S4G, our sample selects 297 targets from the SDSS footprint (excluding low Galactic latitudes, major mergers, and the Virgo cluster). We estimate that the typical surface brightness limit of the SDSS images for these galaxies (after stacking their g, r, and i band images) is 28.1 $\pm$ 0.3 mag arcsec^{-2}.

By visual inspection, we detected a total of 28 confirmed tidal streams, including new features discovered in this study and some previously known tidal streams. Therefore, our most conservative estimate is that 9% of the galaxies in our sample show evidence of diffuse features that may be linked to minor merging events (either stellar or gaseous streams, or a mixture of both). This fraction of galaxies displaying tidal features does not include the possible new, but unconfirmed detections listed in Table 4.1. When we also count the systems with high-confidence detections (i.e., with a DCL of 3 or 4), the frequency of tidal features in our sample rises to 14%. It is important to remark that some of these diffuse-light features may still not be the signature of dwarf satellite remnants, but instead Galactic cirrus, imaging artifacts, or distorted spiral arms. This underscores the importance of deeper observations to confirm the nature of these features (see Fig. 4.1).

These results are consistent with comparable studies cited in Chapter 1. Although the surface brightness limits of the observations used in these earlier studies are more or less compatible, the wide variety of sample selections limits a more detailed comparison of the final results. Bright tidal features are expected to be relatively more likely in ETGs, while the only analogous study for disk galaxies (Miskolczi, Bomans, and Dettmar, 2011) was also less statistically representative of the galaxy population because it was focused on testing the image processing method. Comparisons with simulations are still needed, and will be reported elsewhere.

When reporting galactic tidal features by visual inspection was performed in (Atkinson, Abraham, and Ferguson, 2013), the authors used the Canada-France-Hawaii Telescope Legacy Survey for a sample of 1781 luminous (< -19.3 mag) galaxies in the

magnitude range 15.5 mag $< r <$ 17 mag, and found that around 12% of the galaxies in their sample showed clear tidal features at the highest confidence level, with the fraction rising to 18% when weaker signatures of tidal origin were included. The colors and stellar masses of central galaxies were found to influence these numbers significantly: linear features, shells, and fans were found much more likely to occur in massive galaxies with stellar masses $> 10^{10.5}$ $M_{\odot}$, and red galaxies were found to be two times more likely to show tidal features than blue galaxies.

These results are also broadly consistent with comparable studies of elliptical galaxies, where bright tidal features are expected to be relatively more likely. In Kaviraj (2010), the authors found that $\sim$ 18% of the early-type galaxies (ETGs) in their sample exhibited signs of disturbed morphologies (e.g., shells). This sample was also based on SDSS multiband galaxies, but combined with the significantly ($\sim$ 2 mag) deeper monochromatic images from the public SDSS Stripe 82.

Last, because our procedure for enhancing images to detect low surface brightness features relies on stacking images in multiple filters and because those features have an intrinsically low S/N, we cannot measure their colours. To do so, deeper multiband imaging is needed, and will be valuable to constrain stellar populations and masses of the merging systems. Discussion of the physical properties of the features we detected and their comparison to the newest simulations is beyond the scope of this article. These topics will be addressed in a forthcoming paper.

When simulations are included, Figures A.4, A.5 and A.6 in Appendix A show an overview of the models. When this models are embedded in an identical SDSS environment (yet not entirely representative), this generates the mock images shown in Figures A.7, A.8 and A.9 also in Appendix A.

In this context, it is confirmed once more that mass and surface brightness limit play a defining role on the frequency of detectable streams. Orientation angles have a role to play in the assumed morphologies of these tidal satellites, specially when satellite planes are considered. Regarding the final estimated frequency of observable minor merging processes, it has been found that the occurrence of tidal features from simulations with observational effects are in the range of $16 - 19$%, with a bit of an excess possibly coming from small, compact galaxies, or partially disrupted cores.

While the discussion of the physical properties of the features detected and their comparison to state-of-the-art simulations is covered, their insight is somehow limited:

1. This study only tests a qualitative method based on visual inspection and data analysis. Ultimately, a quantitative measure for the (hopefully automatic) detection of diffuse, extended light structures is crucially needed in this field.

2. The mock catalogue can still be improved. The correct M/L ratio has yet to be inferred and their distribution along the SDSS optical bands computed.

3. More random SDSS backgrounds can be used and selected semi-blindly, to truly span the wide range of effects that can influence stream detectability.

4. The simulations used have no disk component. This means that any structure connected to the presence of disks in real images have no analogue relationship in the mock catalogue. The presence of disk in galaxies could alter and disrupt the presence of satellites very close to them, which in turn may impact somehow their morphologies and detectability by diluting their brigthness contribution in the background.

All of these issues have the potential to be addressed in subsequent publications.

While this work has been proposed as the first step towards using a well-defined sample to make a phenomenological comparison between data and models in the context of diffuse tidal features around galaxies, new simulations and surveys conducted in the future will enable future researchers to continue learning about the role of minor mergers in the local Universe, as shown throught out this thesis, by using tidal streams as a tool for cosmological diagnostics.

Appendix A

Processed images.

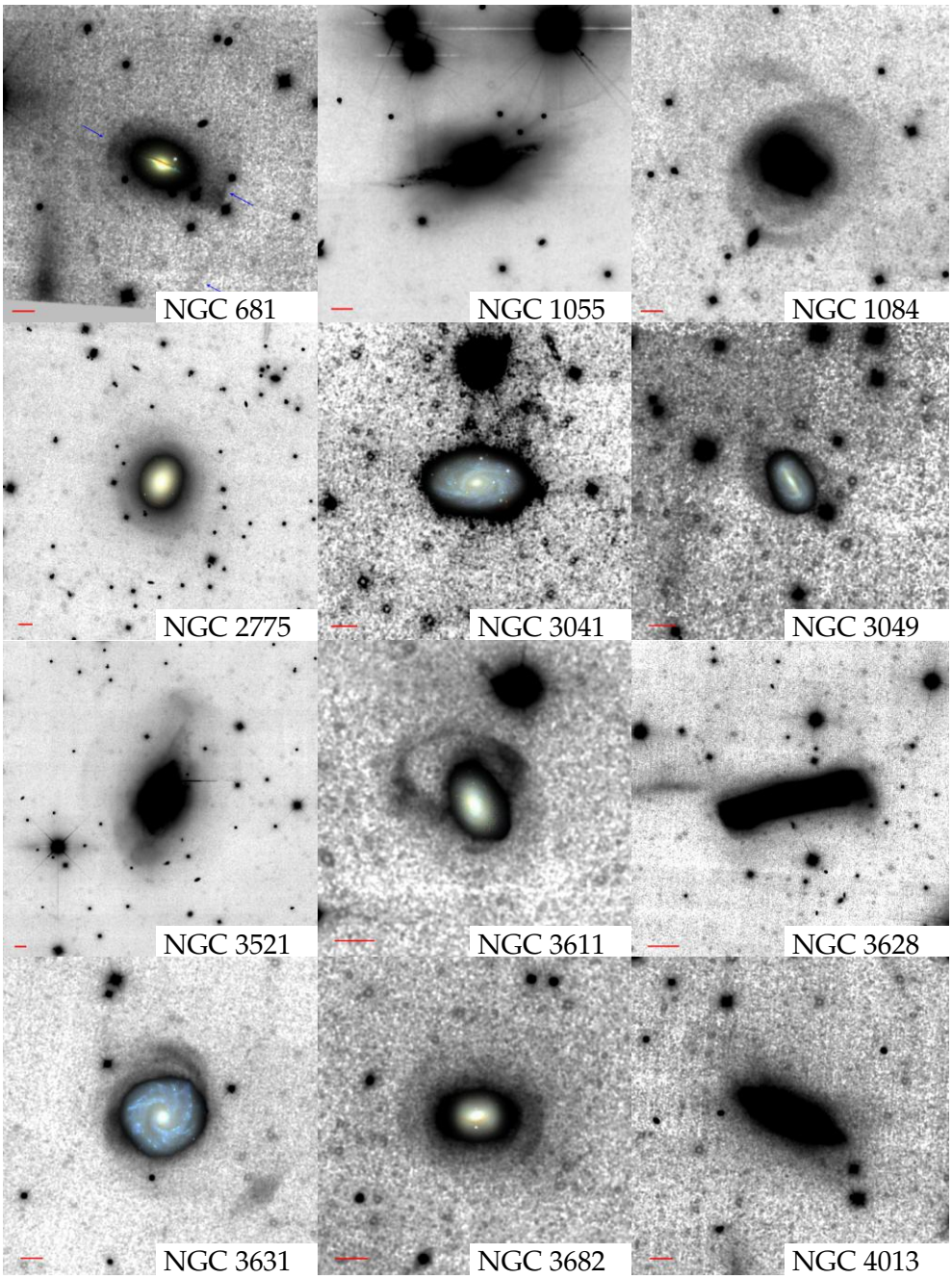

FIGURE A.1: Galaxies from Table 4.1 obtained by stacking *g-r-i* SDSS bands as described in this work. Streams already reported in previous publications are not included. The red lines indicate a scale of 3 arcminutes. In some cases, blue arrows indicatestructures of interest described in Chapter 4. North is up and east to the left.

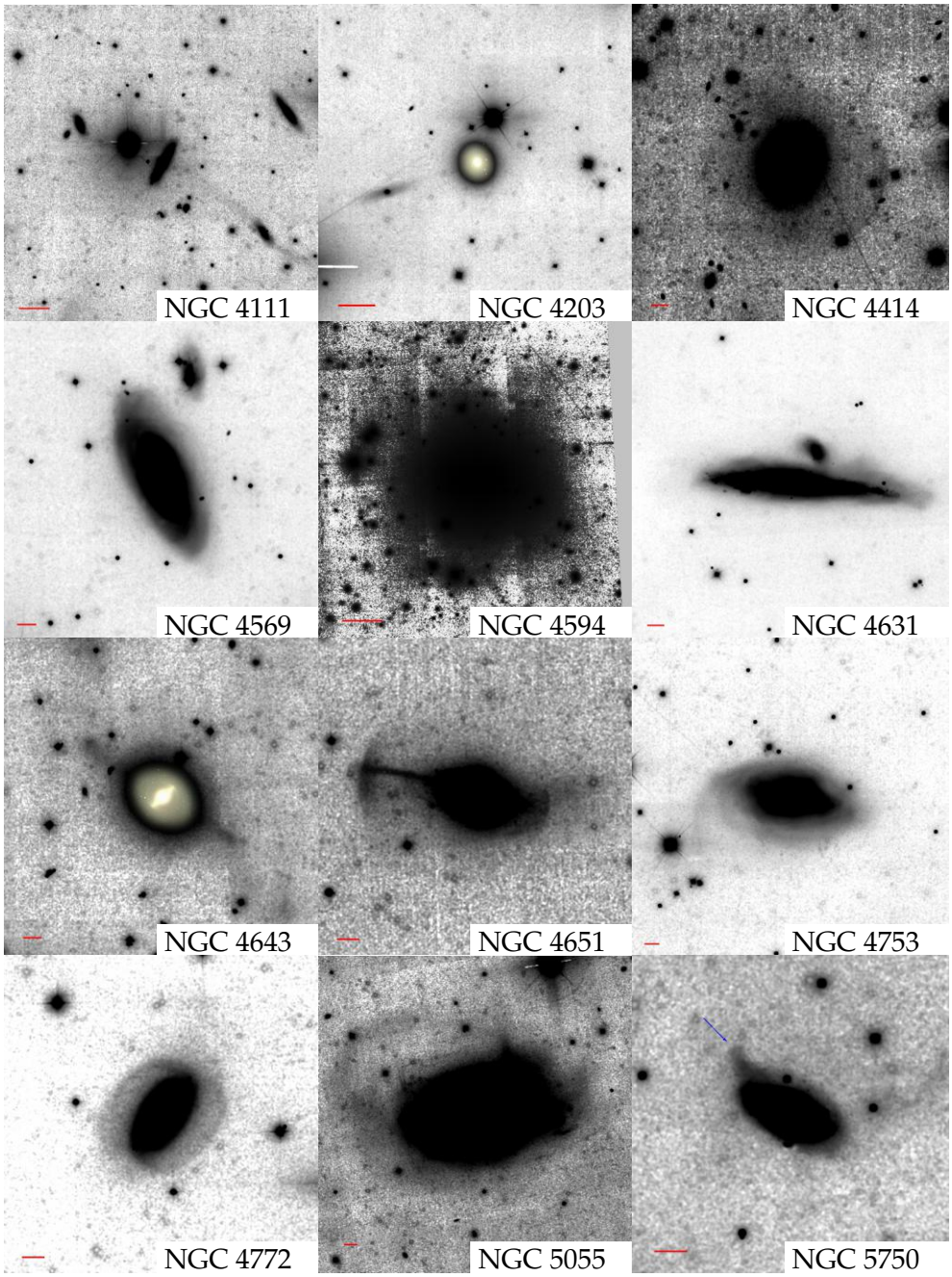

FIGURE A.1: (Continuation)

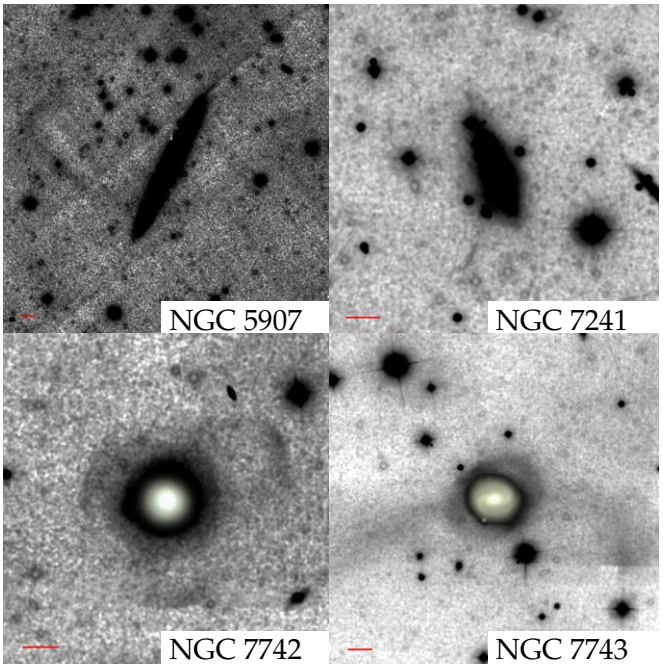

FIGURE A.1: (Continuation)

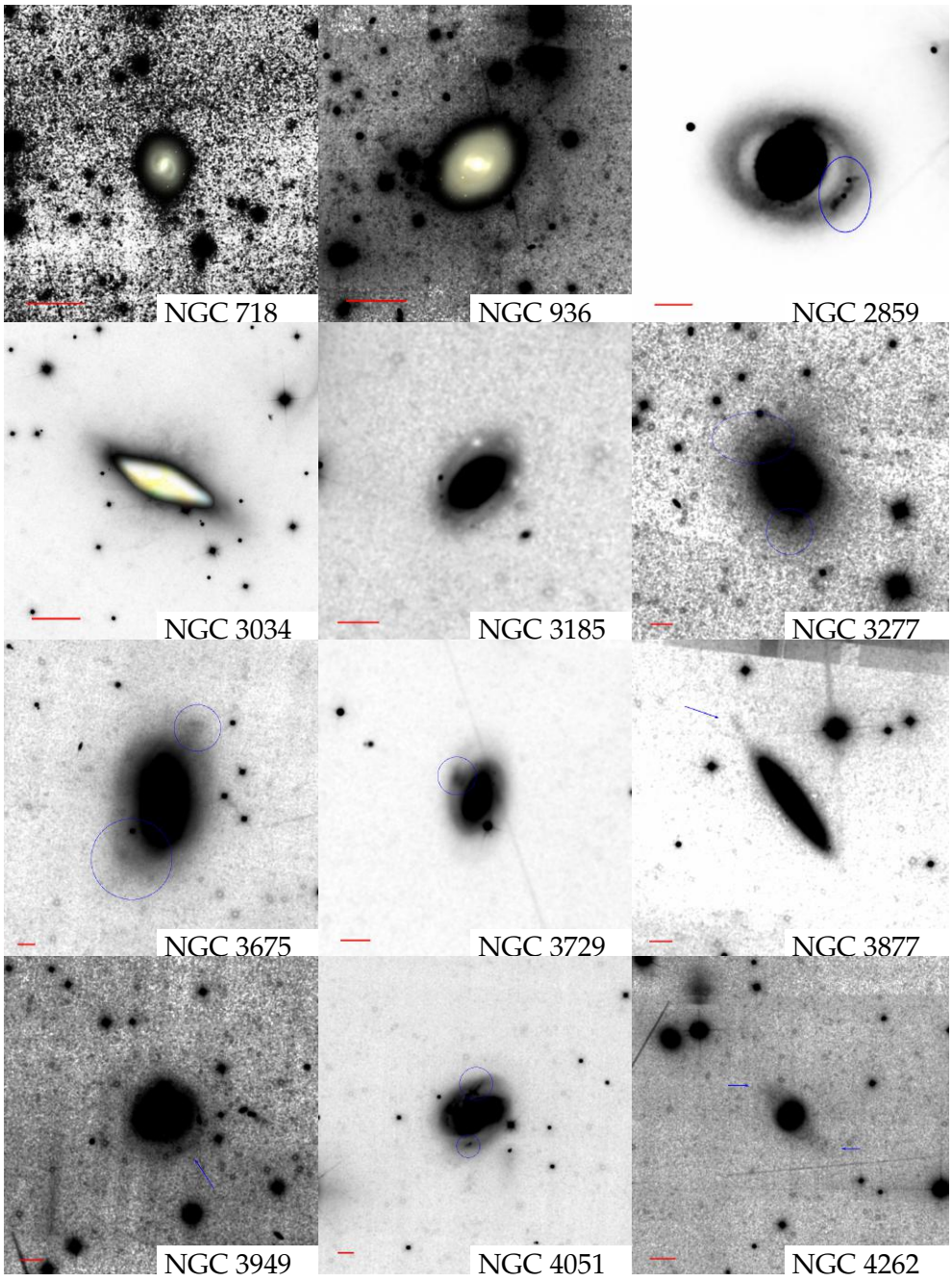

FIGURE A.2: Diffuse light features detected around the galaxies, listed in Table 4.1 with DCL 1 or 2. Deeper data are needed to confirm their origin (e.g., tidal streams, galactic perturbations, extended spiral arms, etc). The red lines indicate a scale of 3 arcminutes, with north pointing upwards and east to the left. Color insets (optical bands) have been added whenever possible.

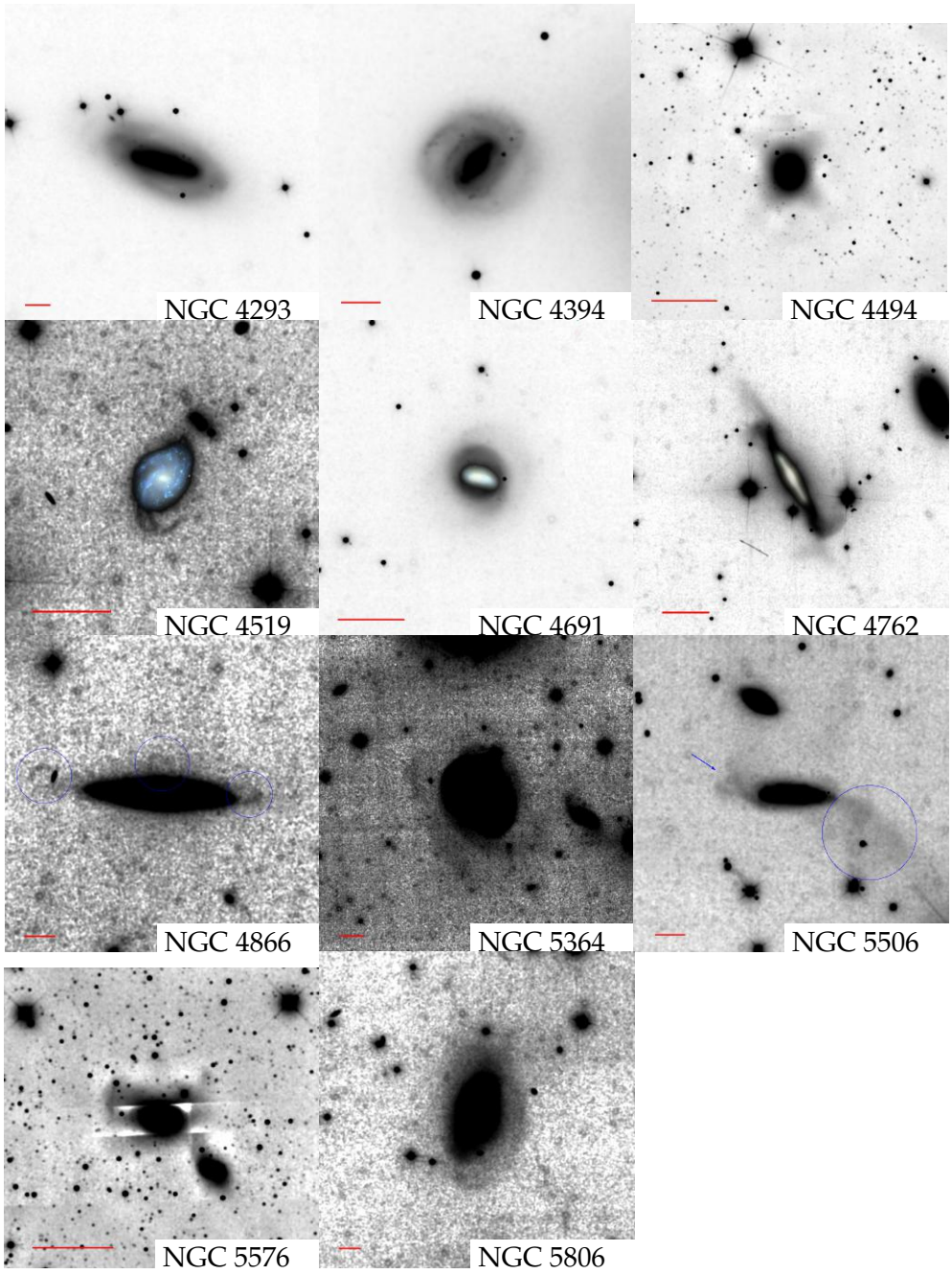

FIGURE A.2: (Continuation)

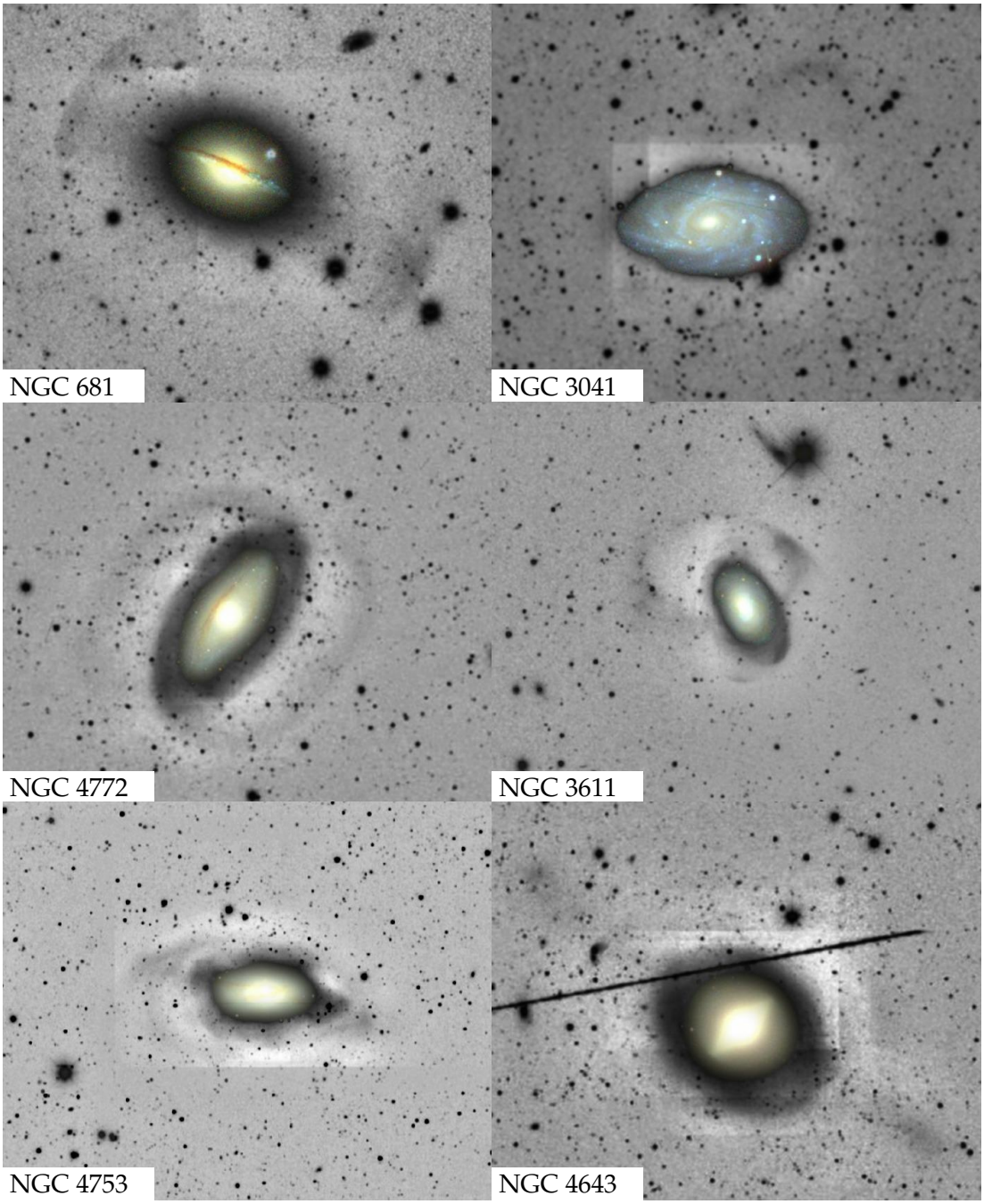

FIGURE A.3: Images taken from DECaLS public survey, confirming some of the findings reported in this thesis. See Figure A.1 for more information. A color inset of the disk of each galaxy taken from this survey has been included as reference.

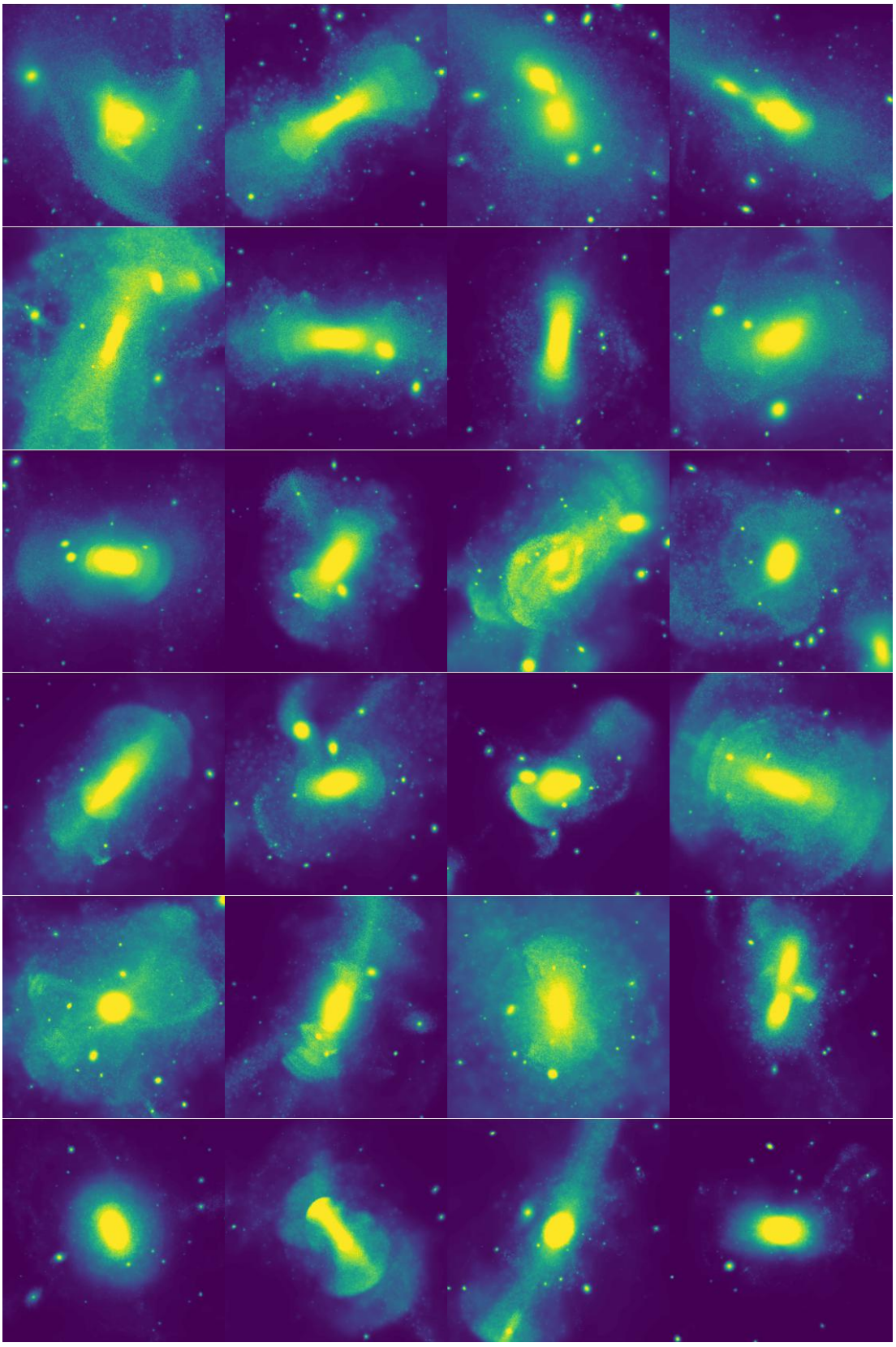

FIGURE A.4: COCO galaxies sorted by decreasing mass, x-axis projection, spanning 300×300 kpc^2. The color encodes logarithmic magnitudes in the AB scale, with a surface brightness limit of 35 mag arcsec^{-2}.

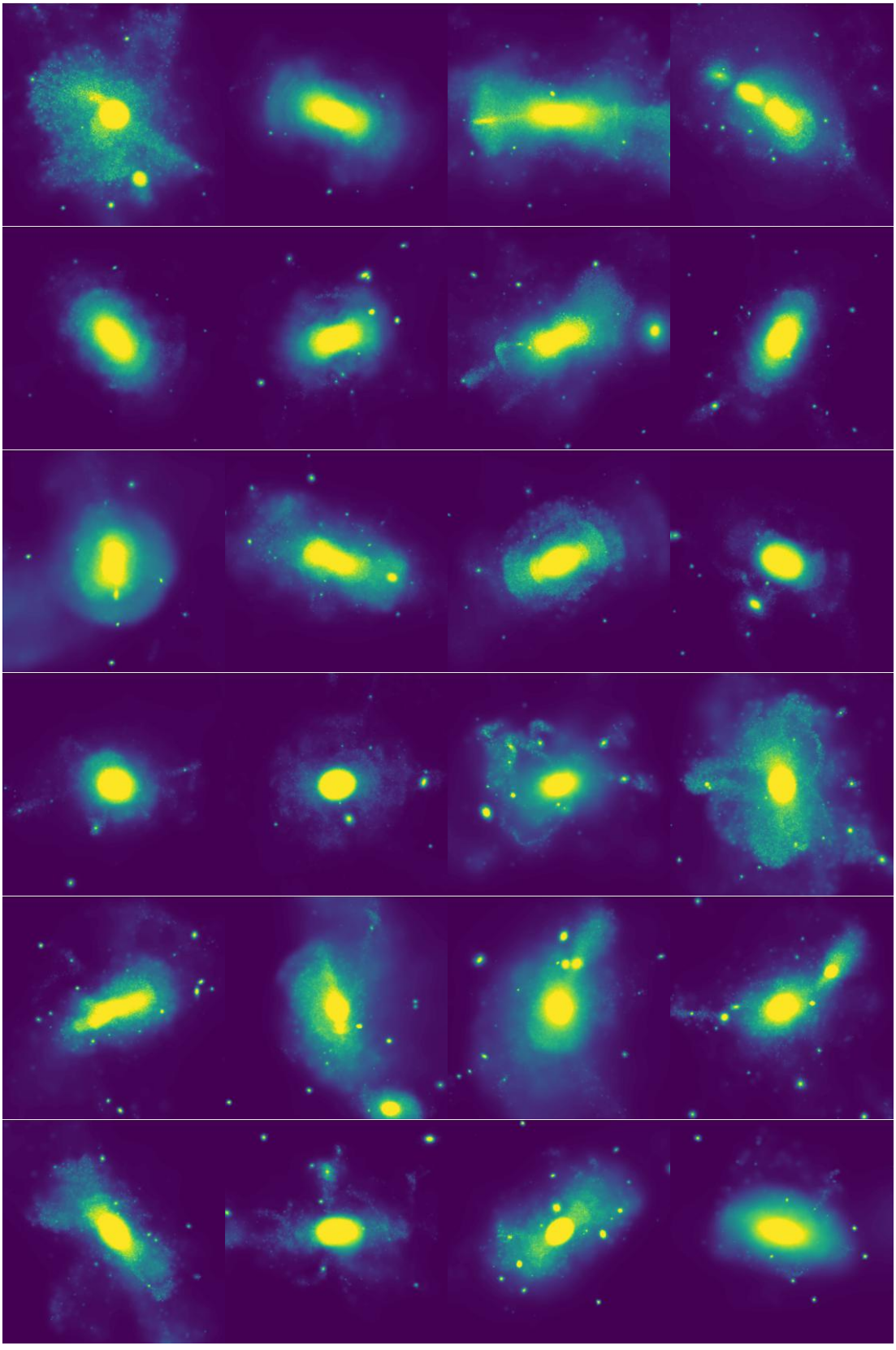

FIGURE A.4: (Continuation)

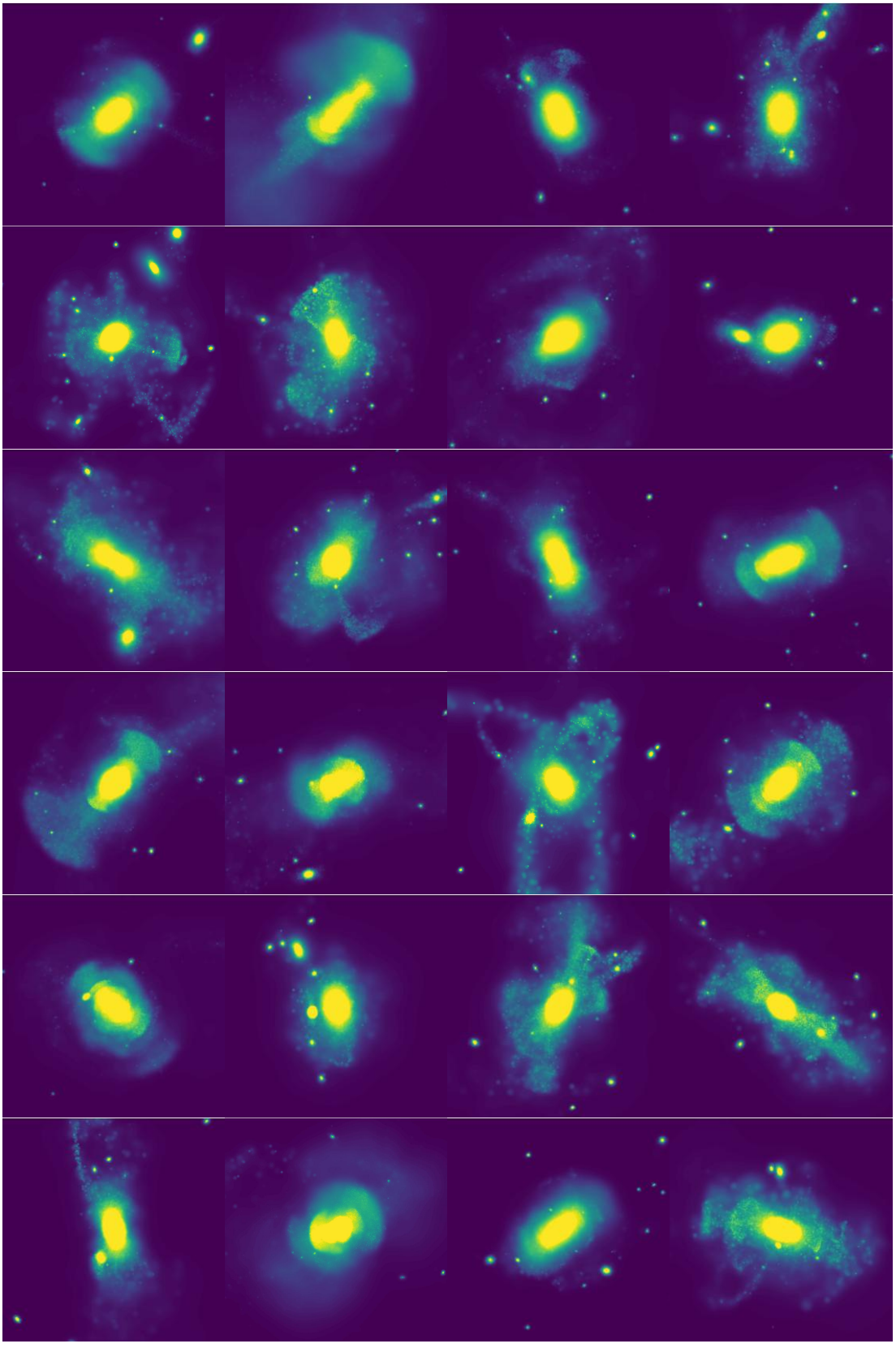

FIGURE A.4: (Continuation)

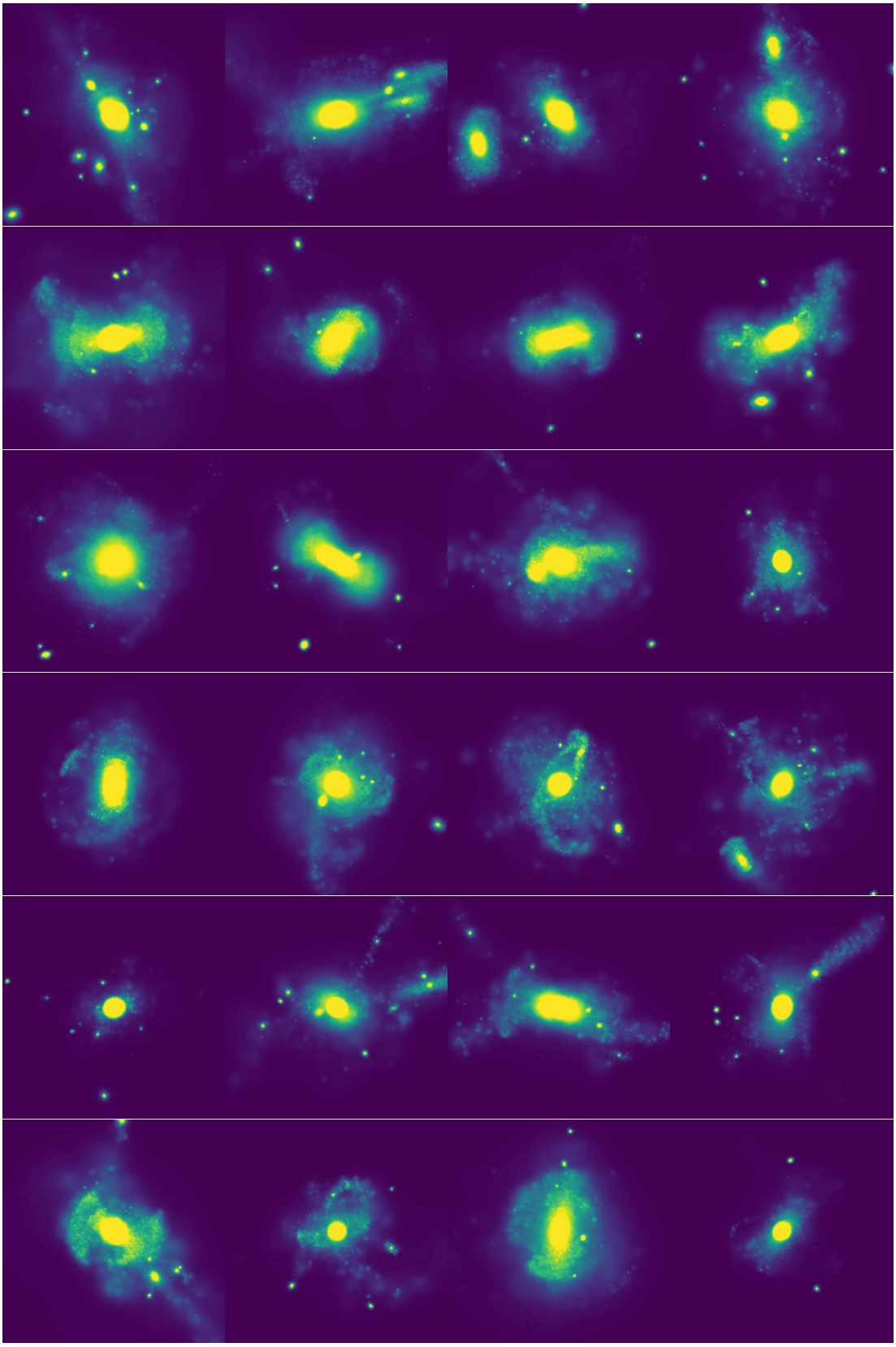

FIGURE A.4: (Continuation)

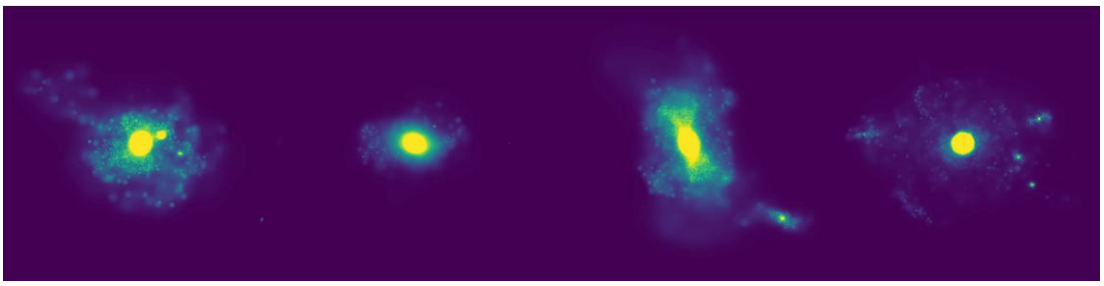

FIGURE A.4: (Continuation)

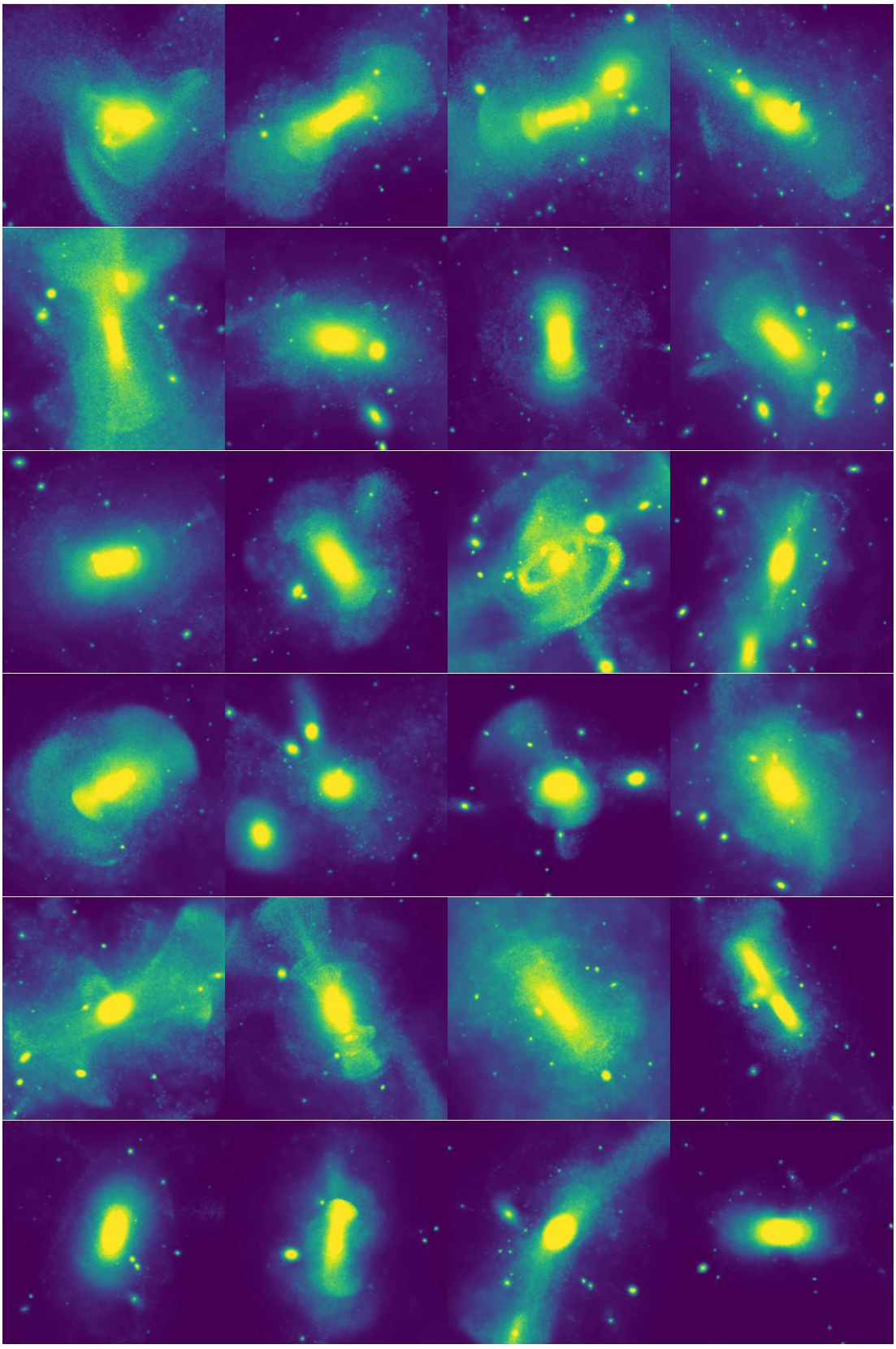

FIGURE A.5: COCO galaxies sorted by decreasing mass, y-axis projection, spanning 300×300 kpc^2. The color encodes logarithmic magnitudes in the AB scale, with a surface brightness limit of 35 mag arcsec^{-2}.

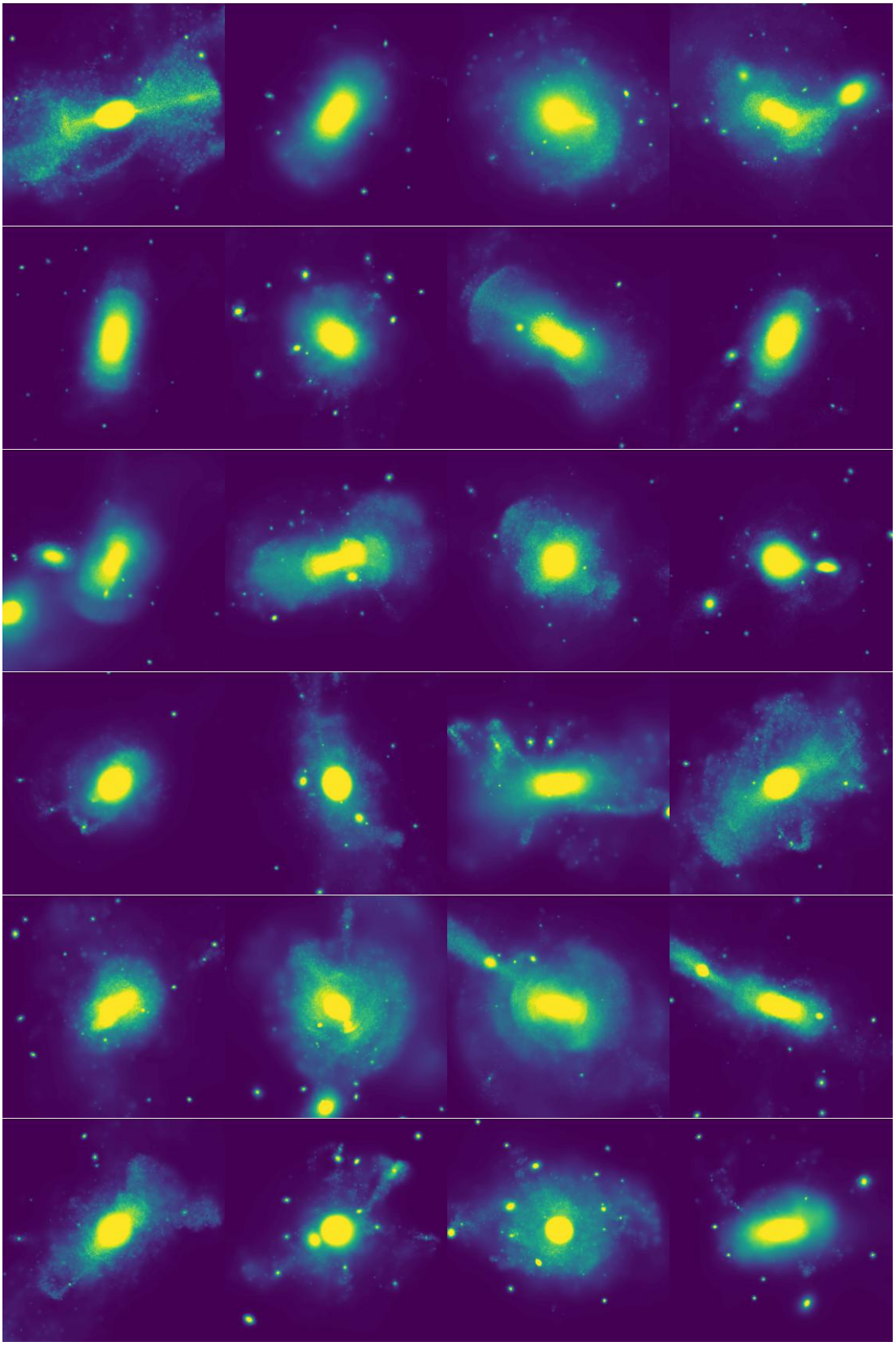

FIGURE A.5: (Continuation)

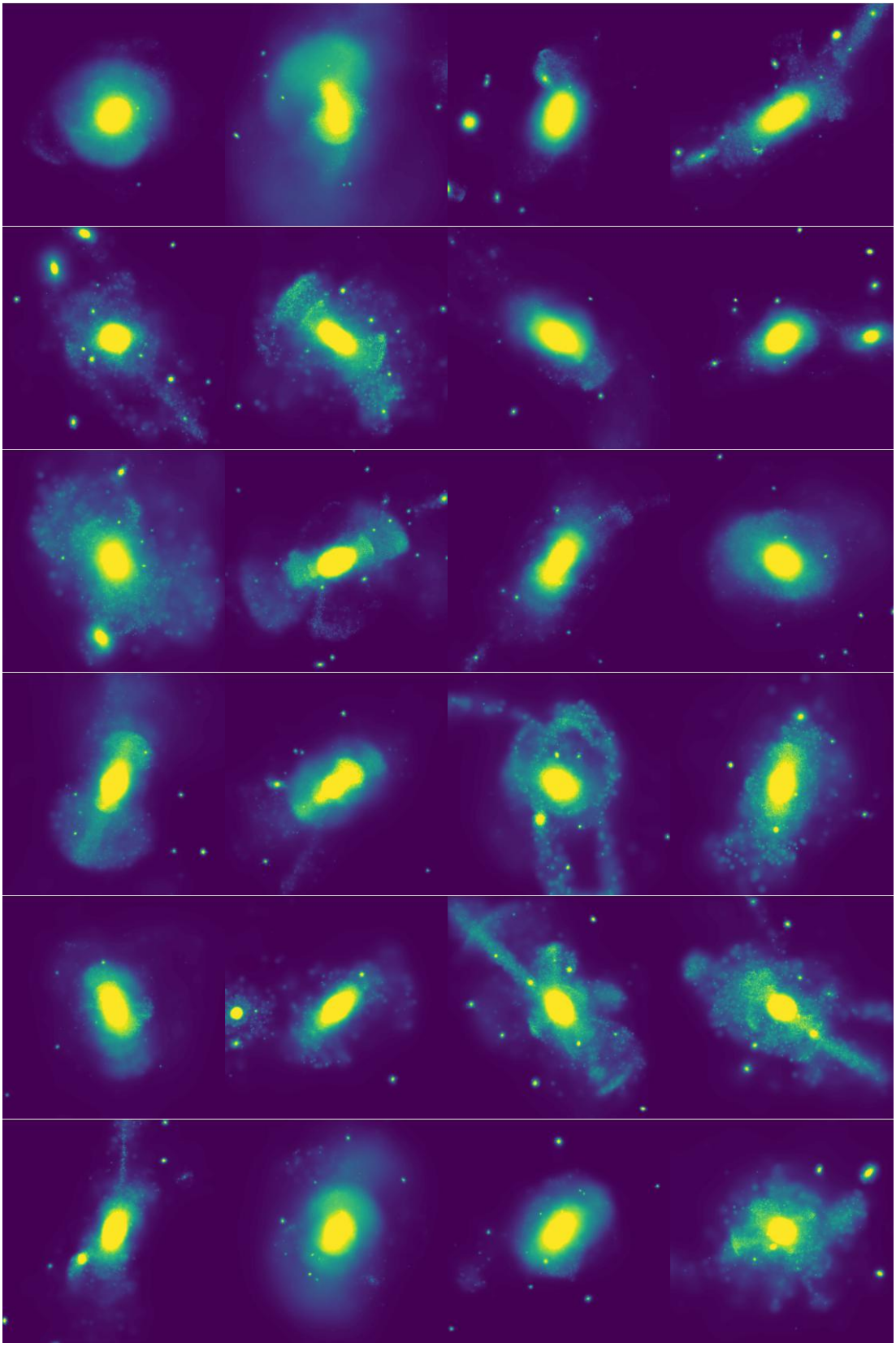

FIGURE A.5: (Continuation)

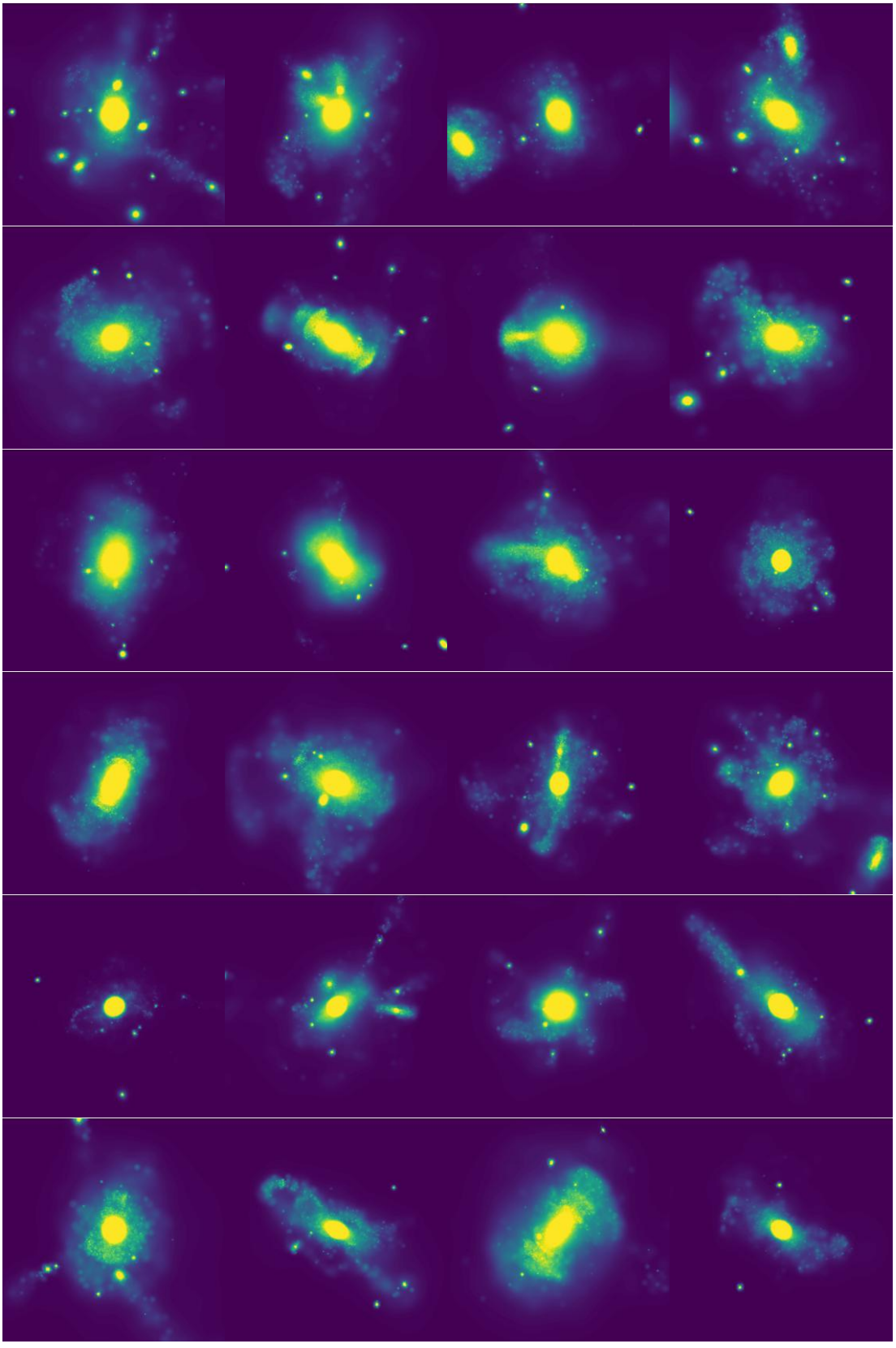

FIGURE A.5: (Continuation)

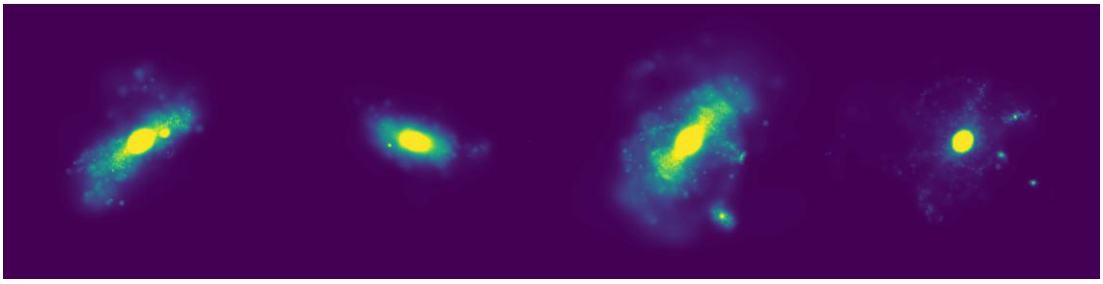

FIGURE A.5: (Continuation)

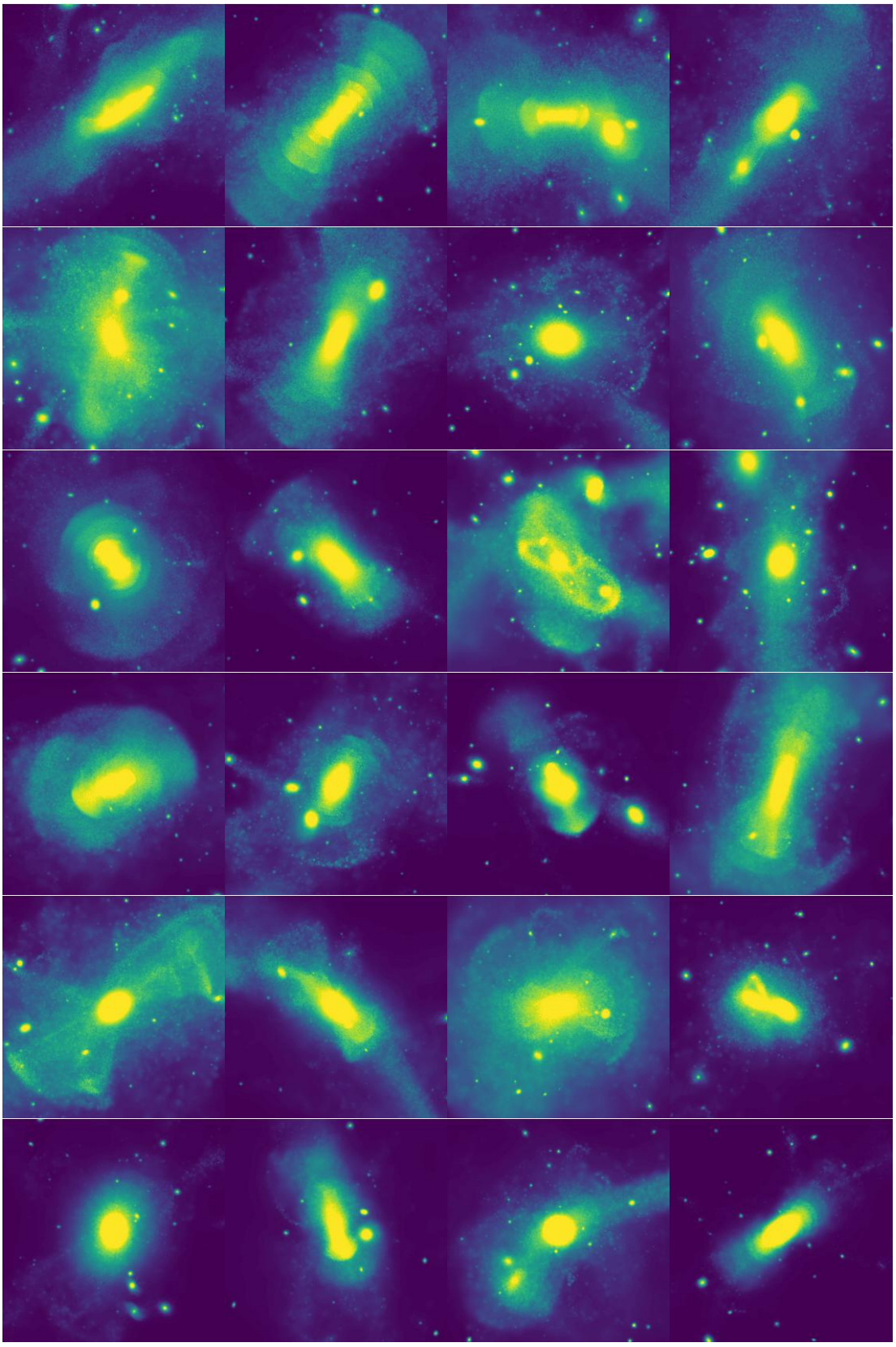

FIGURE A.6: COCO galaxies sorted by decreasing mass, z-axis projection, spanning 300×300 kpc^2. The color encodes logarithmic magnitudes in the AB scale, with a surface brightness limit of 35 mag arcsec^{-2}.

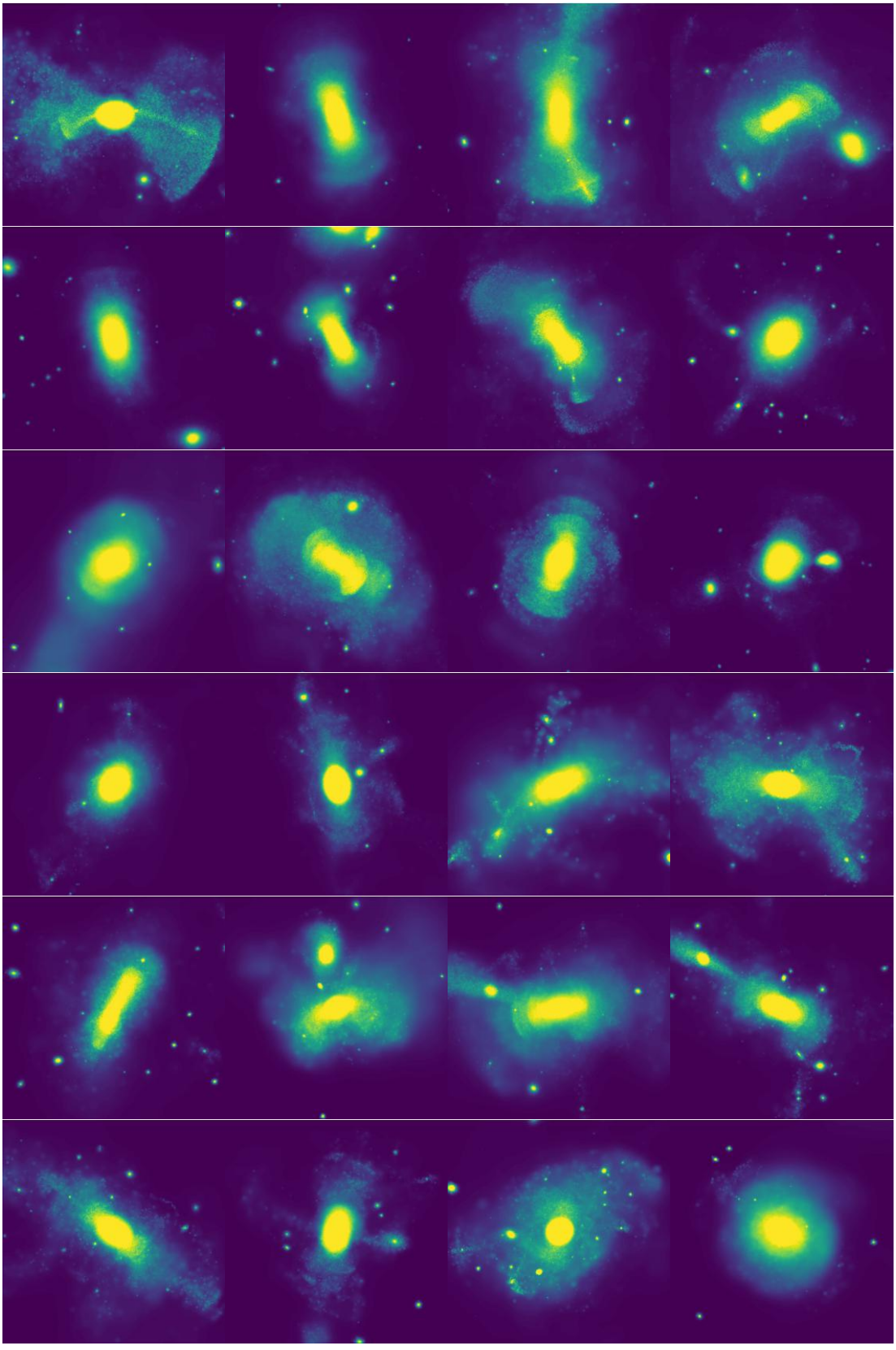

FIGURE A.6: (Continuation)

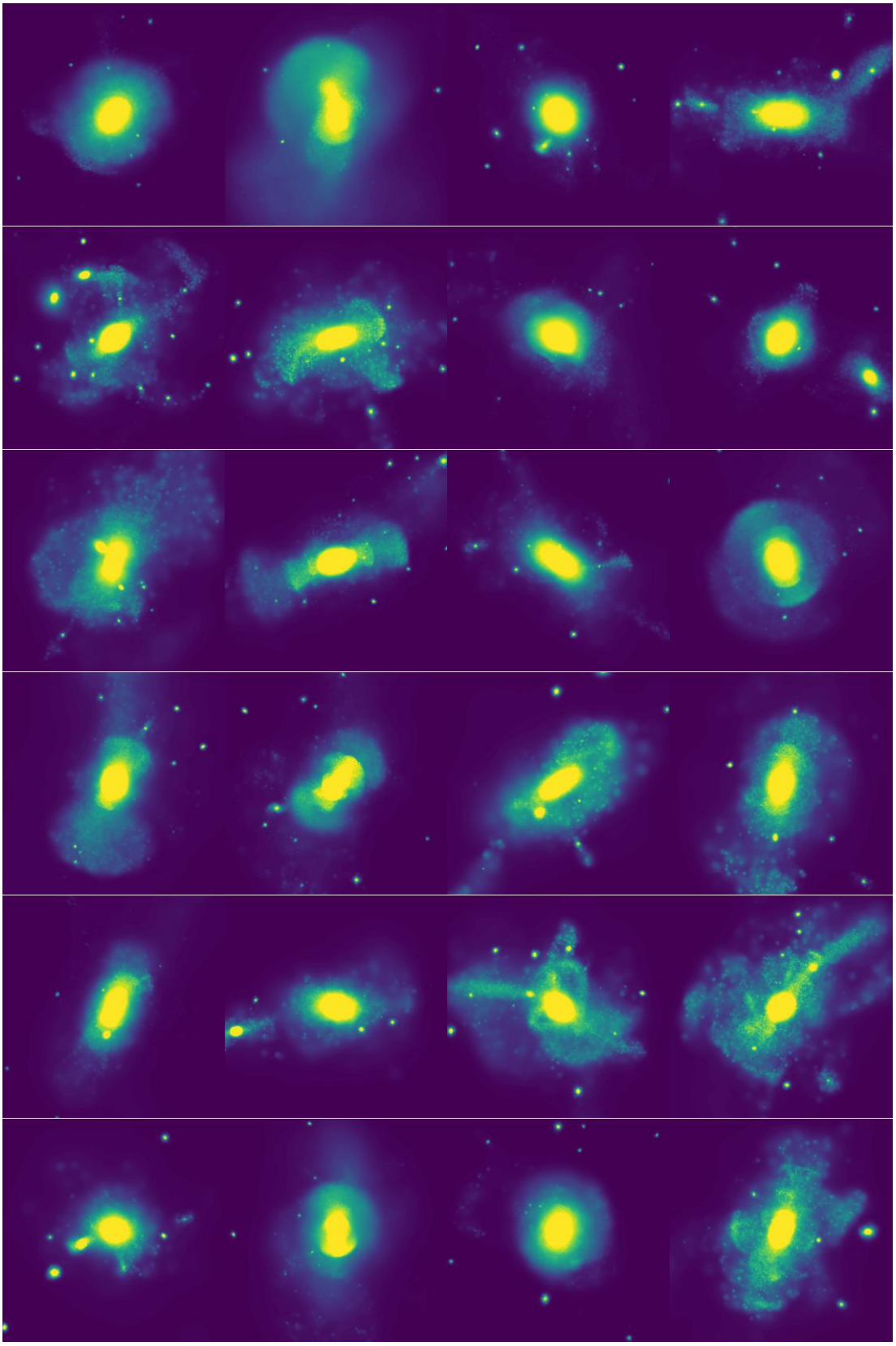

FIGURE A.6: (Continuation)

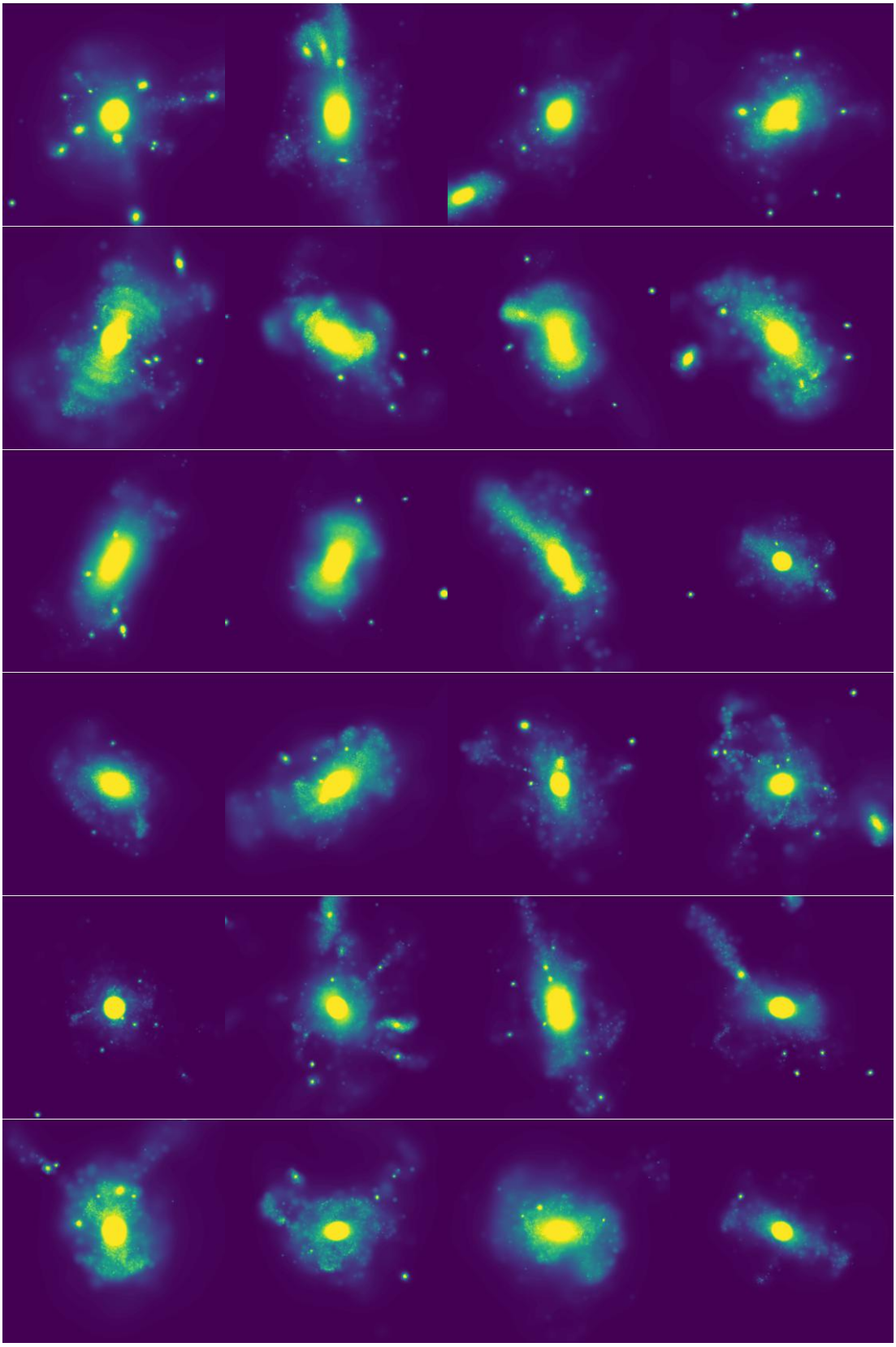

FIGURE A.6: (Continuation)

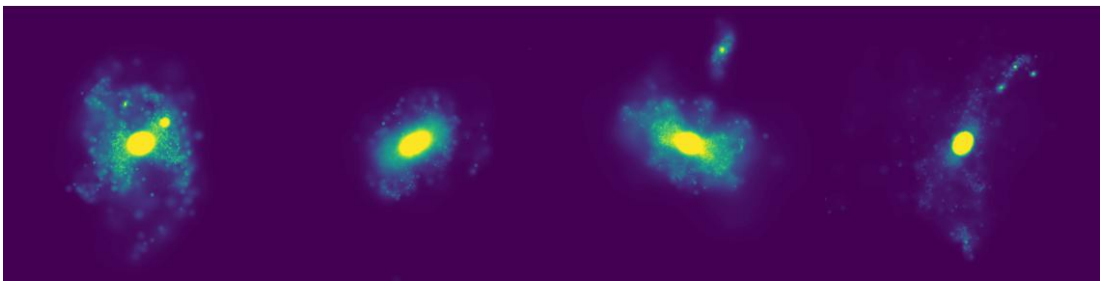

FIGURE A.6: (Continuation)

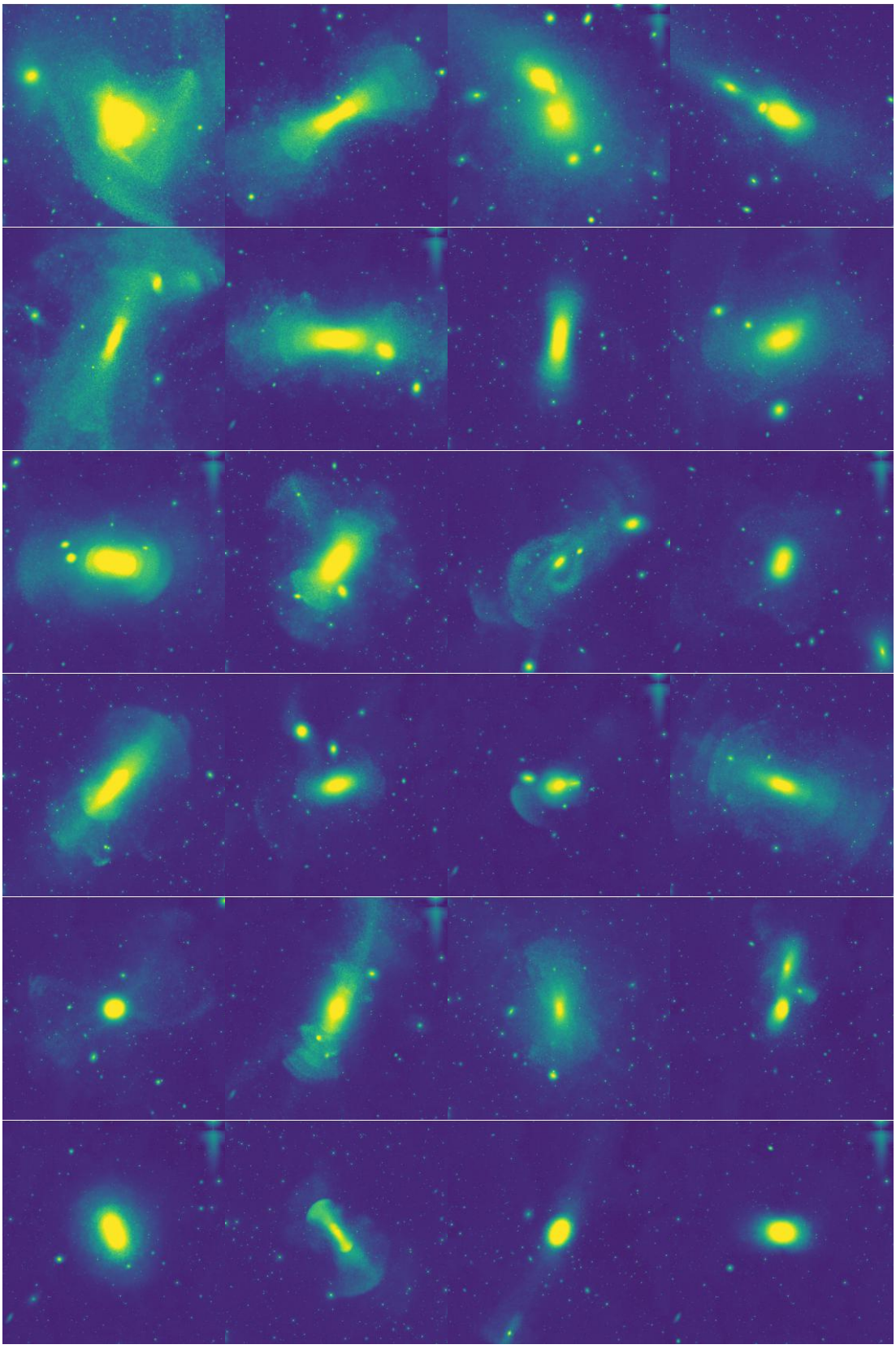

FIGURE A.7: Mock images of COCO galaxies with applied observational effects, sorted by decreasing mass, in the x-axis projection, spanning 300×300 kpc^2. The color encodes logarithmic magnitudes in the AB scale, with a surface brightness limit of 28.1 mag arcsec^{-2}.

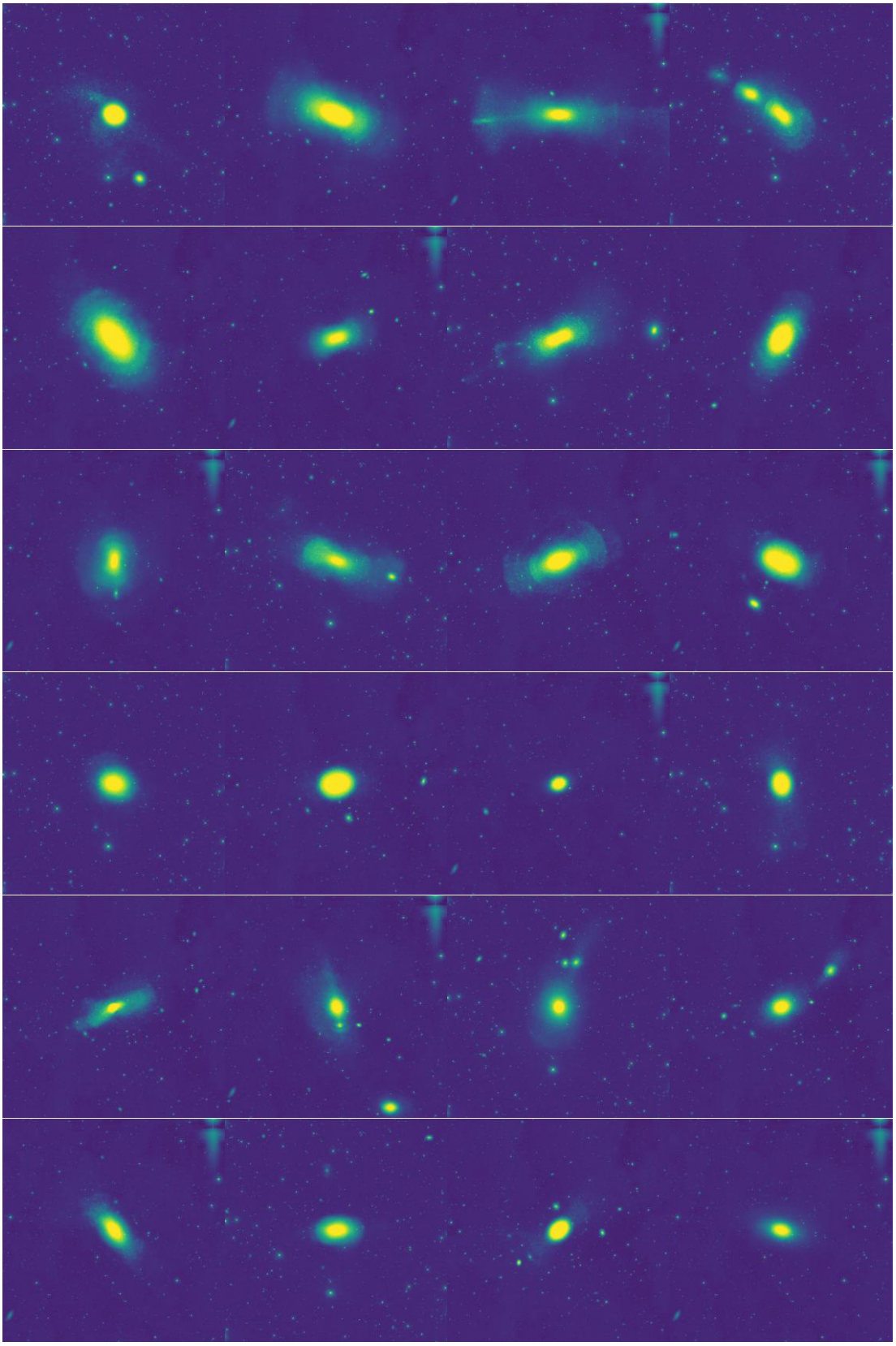

FIGURE A.7: (Continuation)

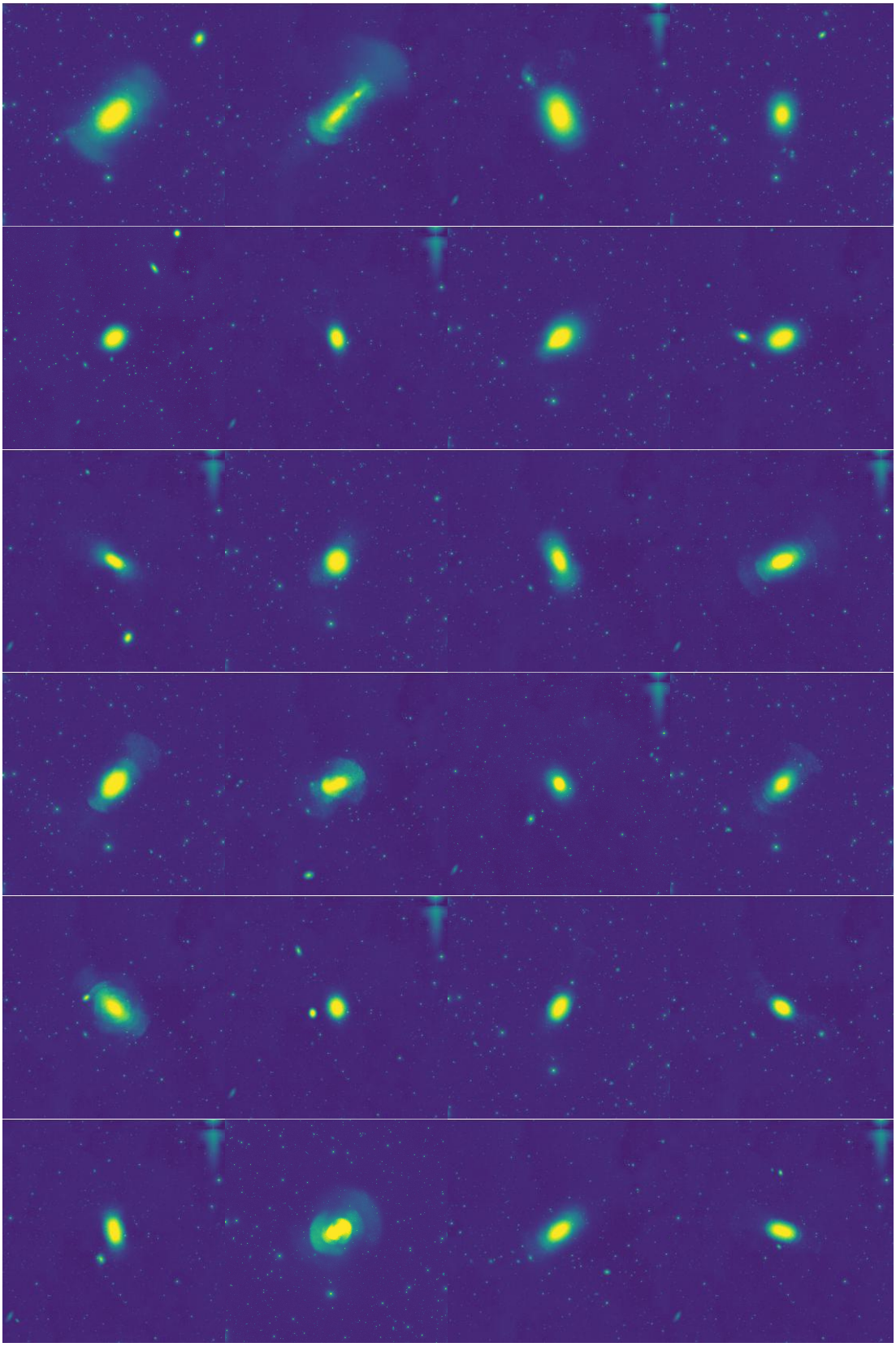

FIGURE A.7: (Continuation)

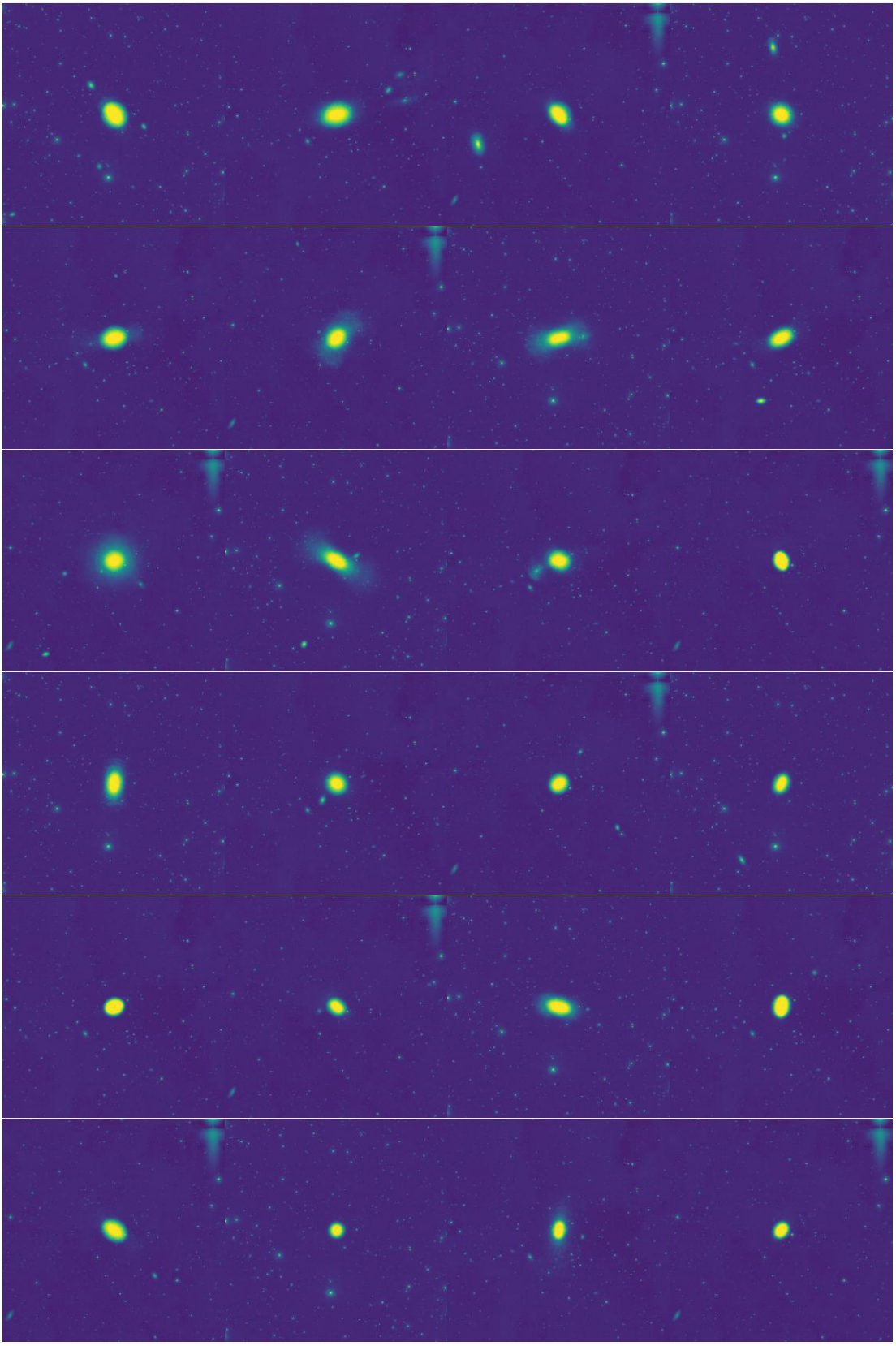

FIGURE A.7: (Continuation)

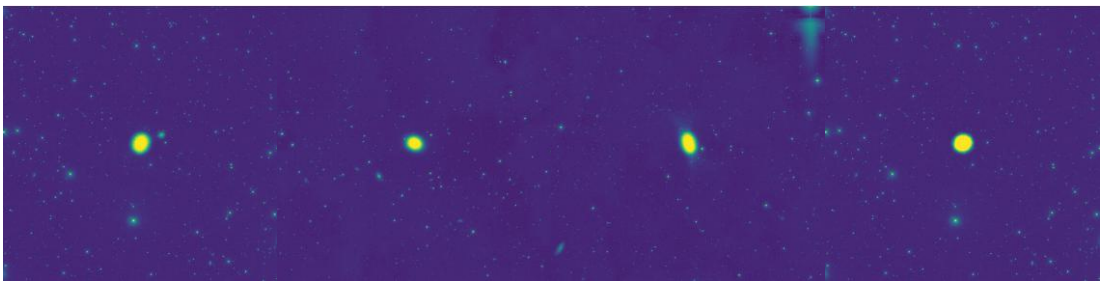

FIGURE A.7: (Continuation)

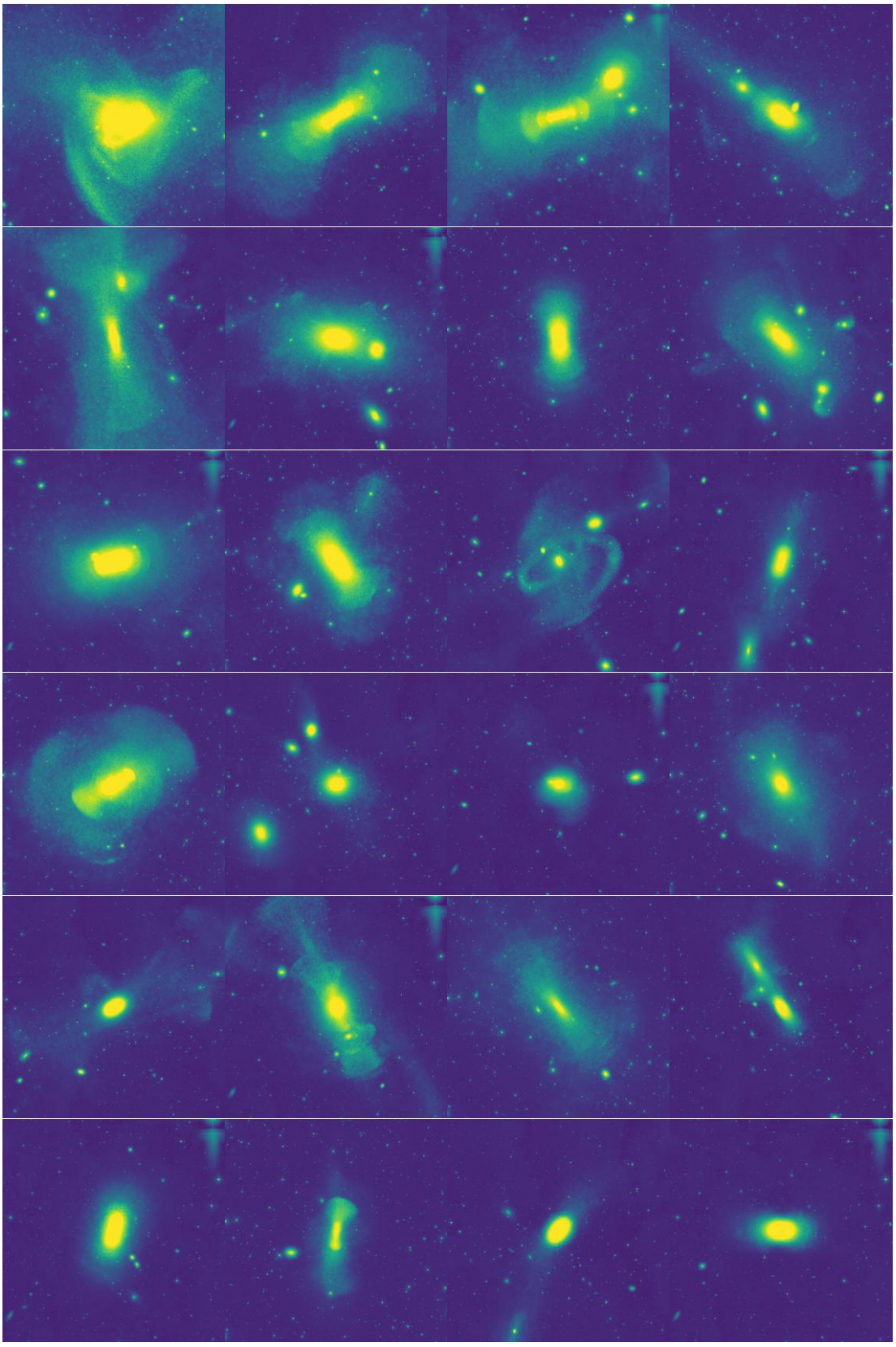

FIGURE A.8: Mock images of COCO galaxies with applied observational effects, sorted by decreasing mass, in the y-axis projection, spanning 300×300 kpc^2. The color encodes logarithmic magnitudes in the AB scale, with a surface brightness limit of 28.1 mag arcsec^{-2}.

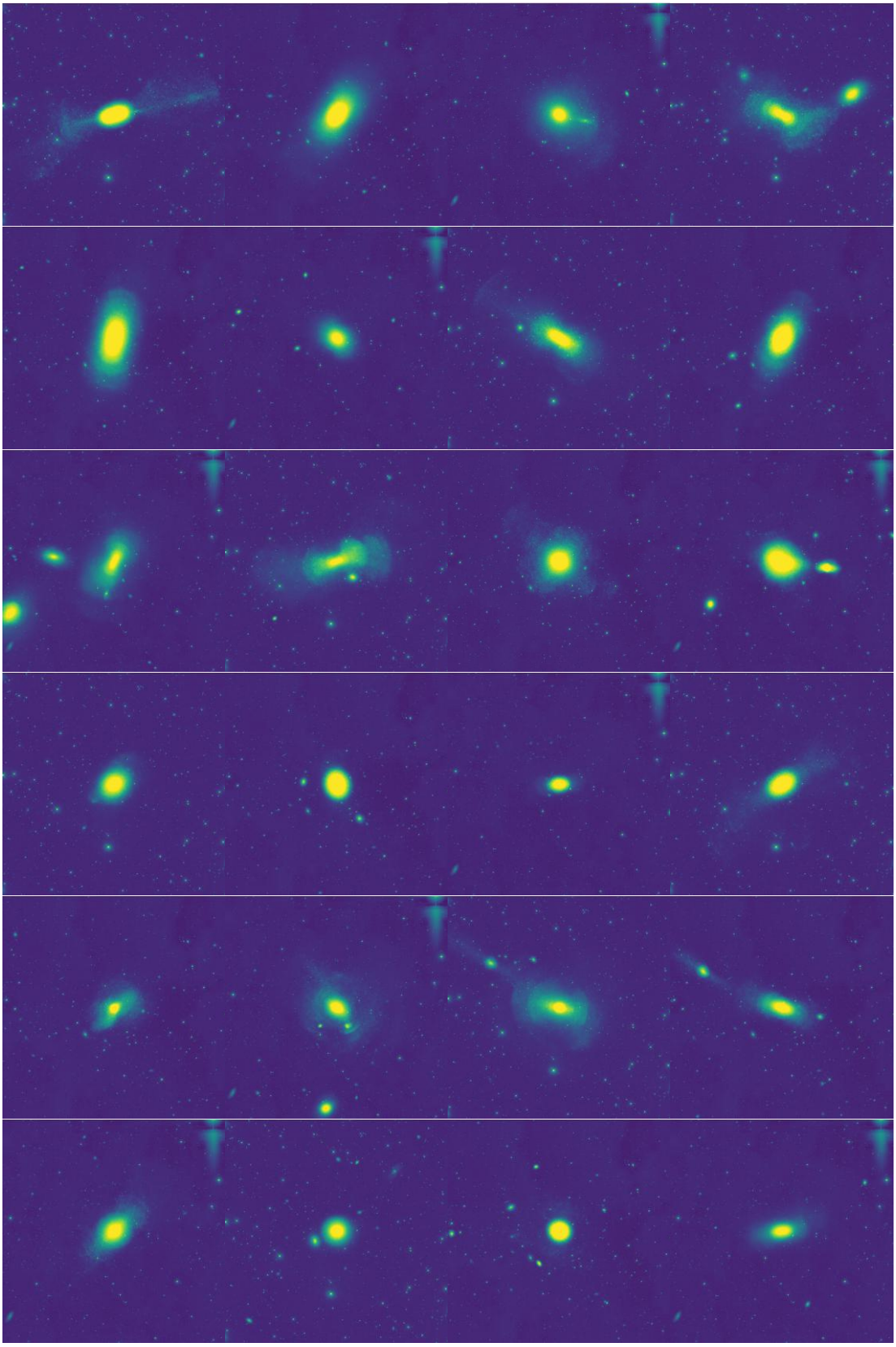

FIGURE A.8: (Continuation)

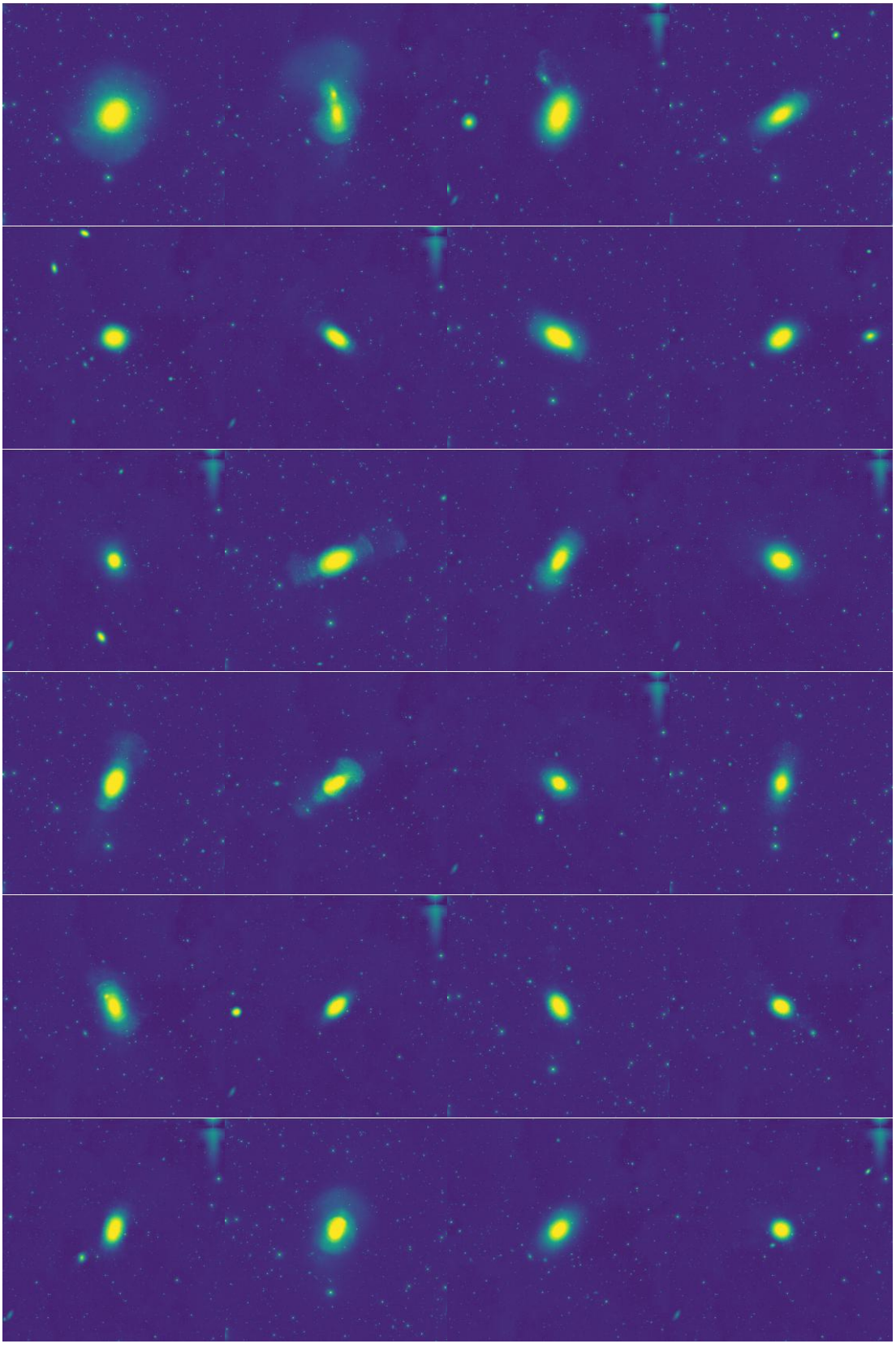

FIGURE A.8: (Continuation)

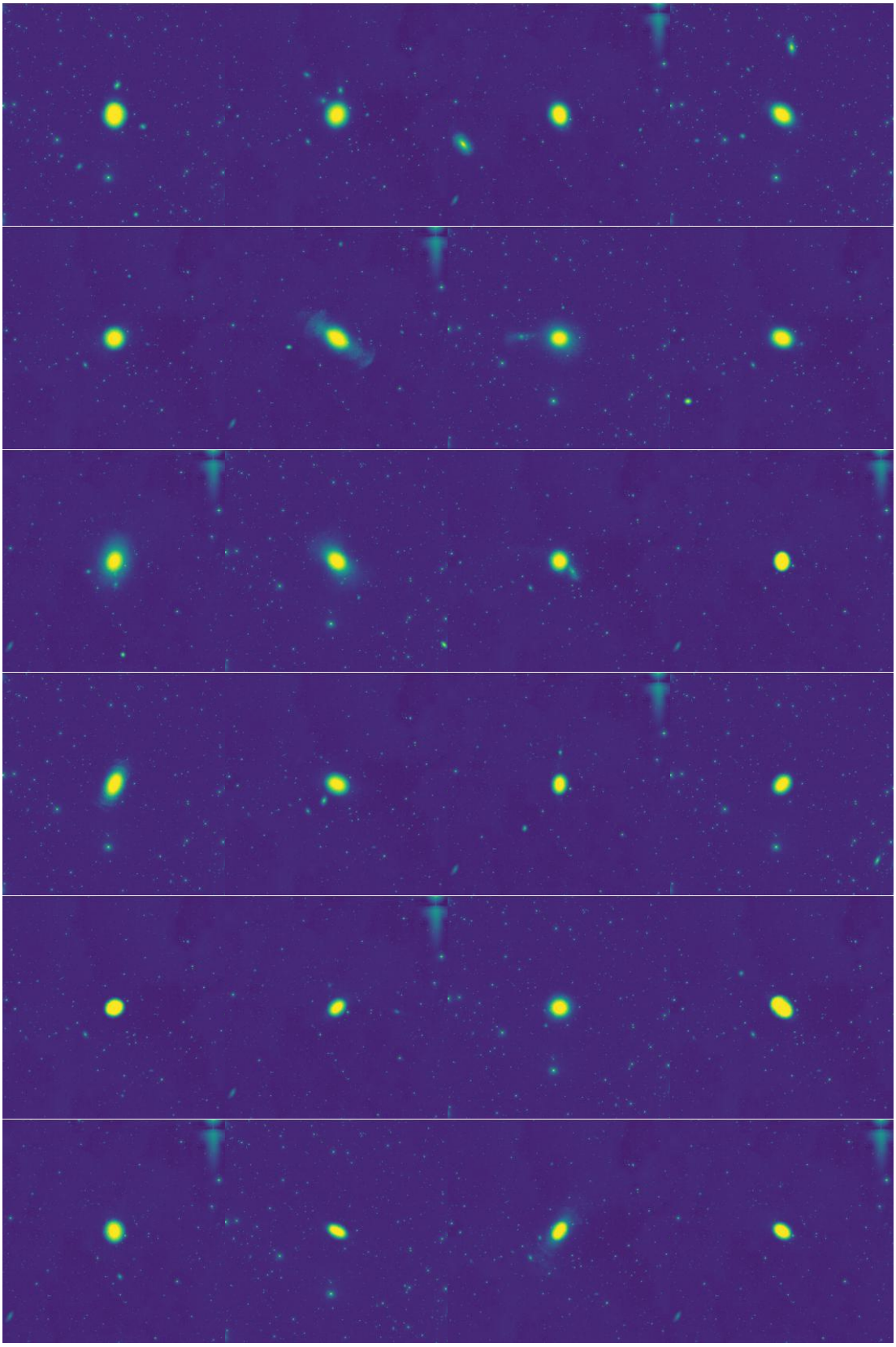

FIGURE A.8: (Continuation)

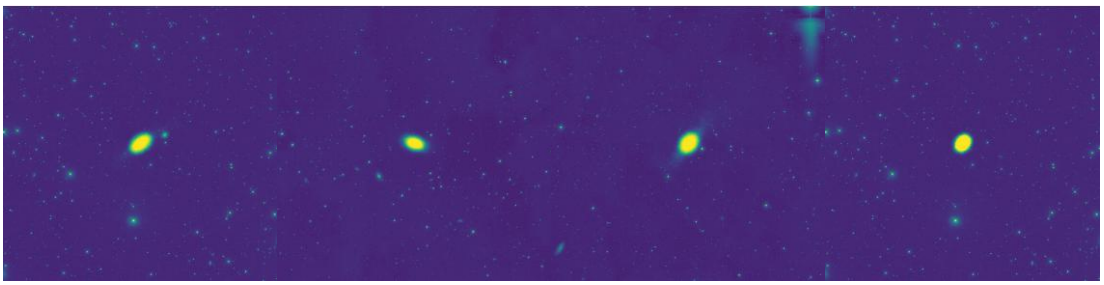

FIGURE A.8: (Continuation)

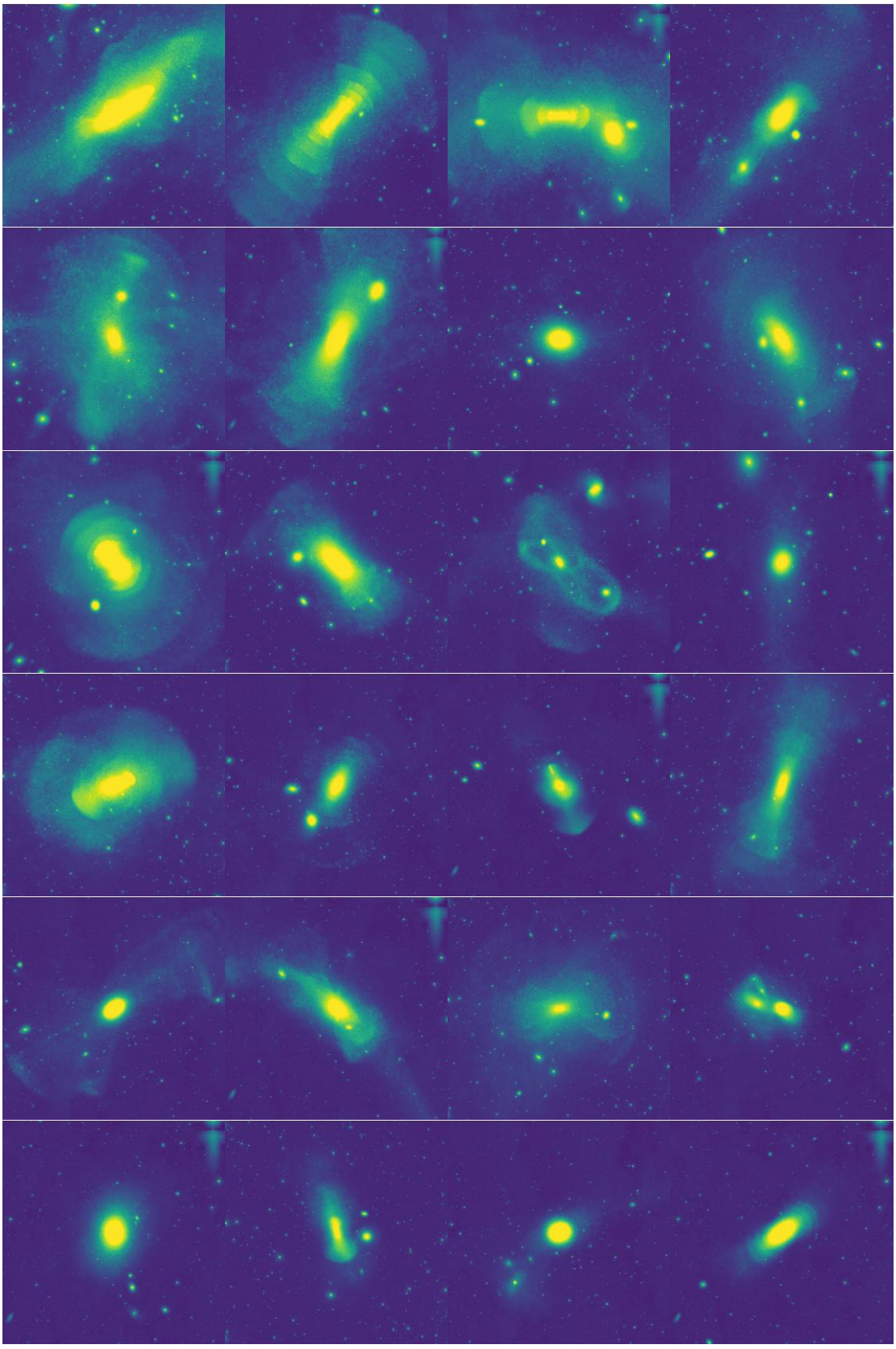

FIGURE A.9: Mock images of COCO galaxies with applied observational effects, sorted by decreasing mass, in the z-axis projection, spanning 300×300 kpc^2. The color encodes logarithmic magnitudes in the AB scale, with a surface brightness limit of 28.1 mag arcsec^{-2}.

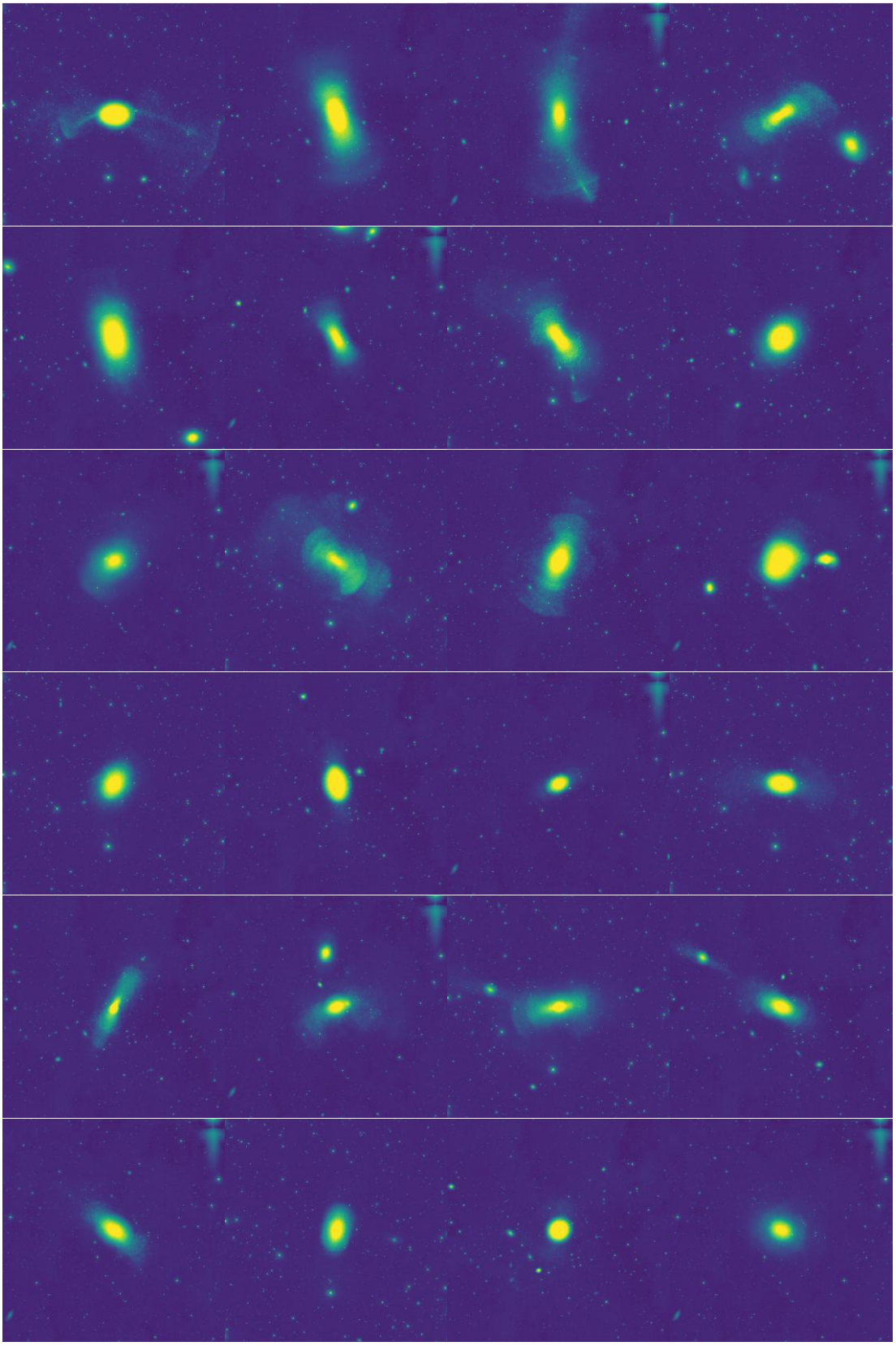

FIGURE A.9: (Continuation)

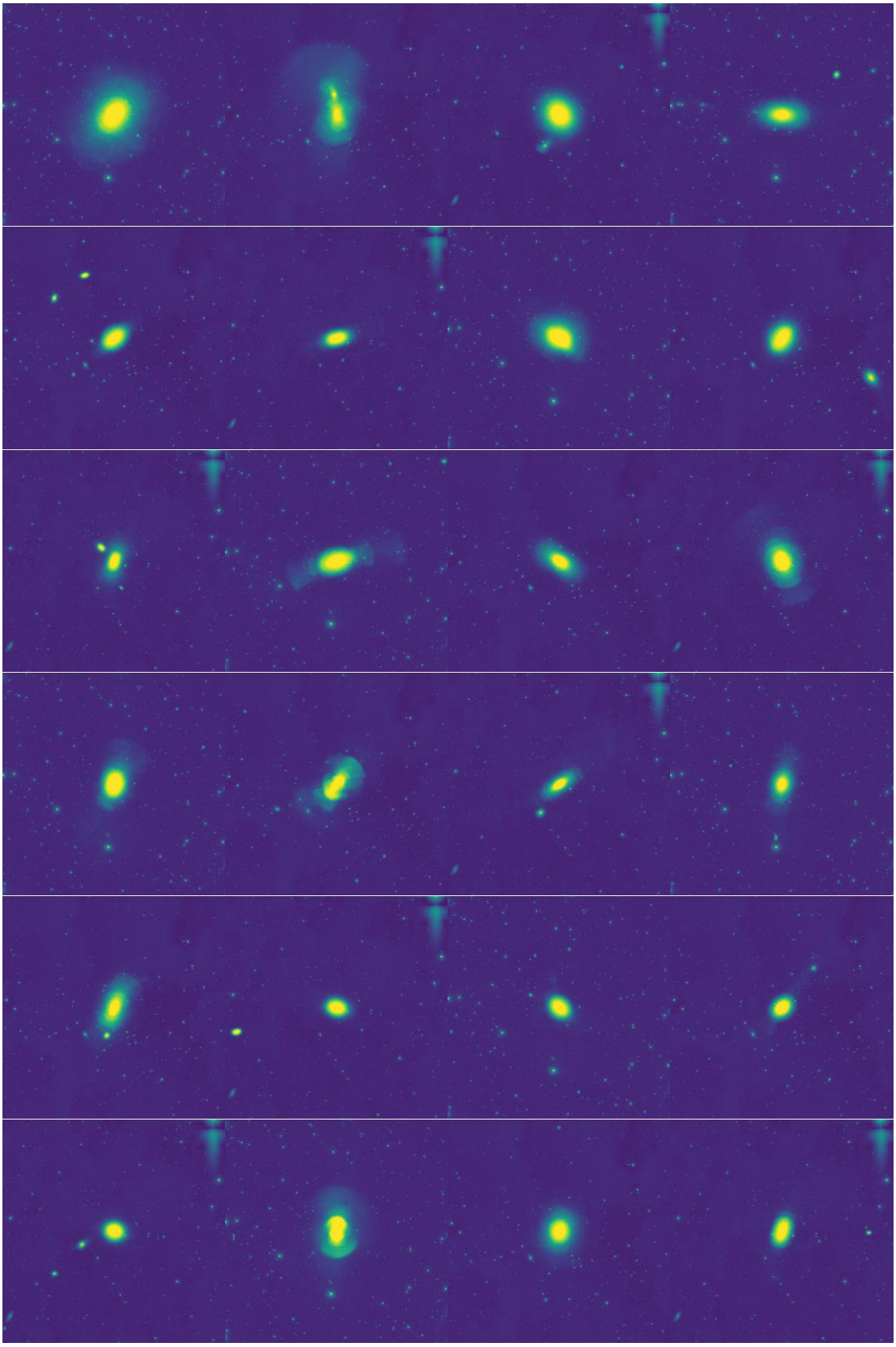

FIGURE A.9: (Continuation)

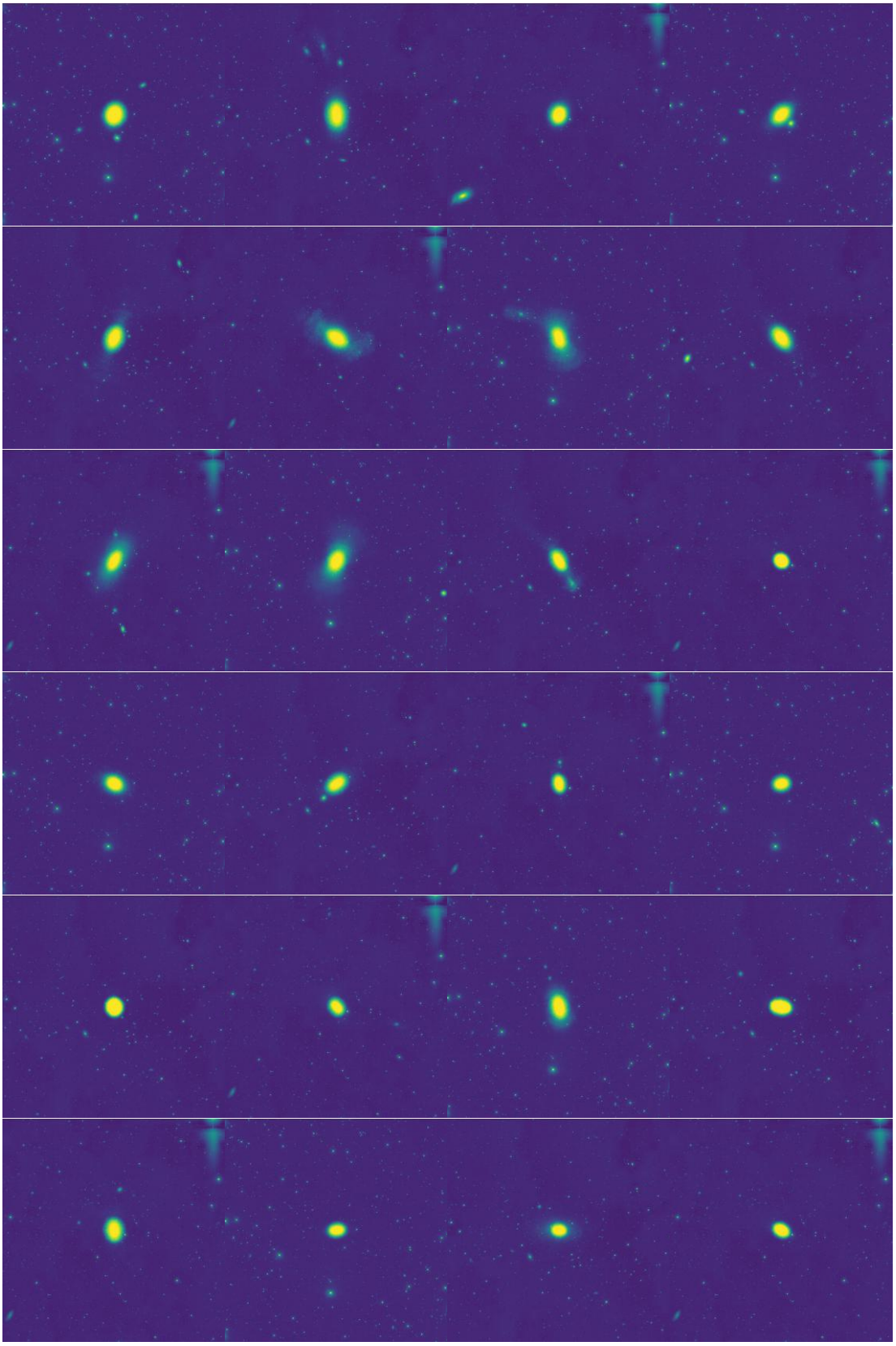

FIGURE A.9: (Continuation)

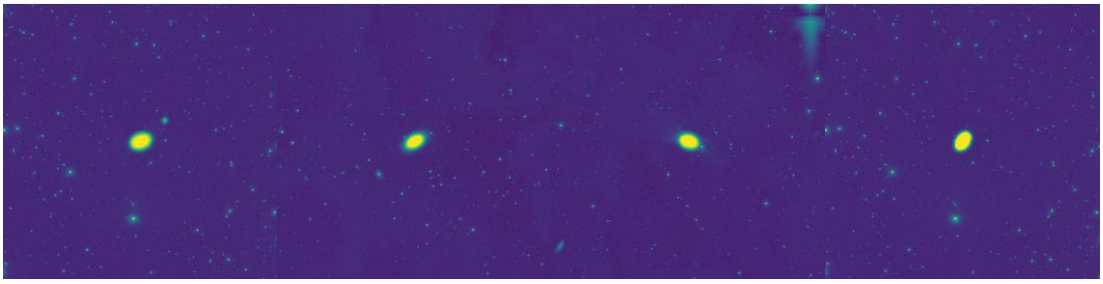

FIGURE A.9: (Continuation)

Appendix B

Auxiliary Tables.

TABLE B.1: Galaxies with no evidence of observable diffuse overdensities in the sample of 297 galaxies.

NGC 7814	NGC 2967	NGC 3495	NGC 3992	NGC 4343	NGC 4904	NGC 5792
NGC 157	NGC 2964	NGC 3501	IC 749	NGC 4356	NGC 5005	NGC 5821
NGC 337	UGC 5228	NGC 3507	IC 750	NGC 4369	NGC 5033	NGC 5854
NGC 584	NGC 3003	NGC 3512	NGC 4030	NGC 4380	NGC 5112	NGC 5864
NGC 615	NGC 3021	NGC 3556	NGC 4045	IC 3322A	NGC 5145	NGC 5879
NGC 628	NGC 3044	NGC 3596	NGC 4062	UGC 7522	NGC 5205	NGC 5921
NGC 660	NGC 3055	NGC 3623	NGC 4085	NGC 4405	IC 902	NGC 5963
NGC 676	NGC 3031	NGC 3626	NGC 4088	NGC 4448	UGC 8614	NGC 5956
NGC 693	NGC 3067	NGC 3629	NGC 4096	NGC 4451	NGC 5248	NGC 5957
NGC 701	NGC 3098	NGC 3637	NGC 4100	NGC 4461	NGC 5301	NGC 5962
NGC 779	NGC 3162	NGC 3642	NGC 4102	NGC 4503	NGC 5300	NGC 5964
IC 210	NGC 3177	NGC 3655	NGC 4123	NGC 4437	NGC 5334	NGC 5970
NGC 864	NGC 3185	NGC 3666	NGC 4138	NGC 4527	NGC 5356	NGC 6015
NGC 955	NGC 3184	NGC 3669	NGC 4145	NGC 4536	NGC 5422	NGC 6012
NGC 1022	NGC 3198	NGC 3681	NGC 4157	NGC 4559	NGC 5443	IC 1158
NGC 1035	IC 610	NGC 3684	UGC 7267	NGC 4565	NGC 5457	NGC 6106
UGC 4551	NGC 3254	NGC 3683	NGC 4212	NGC 4580	NGC 5473	NGC 6217
NGC 2654	NGC 3259	NGC 3686	NGC 4217	NGC 4599	NGC 5480	NGC 7280
NGC 2683	NGC 3279	NGC 3692	NGC 4220	NGC 4632	NGC 5520	NGC 7497
NGC 2712	NGC 3294	NGC 3755	NGC 4237	NGC 4639	NGC 5507	NGC 7625
NGC 2742	NGC 3346	NGC 3756	NGC 4260	NGC 4666	NGC 5584	NGC 1052
NGC 2770	NGC 3351	IC 719	NGC 4274	NGC 4710	NGC 5668	NGC 2768
NGC 2780	NGC 3359	NGC 3810	UGC 7387	NGC 4746	NGC 5690	NGC 3193
NGC 2805	NGC 3370	NGC 3900	NGC 4303	NGC 4771	NGC 5713	NGC 3608
NGC 2820	NGC 3389	NGC 3898	NGC 4307	NGC 4800	IC 1048	NGC 4278
NGC 2844	NGC 3430	NGC 3938	NGC 4314	NGC 4808	NGC 5746	NGC 5173
NGC 2841	NGC 3437	NGC 3953	NGC 4316	NGC 4826	NGC 5768	NGC 5216
NGC 2903	NGC 3486	NGC 3982	NGC 4324	NGC 4845	NGC 5798	NGC 5846

Own publications

Gralla, M. B. et al. (2014). "A measurement of the millimetre emission and the Sunyaev-Zel'dovich effect associated with low-frequency radio sources". In: *MNRAS* 445, pp. 460–478. DOI: 10.1093/mnras/stu1592. arXiv: 1310.8281.

Marsden, D. et al. (2014). "The Atacama Cosmology Telescope: dusty star-forming galaxies and active galactic nuclei in the Southern survey". In: *MNRAS* 439, pp. 1556–1574. DOI: 10.1093/mnras/stu001. arXiv: 1306.2288 [astro-ph.CO].

Martínez-Delgado, D. et al. (2015b). "A Stellar Tidal Stream Around the Whale Galaxy, NGC 4631". In: *AJ* 150, 116, p. 116. DOI: 10.1088/0004-6256/150/4/116. arXiv: 1410.6368.

Morales, G. et al. (2018). "Systematic search for tidal features around nearby galaxies: I. Enhanced SDSS imaging of the Local Volume". In: *ArXiv e-prints*. arXiv: 1804.03330.

Romanowsky, A. J. et al. (2016). "Satellite accretion in action: a tidally disrupting dwarf spheroidal around the nearby spiral galaxy NGC 253". In: *MNRAS* 457, pp. L103–L107. DOI: 10.1093/mnrasl/slv207. arXiv: 1512.03815.

Bibliography

Abadi, M. G., J. F. Navarro, and M. Steinmetz (2006). "Stars beyond galaxies: the origin of extended luminous haloes around galaxies". In: *MNRAS* 365, pp. 747–758. DOI: 10.1111/j.1365-2966.2005.09789.x. eprint: astro-ph/0506659.

Abazajian, K. N. et al. (2009). "The Seventh Data Release of the Sloan Digital Sky Survey". In: *ApJS* 182, 543-558, pp. 543–558. DOI: 10.1088/0067-0049/182/2/543. arXiv: 0812.0649.

Ahn, C. P. et al. (2014). "The Tenth Data Release of the Sloan Digital Sky Survey: First Spectroscopic Data from the SDSS-III Apache Point Observatory Galactic Evolution Experiment". In: *ApJS* 211, 17, p. 17. DOI: 10.1088/0067-0049/211/2/17. arXiv: 1307.7735 [astro-ph.IM].

Amorisco, N. C. (2017a). "Contributions to the accreted stellar halo: an atlas of stellar deposition". In: *MNRAS* 464, pp. 2882–2895. DOI: 10.1093/mnras/stw2229. arXiv: 1511.08806.

– (2017b). "The accreted stellar halo as a window on halo assembly in L* galaxies". In: *MNRAS* 469, pp. L48–L52. DOI: 10.1093/mnrasl/slx044. arXiv: 1701.02741.

Arp, H. (1966). "Atlas of Peculiar Galaxies". In: *ApJS* 14, p. 1. DOI: 10.1086/190147.

Atkinson, A. M., R. G. Abraham, and A. M. N. Ferguson (2013). "Faint Tidal Features in Galaxies within the Canada-France-Hawaii Telescope Legacy Survey Wide Fields". In: *ApJ* 765, 28, p. 28. DOI: 10.1088/0004-637X/765/1/28. arXiv: 1301.4275.

Baumgardt, H. and J. Makino (2003). "Dynamical evolution of star clusters in tidal fields". In: *MNRAS* 340, pp. 227–246. DOI: 10.1046/j.1365-8711.2003.06286.x. eprint: astro-ph/0211471.

Beaton, R. L. et al. (2014). "Cannibalization and Rebirth in the NGC 5387 System. I. The Stellar Stream and Star-forming Region". In: *ApJ* 790, 117, p. 117. DOI: 10.1088/0004-637X/790/2/117. arXiv: 1312.0585.

Behroozi, P. S., R. H. Wechsler, and C. Conroy (2013). "The Average Star Formation Histories of Galaxies in Dark Matter Halos from z = 0-8". In: *ApJ* 770, 57, p. 57. DOI: 10.1088/0004-637X/770/1/57. arXiv: 1207.6105 [astro-ph.CO].

Bell, E. F. et al. (2003). "The Optical and Near-Infrared Properties of Galaxies. I. Luminosity and Stellar Mass Functions". In: *ApJS* 149, pp. 289–312. DOI: 10.1086/378847. eprint: astro-ph/0302543.

Bennert, N. et al. (2008). "Evidence for Merger Remnants in Early-Type Host Galaxies of Low-Redshift QSOs". In: *ApJ* 677, 846-857, pp. 846–857. DOI: 10.1086/529068. arXiv: 0801.0832.

Bertin, E. and S. Arnouts (1996). "SExtractor: Software for source extraction." In: *A&AS* 117, pp. 393–404. DOI: 10.1051/aas:1996164.

Blanton, M. R. et al. (2011). "Improved Background Subtraction for the Sloan Digital Sky Survey Images". In: *AJ* 142, 31, p. 31. DOI: 10.1088/0004-6256/142/1/31. arXiv: 1105.1960 [astro-ph.IM].

Blum, R. D. et al. (2016a). "The DECam Legacy Survey". In: *American Astronomical Society Meeting Abstracts*. Vol. 228. American Astronomical Society Meeting Abstracts, p. 317.01.
– (2016b). "The DECam Legacy Survey". In: *American Astronomical Society Meeting Abstracts*. Vol. 228. American Astronomical Society Meeting Abstracts, p. 317.01.
Blumenthal, G. R. et al. (1984). "Formation of galaxies and large-scale structure with cold dark matter". In: *Nature* 311, pp. 517–525. DOI: 10.1038/311517a0.
Boselli, A. et al. (2016). "Spectacular tails of ionized gas in the Virgo cluster galaxy NGC 4569". In: *A&A* 587, A68, A68. DOI: 10.1051/0004-6361/201527795. arXiv: 1601.04978.
Bower, R. G. et al. (2006). "Breaking the hierarchy of galaxy formation". In: *MNRAS* 370, pp. 645–655. DOI: 10.1111/j.1365-2966.2006.10519.x. eprint: astro-ph/0511338.
Brodie, J. P. et al. (2014). "The SAGES Legacy Unifying Globulars and GalaxieS Survey (SLUGGS): Sample Definition, Methods, and Initial Results". In: *ApJ* 796, 52, p. 52. DOI: 10.1088/0004-637X/796/1/52. arXiv: 1405.2079.
Bullock, J. S. and K. V. Johnston (2005). "Tracing Galaxy Formation with Stellar Halos. I. Methods". In: *ApJ* 635, pp. 931–949. DOI: 10.1086/497422. eprint: astro-ph/0506467.
Bullock, J. S. et al. (2001). "Profiles of dark haloes: evolution, scatter and environment". In: *MNRAS* 321, pp. 559–575. DOI: 10.1046/j.1365-8711.2001.04068.x. eprint: astro-ph/9908159.
Caldwell, J. A. R. et al. (2008). "GEMS Survey Data and Catalog". In: *ApJS* 174, 136-144, pp. 136–144. DOI: 10.1086/521080. eprint: astro-ph/0510782.
Canalizo, G. et al. (2007). "Spectacular Shells in the Host Galaxy of the QSO MC2 1635+119". In: *ApJ* 669, pp. 801–809. DOI: 10.1086/521721. arXiv: 0707.2951.
Cautun, M. et al. (2015). "Planes of satellite galaxies: when exceptions are the rule". In: *MNRAS* 452, pp. 3838–3852. DOI: 10.1093/mnras/stv1557. arXiv: 1506.04151.
Chonis, T. S. and C. M. Gaskell (2008). "Setting UBVRI Photometric Zero-Points Using Sloan Digital Sky Survey ugriz Magnitudes". In: *AJ* 135, pp. 264–267. DOI: 10.1088/0004-6256/135/1/264. arXiv: 0710.5801.
Chonis, T. S. et al. (2011). "A Petal of the Sunflower: Photometry of the Stellar Tidal Stream in the Halo of Messier 63 (NGC 5055)". In: *AJ* 142, 166, p. 166. DOI: 10.1088/0004-6256/142/5/166. arXiv: 1109.0019.
Cole, S. et al. (2000). "Hierarchical galaxy formation". In: *MNRAS* 319, pp. 168–204. DOI: 10.1046/j.1365-8711.2000.03879.x. eprint: astro-ph/0007281.
– (2015). *GALFORM: Galactic modeling*. Astrophysics Source Code Library. ascl: 1510.005.
Cooper, A. P. et al. (2010). "Galactic stellar haloes in the CDM model". In: *MNRAS* 406, pp. 744–766. DOI: 10.1111/j.1365-2966.2010.16740.x. arXiv: 0910.3211 [astro-ph.GA].
Cooper, A. P. et al. (2011). "The Formation of Shell Galaxies Similar to NGC 7600 in the Cold Dark Matter Cosmogony". In: *ApJ* 743, L21, p. L21. DOI: 10.1088/2041-8205/743/1/L21. arXiv: 1111.2864.
Cooper, A. P. et al. (2013). "Galactic accretion and the outer structure of galaxies in the CDM model". In: *MNRAS* 434, pp. 3348–3367. DOI: 10.1093/mnras/stt1245. arXiv: 1303.6283.
Crnojević, D. et al. (2016). "The Extended Halo of Centaurus A: Uncovering Satellites, Streams, and Substructures". In: *ApJ* 823, 19, p. 19. DOI: 10.3847/0004-637X/823/1/19. arXiv: 1512.05366.

Croton, D. J. et al. (2006). "The many lives of active galactic nuclei: cooling flows, black holes and the luminosities and colours of galaxies". In: *MNRAS* 365, pp. 11–28. DOI: 10.1111/j.1365-2966.2005.09675.x. eprint: astro-ph/0508046.

Currie, M. J. et al. (2014). "Starlink Software in 2013". In: *Astronomical Data Analysis Software and Systems XXIII*. Ed. by N. Manset and P. Forshay. Vol. 485. Astronomical Society of the Pacific Conference Series, p. 391.

D'Souza, R. et al. (2014). "Parametrizing the stellar haloes of galaxies". In: *MNRAS* 443, pp. 1433–1450. DOI: 10.1093/mnras/stu1194. arXiv: 1404.2123.

Dalcanton, J. J. et al. (2009). "The ACS Nearby Galaxy Survey Treasury". In: *ApJS* 183, pp. 67–108. DOI: 10.1088/0067-0049/183/1/67. arXiv: 0905.3737 [astro-ph.GA].

Dale, D. A. et al. (2009). "The Spitzer Local Volume Legacy: Survey Description and Infrared Photometry". In: *ApJ* 703, pp. 517–556. DOI: 10.1088/0004-637X/703/1/517. arXiv: 0907.4722.

Danziger, I. J. and H.-E. Schuster (1974). "The interacting galaxy system NGC 646." In: *A&A* 34, pp. 301–303.

Davis, M. et al. (1985). "The evolution of large-scale structure in a universe dominated by cold dark matter". In: *ApJ* 292, pp. 371–394. DOI: 10.1086/163168.

De Lucia, G. and A. Helmi (2008). "The Galaxy and its stellar halo: insights on their formation from a hybrid cosmological approach". In: *MNRAS* 391, pp. 14–31. DOI: 10.1111/j.1365-2966.2008.13862.x. arXiv: 0804.2465.

Doi, M. et al. (2010). "Photometric Response Functions of the Sloan Digital Sky Survey Imager". In: *AJ* 139, pp. 1628–1648. DOI: 10.1088/0004-6256/139/4/1628. arXiv: 1002.3701 [astro-ph.IM].

Duc, P.-A. and F. Renaud (2013). "Tides in Colliding Galaxies". In: *Lecture Notes in Physics, Berlin Springer Verlag*. Ed. by J. Souchay, S. Mathis, and T. Tokieda. Vol. 861. Lecture Notes in Physics, Berlin Springer Verlag, p. 327. DOI: 10.1007/978-3-642-32961-6_9. arXiv: 1112.1922.

Duc, P.-A. et al. (2015). "The ATLAS^{3D} project - XXIX. The new look of early-type galaxies and surrounding fields disclosed by extremely deep optical images". In: *MNRAS* 446, pp. 120–143. DOI: 10.1093/mnras/stu2019. arXiv: 1410.0981.

Eisenstein, D. J. et al. (2011). "SDSS-III: Massive Spectroscopic Surveys of the Distant Universe, the Milky Way, and Extra-Solar Planetary Systems". In: *AJ* 142, 72, p. 72. DOI: 10.1088/0004-6256/142/3/72. arXiv: 1101.1529 [astro-ph.IM].

Epchtein, N. et al. (1994). "DENIS: A Deep Near-Infrared Survey of the southern sky". In: *Ap&SS* 217, pp. 3–9. DOI: 10.1007/BF00990013.

Erwin, P., M. Pohlen, and J. E. Beckman (2008). "The Outer Disks of Early-Type Galaxies. I. Surface-Brightness Profiles of Barred Galaxies". In: *AJ* 135, pp. 20–54. DOI: 10.1088/0004-6256/135/1/20. arXiv: 0709.3505.

Eskridge, P. B. et al. (2002). "Near-Infrared and Optical Morphology of Spiral Galaxies". In: *ApJS* 143, pp. 73–111. DOI: 10.1086/342340. eprint: astro-ph/0206320.

Fazio, G. G. et al. (2004). "The Infrared Array Camera (IRAC) for the Spitzer Space Telescope". In: *ApJS* 154, pp. 10–17. DOI: 10.1086/422843. eprint: astro-ph/0405616.

Font, A. S. et al. (2006). "Chemical Abundance Distributions of Galactic Halos and Their Satellite Systems in a ΛCDM Universe". In: *ApJ* 638, pp. 585–595. DOI: 10.1086/498970. eprint: astro-ph/0507114.

Foster, C. et al. (2014). "Kinematics and simulations of the stellar stream in the halo of the Umbrella Galaxy". In: *MNRAS* 442, pp. 3544–3564. DOI: 10.1093/mnras/stu1074. arXiv: 1406.5511.

Frenk, C. S., C. M. Baugh, and S. M. Cole (1996). "Galaxy Formation and Evolution What to Expect from Hierarchical Clustering Models". In: *New Light on Galaxy Evolution*. Ed. by R. Bender and R. L. Davies. Vol. 171. IAU Symposium, p. 247. eprint: astro-ph/9512088.

Fritze, K. et al. (1977). "A scanning microphotometer with an on-line data reduction for large field Schmidt plates". In: *Astronomische Nachrichten* 298, pp. 189–196. DOI: 10.1002/asna.19772980402.

Gil de Paz, A. et al. (2005). "Discovery of an Extended Ultraviolet Disk in the Nearby Galaxy NGC 4625". In: *ApJ* 627, pp. L29–L32. DOI: 10.1086/432054. eprint: astro-ph/0506357.

Gonzalez-Perez, V. et al. (2014). "How sensitive are predicted galaxy luminosities to the choice of stellar population synthesis model?" In: *MNRAS* 439, pp. 264–283. DOI: 10.1093/mnras/stt2410. arXiv: 1309.7057 [astro-ph.CO].

Gottlöber, S., A. Klypin, and A. V. Kravtsov (2001). "Merging History as a Function of Halo Environment". In: *ApJ* 546, pp. 223–233. DOI: 10.1086/318248. eprint: astro-ph/0004132.

Gralla, M. B. et al. (2014). "A measurement of the millimetre emission and the Sunyaev-Zel'dovich effect associated with low-frequency radio sources". In: *MNRAS* 445, pp. 460–478. DOI: 10.1093/mnras/stu1592. arXiv: 1310.8281.

Gunn, J. E. et al. (1998). "The Sloan Digital Sky Survey Photometric Camera". In: *AJ* 116, pp. 3040–3081. DOI: 10.1086/300645. eprint: astro-ph/9809085.

Gunn, J. E. et al. (2006). "The 2.5 m Telescope of the Sloan Digital Sky Survey". In: *AJ* 131, pp. 2332–2359. DOI: 10.1086/500975. eprint: astro-ph/0602326.

Guo, Q. and S. D. M. White (2008). "Galaxy growth in the concordance ΛCDM cosmology". In: *MNRAS* 384, pp. 2–10. DOI: 10.1111/j.1365-2966.2007.12619.x. arXiv: 0708.1814.

Guo, Q. et al. (2010). "How do galaxies populate dark matter haloes?" In: *MNRAS* 404, pp. 1111–1120. DOI: 10.1111/j.1365-2966.2010.16341.x. arXiv: 0909.4305 [astro-ph.CO].

Hammer, F. et al. (2007). "The Milky Way, an Exceptionally Quiet Galaxy: Implications for the Formation of Spiral Galaxies". In: *ApJ* 662, pp. 322–334. DOI: 10.1086/516727. eprint: astro-ph/0702585.

Harmsen, B. et al. (2017). "Diverse stellar haloes in nearby Milky Way mass disc galaxies". In: *MNRAS* 466, pp. 1491–1512. DOI: 10.1093/mnras/stw2992. arXiv: 1611.05448.

Haynes, M. P. et al. (2000). "Kinematic Evidence of Minor Mergers in Normal SA Galaxies: NGC 3626, NGC 3900, NGC 4772, and NGC 5854". In: *AJ* 120, pp. 703–727. DOI: 10.1086/301457. eprint: astro-ph/0004340.

Hellwing, W. A. et al. (2016). "The Copernicus Complexio: a high-resolution view of the small-scale Universe". In: *MNRAS* 457, pp. 3492–3509. DOI: 10.1093/mnras/stw214. arXiv: 1505.06436.

Helmi, A., S. D. M. White, and V. Springel (2003). "The phase-space structure of cold dark matter haloes: insights into the Galactic halo". In: *MNRAS* 339, pp. 834–848. DOI: 10.1046/j.1365-8711.2003.06227.x. eprint: astro-ph/0208041.

Hubble, E. (1929). "A Relation between Distance and Radial Velocity among Extra-Galactic Nebulae". In: *Proceedings of the National Academy of Science* 15, pp. 168–173. DOI: 10.1073/pnas.15.3.168.

Ibata, R. A. et al. (2014). "The Large-scale Structure of the Halo of the Andromeda Galaxy. I. Global Stellar Density, Morphology and Metallicity Properties". In: *ApJ* 780, 128, p. 128. DOI: 10.1088/0004-637X/780/2/128. arXiv: 1311.5888.

Javanmardi, B. et al. (2016). "DGSAT: Dwarf Galaxy Survey with Amateur Telescopes. I. Discovery of low surface brightness systems around nearby spiral galaxies". In: *A&A* 588, A89, A89. DOI: 10.1051/0004-6361/201527745. arXiv: 1511.04446.

Johnston, K. V., P. D. Sackett, and J. S. Bullock (2001). "Interpreting Debris from Satellite Disruption in External Galaxies". In: *ApJ* 557, pp. 137–149. DOI: 10.1086/321644. eprint: astro-ph/0101543.

Johnston, K. V. et al. (2008). "Tracing Galaxy Formation with Stellar Halos. II. Relating Substructure in Phase and Abundance Space to Accretion Histories". In: *ApJ* 689, 936-957, pp. 936–957. DOI: 10.1086/592228. arXiv: 0807.3911.

Karachentsev, I. D. and O. G. Kashibadze (2006). "Masses of the local group and of the M81 group estimated from distortions in the local velocity field". In: *Astrophysics* 49, pp. 3–18. DOI: 10.1007/s10511-006-0002-6.

Katz, N. and S. D. M. White (1993). "Hierarchical galaxy formation - Overmerging and the formation of an X-ray cluster". In: *ApJ* 412, pp. 455–478. DOI: 10.1086/172935.

Kauffmann, G., S. D. M. White, and B. Guiderdoni (1993). "The Formation and Evolution of Galaxies Within Merging Dark Matter Haloes". In: *MNRAS* 264, p. 201. DOI: 10.1093/mnras/264.1.201.

Kaviraj, S. (2010). "Peculiar early-type galaxies in the Sloan Digital Sky Survey Stripe82". In: *MNRAS* 406, pp. 382–394. DOI: 10.1111/j.1365-2966.2010.16714.x. arXiv: 1004.3775.

Kazantzidis, S. et al. (2004). "Density Profiles of Cold Dark Matter Substructure: Implications for the Missing-Satellites Problem". In: *ApJ* 608, pp. 663–679. DOI: 10.1086/420840. eprint: astro-ph/0312194.

Keenan, D. W. and K. A. Innanen (1975). "Numerical investigation of galactic tidal effects on spherical stellar systems". In: *AJ* 80, pp. 290–302. DOI: 10.1086/111744.

Kennicutt Jr., R. C. et al. (2003). "SINGS: The SIRTF Nearby Galaxies Survey". In: *PASP* 115, pp. 928–952. DOI: 10.1086/376941. eprint: astro-ph/0305437.

Kennicutt Jr., R. C. et al. (2008). "An Hα Imaging Survey of Galaxies in the Local 11 Mpc Volume". In: *ApJS* 178, 247-279, pp. 247–279. DOI: 10.1086/590058. arXiv: 0807.2035.

Komatsu, E. et al. (2011). "Seven-year Wilkinson Microwave Anisotropy Probe (WMAP) Observations: Cosmological Interpretation". In: *ApJS* 192, 18, p. 18. DOI: 10.1088/0067-0049/192/2/18. arXiv: 1001.4538 [astro-ph.CO].

Kravtsov, A. V., O. Y. Gnedin, and A. A. Klypin (2004). "The Tumultuous Lives of Galactic Dwarfs and the Missing Satellites Problem". In: *ApJ* 609, pp. 482–497. DOI: 10.1086/421322. eprint: astro-ph/0401088.

Lacey, C. and S. Cole (1993). "Merger rates in hierarchical models of galaxy formation". In: *MNRAS* 262, pp. 627–649. DOI: 10.1093/mnras/262.3.627.

Laine, S. et al. (2014). "Spitzer/Infrared Array Camera near-infrared features in the outer parts of S^{4}G galaxies". In: *MNRAS* 444, pp. 3015–3039. DOI: 10.1093/mnras/stu1642. arXiv: 1408.2602.

Laurikainen, E. et al. (2010). "Photometric scaling relations of lenticular and spiral galaxies". In: *MNRAS* 405, pp. 1089–1118. DOI: 10.1111/j.1365-2966.2010.16521.x. arXiv: 1002.4370.

Leaman, R. et al. (2015). "Triggered star formation in a merging, gas-rich dwarf galaxy around NGC 7241". In: *MNRAS* 450, pp. 2473–2485. DOI: 10.1093/mnras/stv626.

Lee, J. C. et al. (2009). "Comparison of Hα and UV Star Formation Rates in the Local Volume: Systematic Discrepancies for Dwarf Galaxies". In: *ApJ* 706, 599-613, pp. 599–613. DOI: 10.1088/0004-637X/706/1/599. arXiv: 0909.5205 [astro-ph.CO].

Lee, J. C. et al. (2011). "A GALEX Ultraviolet Imaging Survey of Galaxies in the Local Volume". In: *ApJS* 192, 6, p. 6. DOI: 10.1088/0067-0049/192/1/6. arXiv: 1009.4705.

Ludwig, J. et al. (2012). "Giant Galaxies, Dwarfs, and Debris Survey. I. Dwarf Galaxies and Tidal Features around NGC 7331". In: *AJ* 144, 190, p. 190. DOI: 10.1088/0004-6256/144/6/190. arXiv: 1211.3764.

Luo, G. and T. Y. Hou (2014). "Potentially singular solutions of the 3D axisymmetric Euler equations". In: *Proceedings of the National Academy of Science* 111, pp. 12968–12973. DOI: 10.1073/pnas.1405238111. arXiv: 1310.0497 [physics.flu-dyn].

Malin, D. and B. Hadley (1997). "HI in Shell Galaxies and Other Merger Remnants". In: *PASA* 14, pp. 52–58. DOI: 10.1071/AS97052.

Maller, A. H. et al. (2006). "Galaxy Merger Statistics and Inferred Bulge-to-Disk Ratios in Cosmological SPH Simulations". In: *ApJ* 647, pp. 763–772. DOI: 10.1086/503319. eprint: astro-ph/0509474.

Marsden, D. et al. (2014). "The Atacama Cosmology Telescope: dusty star-forming galaxies and active galactic nuclei in the Southern survey". In: *MNRAS* 439, pp. 1556–1574. DOI: 10.1093/mnras/stu001. arXiv: 1306.2288 [astro-ph.CO].

Martin, D. C. et al. (2005). "The Galaxy Evolution Explorer: A Space Ultraviolet Survey Mission". In: *ApJ* 619, pp. L1–L6. DOI: 10.1086/426387. eprint: astro-ph/0411302.

Martínez-Delgado, D. et al. (2007). "The Virgo Stellar Overdensity: Mapping the Infall of the Sagittarius Tidal Stream onto the Milky Way Disk". In: *ApJ* 660, pp. 1264–1272. DOI: 10.1086/513067. eprint: astro-ph/0609104.

Martínez-Delgado, D. et al. (2008a). "The Ghost of a Dwarf Galaxy: Fossils of the Hierarchical Formation of the Nearby Spiral Galaxy NGC 5907". In: *ApJ* 689, 184-193, pp. 184–193. DOI: 10.1086/592555. arXiv: 0805.1137.

– (2008b). "The Ghost of a Dwarf Galaxy: Fossils of the Hierarchical Formation of the Nearby Spiral Galaxy NGC 5907". In: *ApJ* 689, 184-193, pp. 184–193. DOI: 10.1086/592555. arXiv: 0805.1137.

Martínez-Delgado, D. et al. (2009). "Discovery of a Giant Stellar Tidal Stream Around The Disk Galaxy NGC 4013". In: *ApJ* 692, pp. 955–963. DOI: 10.1088/0004-637X/692/2/955. arXiv: 0812.3219.

Martínez-Delgado, D. et al. (2010). "Stellar Tidal Streams in Spiral Galaxies of the Local Volume: A Pilot Survey with Modest Aperture Telescopes". In: *AJ* 140, pp. 962–967. DOI: 10.1088/0004-6256/140/4/962. arXiv: 1003.4860.

Martínez-Delgado, D. et al. (2012). "Dwarfs Gobbling Dwarfs: A Stellar Tidal Stream around NGC 4449 and Hierarchical Galaxy Formation on Small Scales". In: *ApJ* 748, L24, p. L24. DOI: 10.1088/2041-8205/748/2/L24. arXiv: 1112.2154.

Martínez-Delgado, D. et al. (2015a). "A Stellar Tidal Stream Around the Whale Galaxy, NGC 4631". In: *AJ* 150, 116, p. 116. DOI: 10.1088/0004-6256/150/4/116. arXiv: 1410.6368.

– (2015b). "A Stellar Tidal Stream Around the Whale Galaxy, NGC 4631". In: *AJ* 150, 116, p. 116. DOI: 10.1088/0004-6256/150/4/116. arXiv: 1410.6368.

Mayer, L. et al. (2006). "Simultaneous ram pressure and tidal stripping; how dwarf spheroidals lost their gas". In: *MNRAS* 369, pp. 1021–1038. DOI: 10.1111/j.1365-2966.2006.10403.x. eprint: astro-ph/0504277.

McConnachie, A. W. et al. (2009). "The remnants of galaxy formation from a panoramic survey of the region around M31". In: *Nature* 461, pp. 66–69. DOI: 10.1038/nature08327. arXiv: 0909.0398.

McMillan, P. J. (2011). "Mass models of the Milky Way". In: *MNRAS* 414, pp. 2446–2457. DOI: 10.1111/j.1365-2966.2011.18564.x. arXiv: 1102.4340.

– (2017). "The mass distribution and gravitational potential of the Milky Way". In: *MNRAS* 465, pp. 76–94. DOI: 10.1093/mnras/stw2759. arXiv: 1608.00971.

Merritt, A. et al. (2016). "The Dragonfly Nearby Galaxies Survey. II. Ultra-Diffuse Galaxies near the Elliptical Galaxy NGC 5485". In: *ApJ* 833, 168, p. 168. DOI: 10.3847/1538-4357/833/2/168. arXiv: 1610.01609.

Miskolczi, A., D. J. Bomans, and R.-J. Dettmar (2011). "Tidal streams around galaxies in the SDSS DR7 archive. I. First results". In: *A&A* 536, A66, A66. DOI: 10.1051/0004-6361/201116716. arXiv: 1102.2905.

Morales, G. et al. (2018). "Systematic search for tidal features around nearby galaxies: I. Enhanced SDSS imaging of the Local Volume". In: *ArXiv e-prints*. arXiv: 1804.03330.

Moster, B. P., T. Naab, and S. D. M. White (2017). "EMERGE - An empirical model for the formation of galaxies since $z \sim 10$". In: *ArXiv e-prints*. arXiv: 1705.05373.

Moster, B. P. et al. (2010). "Constraints on the Relationship between Stellar Mass and Halo Mass at Low and High Redshift". In: *ApJ* 710, pp. 903–923. DOI: 10.1088/0004-637X/710/2/903. arXiv: 0903.4682 [astro-ph.CO].

Mouhcine, M. and R. Ibata (2009). "A panoramic view of M81: new stellar systems in the debris field". In: *MNRAS* 399, pp. 737–743. DOI: 10.1111/j.1365-2966.2009.15135.x.

Muñoz-Mateos, J. C. et al. (2007). "Specific Star Formation Rate Profiles in Nearby Spiral Galaxies: Quantifying the Inside-Out Formation of Disks". In: *ApJ* 658, pp. 1006–1026. DOI: 10.1086/511812. eprint: astro-ph/0612017.

Muñoz-Mateos, J. C. et al. (2015). "The Spitzer Survey of Stellar Structure in Galaxies (S^4G): Stellar Masses, Sizes, and Radial Profiles for 2352 Nearby Galaxies". In: *ApJS* 219, 3, p. 3. DOI: 10.1088/0067-0049/219/1/3. arXiv: 1505.03534.

Muñoz, R. P. et al. (2014). "The Next Generation Virgo Cluster Survey-Infrared (NGVS-IR). I. A New Near-Ultraviolet, Optical, and Near-Infrared Globular Cluster Selection Tool". In: *ApJS* 210, 4, p. 4. DOI: 10.1088/0067-0049/210/1/4. arXiv: 1311.0873.

Ninković, S. (2017). "Mass Distribution and Gravitational Potential of the Milky Way". In: *Open Astronomy* 26, pp. 1–6. DOI: 10.1515/astro-2017-0002.

Okamoto, S. et al. (2015). "A Hyper Suprime-Cam View of the Interacting Galaxies of the M81 Group". In: *ApJ* 809, L1, p. L1. DOI: 10.1088/2041-8205/809/1/L1. arXiv: 1507.04889.

Paturel, G. et al. (2003). "The provisional DENIS I-band catalog of galaxies revisited". In: *A&A* 405, pp. 1–3. DOI: 10.1051/0004-6361:20030535.

Peng, C. Y. et al. (2002). "Detailed Structural Decomposition of Galaxy Images". In: *AJ* 124, pp. 266–293. DOI: 10.1086/340952. eprint: astro-ph/0204182.

– (2010). "Detailed Decomposition of Galaxy Images. II. Beyond Axisymmetric Models". In: *AJ* 139, pp. 2097–2129. DOI: 10.1088/0004-6256/139/6/2097. arXiv: 0912.0731.

Pillepich, A., P. Madau, and L. Mayer (2015). "Building Late-type Spiral Galaxies by In-situ and Ex-situ Star Formation". In: *ApJ* 799, 184, p. 184. DOI: 10.1088/0004-637X/799/2/184. arXiv: 1407.7855.

Pohlen, M. and I. Trujillo (2006). "The structure of galactic disks. Studying late-type spiral galaxies using SDSS". In: *A&A* 454, pp. 759–772. DOI: 10.1051/0004-6361:20064883. eprint: astro-ph/0603682.

Press, W. H. and P. Schechter (1974). "Formation of Galaxies and Clusters of Galaxies by Self-Similar Gravitational Condensation". In: *ApJ* 187, pp. 425–438. DOI: 10.1086/152650.

Purcell, C. W., J. S. Bullock, and A. R. Zentner (2007). "Shredded Galaxies as the Source of Diffuse Intrahalo Light on Varying Scales". In: *ApJ* 666, pp. 20–33. DOI: 10.1086/519787. eprint: astro-ph/0703004.

Read, J. I. et al. (2005). "The mass of dwarf spheroidal galaxies and the missing satellite problem". In: *IAU Colloq. 198: Near-fields cosmology with dwarf elliptical galaxies*. Ed. by H. Jerjen and B. Binggeli, pp. 235–239. DOI: 10.1017/S1743921305003807. eprint: astro-ph/0505226.

Rodriguez-Gomez, V. et al. (2016). "The stellar mass assembly of galaxies in the Illustris simulation: growth by mergers and the spatial distribution of accreted stars". In: *MNRAS* 458, pp. 2371–2390. DOI: 10.1093/mnras/stw456. arXiv: 1511.08804.

Romanowsky, A. J. et al. (2016). "Satellite accretion in action: a tidally disrupting dwarf spheroidal around the nearby spiral galaxy NGC 253". In: *MNRAS* 457, pp. L103–L107. DOI: 10.1093/mnrasl/slv207. arXiv: 1512.03815.

Schaye, J. et al. (2015). "The EAGLE project: simulating the evolution and assembly of galaxies and their environments". In: *MNRAS* 446, pp. 521–554. DOI: 10.1093/mnras/stu2058. arXiv: 1407.7040.

Schweizer, F. and P. Seitzer (1990). "The peculiar, off-centered ring of the SA galaxy NGC 3611". In: *PASP* 102, pp. 615–620. DOI: 10.1086/132680.

– (1992). "Correlations between UBV colors and fine structure in E and S0 galaxies - A first attempt at dating ancient merger events". In: *AJ* 104, pp. 1039–1067. DOI: 10.1086/116296.

Searle, L. and R. Zinn (1978). "Compositions of halo clusters and the formation of the galactic halo". In: *ApJ* 225, pp. 357–379. DOI: 10.1086/156499.

Sheth, K. et al. (2010). "The Spitzer Survey of Stellar Structure in Galaxies ()". In: *PASP* 122, p. 1397. DOI: 10.1086/657638. arXiv: 1010.1592.

Skrutskie, M. F. et al. (2006). "The Two Micron All Sky Survey (2MASS)". In: *AJ* 131, pp. 1163–1183. DOI: 10.1086/498708.

Snyder, G. F. et al. (2015). "Galaxy morphology and star formation in the Illustris Simulation at z = 0". In: *MNRAS* 454, pp. 1886–1908. DOI: 10.1093/mnras/stv2078. arXiv: 1502.07747.

Sollima, A. et al. (2010). "A multi-wavelength analysis of M 81: insight on the nature of Arp's loop". In: *A&A* 516, A83, A83. DOI: 10.1051/0004-6361/201014085. arXiv: 1004.1610.

Spavone, M. et al. (2017). "VEGAS: A VST Early-type GAlaxy Survey. II. Photometric study of giant ellipticals and their stellar halos". In: *A&A* 603, A38, A38. DOI: 10.1051/0004-6361/201629111. arXiv: 1703.10835.

Springel, V. (2005). "The cosmological simulation code GADGET-2". In: *MNRAS* 364, pp. 1105–1134. DOI: 10.1111/j.1365-2966.2005.09655.x. eprint: astro-ph/0505010.

Springel, V. et al. (2008). "The Aquarius Project: the subhaloes of galactic haloes". In: *MNRAS* 391, pp. 1685–1711. DOI: 10.1111/j.1365-2966.2008.14066.x. arXiv: 0809.0898.

Steiman-Cameron, T. Y. (1992). "The remarkable twisted disk of NGC 4753 and the shapes of galactic halos". In: *AJ* 104, pp. 1339–1348. DOI: 10.1086/116323.

Stockton, A. (1974). "ON the Tidal Origin of the Bridge of ARP 295". In: *ApJ* 190, p. L47. DOI: 10.1086/181501.

Takahashi, K., H. M. Lee, and S. Inagaki (1997). "Evolution of tidally truncated globular clusters with anisotropy". In: *MNRAS* 292, p. 331. DOI: 10.1093/mnras/292.2.331. eprint: astro-ph/9705012.

Thilker, D. A. et al. (2005). "Recent Star Formation in the Extreme Outer Disk of M83". In: *ApJ* 619, pp. L79–L82. DOI: 10.1086/425251. eprint: astro-ph/0411306.

Thilker, D. A. et al. (2007). "A Search for Extended Ultraviolet Disk (XUV-Disk) Galaxies in the Local Universe". In: *ApJS* 173, pp. 538–571. DOI: 10.1086/523853. arXiv: 0712.3555.

Thomas, G. F. et al. (2017). "Stellar streams as gravitational experiments. I. The case of Sagittarius". In: *A&A* 603, A65, A65. DOI: 10.1051/0004-6361/201730531. arXiv: 1705.01552.

Toomre, A. and J. Toomre (1972). "Galactic Bridges and Tails". In: *ApJ* 178, pp. 623–666. DOI: 10.1086/151823.

Trujillo, I. et al. (2009). "Unveiling the Nature of M94's (NGC4736) Outer Region: A Panchromatic Perspective". In: *ApJ* 704, pp. 618–628. DOI: 10.1088/0004-637X/704/1/618. arXiv: 0907.4884.

Vogelsberger, M. et al. (2014). "Introducing the Illustris Project: simulating the coevolution of dark and visible matter in the Universe". In: *MNRAS* 444, pp. 1518–1547. DOI: 10.1093/mnras/stu1536. arXiv: 1405.2921.

Vorontsov-Vel'Yaminov, B. A. and V. P. Arkhipova (1962). "Morphological catalogue of galaxies. Part 1." In: *Morphological catalogue of galaxies., 1 (1962)*.

– (1964). "Morphological catalogue of galaxies. Part 2." In: *Morphological catalogue of galaxies., 2 (1964)*.

Wang, M.-Y. et al. (2017). "Tidal features of classical Milky Way satellites in a Λ cold dark matter universe". In: *MNRAS* 468, pp. 4887–4901. DOI: 10.1093/mnras/stx742. arXiv: 1611.00778.

Werner, M. W. et al. (2004). "The Spitzer Space Telescope Mission". In: *ApJS* 154, pp. 1–9. DOI: 10.1086/422992. eprint: astro-ph/0406223.

Weżgowiec, M. et al. (2012). "Tidal interaction vs. ram pressure stripping effects as seen in X-rays. Hot gas in group and cluster galaxies". In: *A&A* 544, A99, A99. DOI: 10.1051/0004-6361/201117652. arXiv: 1207.1684.

White, S. D. M. and M. J. Rees (1978). "Core condensation in heavy halos - A two-stage theory for galaxy formation and clustering". In: *MNRAS* 183, pp. 341–358. DOI: 10.1093/mnras/183.3.341.

Whitmore, B. C. et al. (1990). "New observations and a photographic atlas of polar-ring galaxies". In: *AJ* 100, pp. 1489–1522. DOI: 10.1086/115614.

Xue, X. X. et al. (2008). "The Milky Way's Circular Velocity Curve to 60 kpc and an Estimate of the Dark Matter Halo Mass from the Kinematics of ~2400 SDSS Blue Horizontal-Branch Stars". In: *ApJ* 684, 1143-1158, pp. 1143–1158. DOI: 10.1086/589500. arXiv: 0801.1232.

Yabushita, S. (1977). "On the formation of galactic binary systems by tidal encounters". In: *MNRAS* 178, pp. 289–299. DOI: 10.1093/mnras/178.2.289.

York, D. G. and SDSS Collaboration (2000). "The Sloan Digital Sky Survey: Technical Summary". In: *AJ* 120, pp. 1579–1587. DOI: 10.1086/301513. eprint: astro-ph/0006396.

Zaritsky, D. and D. Christlein (2007). "On the Extended Knotted Disks of Galaxies". In: *AJ* 134, pp. 135–141. DOI: 10.1086/518238. eprint: astro-ph/0703487.

Zucker, D. B. et al. (2004). "Andromeda IX: A New Dwarf Spheroidal Satellite of M31". In: *ApJ* 612, pp. L121–L124. DOI: 10.1086/424691. eprint: astro-ph/0404268.

Zwicky, F., E. Herzog, and P. Wild (1963). *Catalogue of galaxies and of clusters of galaxies, Vol. 2*.

Zwicky, F. et al. (1961). *Catalogue of galaxies and of clusters of galaxies, Vol. I*.

de Blok, W. J. G. et al. (2014). "HALOGAS observations of NGC 4414: fountains, interaction, and ram pressure". In: *A&A* 566, A80, A80. DOI: 10.1051/0004-6361/201322517. arXiv: 1405.2160.

de Vaucouleurs, G. et al. (1991). *Third Reference Catalogue of Bright Galaxies. Volume I: Explanations and references. Volume II: Data for galaxies between 0^h and 12^h. Volume III: Data for galaxies between 12^h and 24^h*.